

ABSTRACT

Title of dissertation: **DESIGN OF A PROGRAMMABLE ACTIVE
ACOUSTICS METAMATERIAL**

Jason J. Smoker, Doctor of Philosophy, 2012

Directed by: **Professor Amr Baz
Department of Mechanical Engineering**

Metamaterials are artificial materials engineered to provide properties which may not be readily available in nature. The development of such class of materials constitutes a new area of research that has grown significantly over the past decade. Acoustic metamaterials, specifically, are even more novel than their electromagnetic counterparts arising only in the latter half of the decade. Acoustic metamaterials provide a new tool in controlling the propagation of pressure waves. However, physical design and frequency tuning, is still a large obstacle when creating a new acoustic metamaterial. This dissertation describes active and programmable design for acoustic metamaterials which allows the same basic physical design principles to be used for a variety of application.

With cloaking technology being of a great interest to the US Navy, the proposed design approach would enable the development of a metamaterial with spatially changing effective parameters while retaining a uniform physical design features. The effective parameters would be controlled by tuning smart actuators embedded inside the metamaterial structure. Since this design is based on dynamic effective parameters that

can be electrically controlled, material property ranges of several orders of magnitude could potentially be achieved without changing any physical parameters. With such unique capabilities, physically realizable acoustic cloaks can be achieved and objects treated with these active metamaterials can become acoustically invisible.

DESIGN OF A PROGRAMMABLE ACTIVE ACOUSTICS METAMATERIAL

Submitted by

Jason J. Smoker

Dissertation submitted to the Faculty of the Graduate School of the
University of Maryland, College Park in partial fulfillment
of the requirements for the degree of
Doctor of Philosophy
2012

Advisory Committee:

Professor Amr Baz, Chairman/Advisor
Professor Balakumar Balachandran
Professor Nikhil Chopra
Professor Sarah Bergbreiter
Professor Norman Wereley (Dean's Representative)

©Copyright by

Jason Smoker

2012

Dedication

This dissertation is dedicated to...

my parents, *Kyong Hui and Ronald Smoker*
and my fiancée, *Kristen Hand*

...for their never ending patience and support.

Acknowledgements

Thanks to all my colleagues from the lab including Daniel Chinn, Chang Lee, Mostafa Nouh, Mohammed Rifaat, and Dr. Wael Akl for the support in the labs and also Dr. Adel Elsabbagh and Dr. Soon-Neo Poh who showed me the ropes when I started.

Thanks to all my friends in and out of gradschool who kept me entertained and sane over the years while working on both my masters and doctorate.

And special thanks to Dr. Baz for his patience, his mentorship and for giving me the chance to pursue this doctorate.

Table of Contents

Table of Contents	iv
List of Tables	vi
List of Figures	vii
List of Symbols	xi
List of Symbols	xi
Chapter 1 : Introduction	1
1.1: Motivation.....	1
1.2: Literature Review	2
1.2.1: Metamaterials.....	2
1.2.2: Electromagnetic Cloak.....	6
1.2.3: Acoustic Cloaking Technology	13
1.3: Scope of Dissertation.....	23
1.4: Summary.....	23
Chapter 2 : Derivation for change of coordinate system	24
2.1: Generalized derivation for change of coordinate system in an acoustic medium .	24
2.2: Coordinate Change Derivation for an Acoustic Cloak	30
2.3: Coordinate Change Derivation for Directivity and Dispersion	33
2.4: Summary.....	36
Chapter 3 : Computer Modeling	37
3.1: Derivation of the second order acoustic wave equation	37
3.1.1: Acoustic reflection to the cloak	41
3.2: Implementation into Finite Difference	42
3.2.1: Stability.....	43
3.2.2: Boundary Conditions	44
3.3.1: Cloak with Line Source	53
3.3.2: Cloak with Internal Source	56
3.3.3: Directivity and Dispersion Metamaterial.....	57
3.3.4: Velocities for Focusing Waves	63
3.4: Summary.....	72
Chapter 4 : Active Acoustic Metamaterial (AAMM) with Tunable Effective Density... 73	
4.1: Overview.....	73
4.2: Motivation for the Active Acoustic Metamaterial.....	74
4.3: Description of the Active Acoustic Metamaterial.....	76
4.3.1: Using an active acoustic metamaterial for the purpose of a cloak.....	76
4.3.2: The configuration of the active acoustic metamaterial	79
4.4: Circuit Analog	81
4.5: Plain Acoustic Cavity	82
4.6: Acoustic Cavity with Flexible Diaphragm	84
4.7: Acoustic Cavity with Piezoelectric Diaphragm.....	86
4.7.1: Basic Equations.....	86
4.7.2: Analysis of the effective density	89
4.8: Numerical Performance of an Acoustic Cavity with Piezoelectric Diaphragm	91
4.9: Summary.....	96

Chapter 5 : Experimental Demonstration of an Active Acoustic Metamaterial with Tunable Effective Density	97
5.1: Overview.....	97
5.2: Introduction.....	98
5.3: Analytical Model for the Developed Active Metamaterial Cell.....	100
5.4: Calculation of the Acoustic Impedance using Two Microphone Measurements	103
5.5: Acoustic Metamaterial Cell Construction	104
5.6: Experimental Setup.....	106
5.7: Finite Element Model	108
5.8: Results.....	109
5.9: Summary	114
Chapter 6 : Dually Tunable Effective Density and Bulk Modulus	116
6.1: Introduction.....	116
6.2: Electro-Acoustic Analogy	119
6.2.1: Inertial Forces	119
6.2.2: Elastic Forces	120
6.3: Experimental Realization of the Active Metamaterial Cell.....	130
6.4: Experimental Verification	132
6.4.1: Density Control (First Step).....	132
6.4.2: Bulk Modulus Control (Second Step).....	135
6.5: Summary and Conclusions	137
Chapter 7 : Loss Analysis	139
7.1: Addition of Resistances to Model.....	139
7.2: Results.....	142
7.3: Summary and Conclusions	146
Chapter 8 : Conclusion.....	147
8.1: Summary.....	147
8.2: Original Contributions	149
8.2: Future Work.....	150
Appendix I: Descritization into Finite Difference	153
Appendix II: Stability Analysis	155
Appendix III: Discretization of the Perfectly Matched Layer equations	161
Bibliography	163

List of Tables

Table 1.1: Common wave speeds and wavelengths.....	3
Table 4.1: Analogs adapted from Bauer ⁷²	81
Table 4.2: Parameters of acoustic cavity and.....	91
Table 5.1: PZT4 material properties (adapted from Akl and Baz ⁷⁷).....	105
Table 6.1: Material Properties.....	130
Table 7.1: Parameters of the model with resistance	142

List of Figures

Figure 1.1: Arbitrary change of coordinate system (Pendry <i>et al.</i> ⁵). (a) A field line with the background of a Cartesian coordinate system. (b) A distorted field line with the background of a similarly distorted coordinate system; the field line may be an electric displacement, magnetic induction or Poynting vector.....	6
Figure 1.2: Change of coordinate system to exclude a void. (a) Normal Polar coordinates (b) Polar Coordinate with the beginnings of a small void exclusion (c) Polar coordinate with a large void exclusion in which R_1 is half of R_2	7
Figure 1.3: Descritization of cloak layers (Cummer <i>et al.</i> ¹⁷).....	11
Figure 1.4: Electromagnetic cloak experiment (Schurig <i>et al.</i> ¹⁸) (a) Experimental setup for the electromagnetic cloak for the X-band of microwaves. (b) Actual picture of the split ring cloak used in the experiement.	12
Figure 1.5: Acoustic cloak profile (Cummer and Schurig ¹⁹).....	15
Figure 1.6: Acoustic cloak scattering (Cai and Sanchez-Dehesa ²⁰) (a) Scatter form factor and (b) scattering cross section as a function of ka for the original Cummer-Schurig cloak with rigid core, a rigid core only, a cloaked void core and a cloaked water core.....	17
Figure 1.7: Scattering for $ka=1.5$ with resemblance of monopole resonance (Cai and Sanchez-Dehesa).....	18
Figure 1.8: Layered isotropic parameters (Cheng <i>et al.</i> ²⁸). (a) Idealized structure with layers for a 2D cloak. (b) Ideal and actual parameters necessary for the layers of a cloak for a 20 layer approximation.....	21
Figure 1.9: Possible metamaterial design (Pendry and Jensen ³²).....	22
Figure 2.1: Parallelepiped.....	25
Figure 2.2: Change of polar coordinates (a) Normal polar coordinates (b) Polar Coordinate with the beginnings of a small void exclusion (c) Polar coordinate with a large void exclusion in which R_1 is half of R_2	30
Figure 2.3: Change of Cartesian Coordinates (a) Normal Cartesian Coordinates (b) Cartesian Coordinates with change in directivity and dispersion.....	33
Figure 3.1: Conceptualization for a rotation of the density matrix to give equivalent values of polar properties in Cartesian coordinates.	39
Figure 3.2: Boundary Conditions for (a) Infinite Medium (b) Finite Medium with no defined boundary conditions (c) Finite medium with absorbing boundary conditions.....	45
Figure 3.3: Effect of PML boundary condition on wave (a) propagation cross section through a normal system (b) propagation cross section showing absorption through a perfectly matched layer.....	46
Figure 3.4: PML boundary conditions on field where domains (a), (b), and (c) represent changes in coordinate systems in the x direction, y direction, and both the x and y directions respectively.....	48
Figure 3.5: Density cross section.....	51
Figure 3.6: Bulk modulus cross section.....	52

Figure 3.7: Anisotropic speed of sound: radial (left) and tangential (right)	52
Figure 3.8: Line source from left on a cylinder with Dirichelet boundary conditions for (a) COMSOL FEM and (b) the Custom FDTD model.....	53
Figure 3.9: Line source from left on above cylinder with addition of cloak layer for (a) COMSOL FEM and (b) the Custom FDTD model	55
Figure 3.10: Internal point source for (a) COMSOL FEM and (b) the Custom FDTD model	57
Figure 3.11: $a=0, b=1$ for (a) COMSOL FEM and (b) the Custom FDTD model	58
Figure 3.12: $a=-0.5, b=1$ for (a) COMSOL FEM and (b) the Custom FDTD model	59
Figure 3.13: $a=0.5, b=1$ for (a) COMSOL FEM and (b) the Custom FDTD model	60
Figure 3.14: $a=0.5, b=1.5$ for (a) COMSOL FEM and (b) the Custom FDTD model.....	61
Figure 3.15: $a=0.5, b=0.5$ for (a) COMSOL FEM and (b) the Custom FDTD model.....	62
Figure 3.16: Linear increase in sound speed in a wide domain with (a), (b), and (c) corresponding to 1, 3 and 5 meters per second increase per meter respectively.	65
Figure 3.17: Linear increase in sound speed in a short domain with (a), (b), and (c) corresponding to 1, 3 and 5 meters per second increase per meter respectively.	67
Figure 3.18: Quadratic increase in sound speed in a wide domain with (a), (b), and (c) corresponding to 1, 9 and 25 meters per second increase at one meter from the center.	69
Figure 3.19: Quadratic increase in sound speed in a short domain with (a), (b), and (c) corresponding to 1, 9 and 25 meters per second increase at one meter from the center.	71
Figure 4.1: Layout of the acoustic cloak (Baz ⁶³)	76
Figure 4.2: Multi-layered acoustic cloak (Baz ⁶³).....	77
Figure 4.3: Density (Baz ⁶³) (a) and bulk modulus (b) distributions	78
Figure 4.4: Configuration of active acoustic metamaterial (Baz ⁶³)	80
Figure 4.5: Plain acoustic cavity (Baz ⁶³) (a) schematic (b) electric analog.....	82
Figure 4.6: Acoustic cavity with flexible diaphragm cavity (Baz ⁶³) (a) schematic (b) electric analog	84
Figure 4.7: Acoustic cavity with open-loop piezoelectric diaphragm cavity (Baz ⁶³) (a) schematic	86
Figure 4.8: Acoustic cavity with closed-loop piezoelectric diaphragm cavity (Baz ⁶³).....	88
Figure 4.9: Comparison between passive and active cavities cavity (Baz ⁶³) (a) passive (b) active.....	92
Figure 4.10: Active acoustic metamaterial (A) with increasing density distribution cavity (Baz ⁶³)	93
Figure 4.11: Active acoustic metamaterial (B) with decreasing density distribution cavity (Baz ⁶³)	94
Figure 4.12: Comparison between the predictions of the full (exact) and reduced (approximate) order feedback gain models (— exact , • approximate) cavity (Baz ⁶³)	95

Figure 5.1: (a) Schematic of the metamaterial cell with property values.	101
Figure 5.2: (a) Drawing of the impedance tube with metamaterial cell mounted (b) Actual mount of the metamaterial cell with holder (Akl and Baz ⁷⁷)	103
Figure 5.3: (a)End construction of metamaterial cell (b) Dimensional layout of the PZT4 bimorph (Akl and Baz ⁷⁷).....	105
Figure 5.4: Schematic of the operation mechanism of the proposed cell (Akl and Baz ⁷⁷)	106
Figure 5.5: Schematic drawing and picture of the impedance tube with attached prototype and transmission loss attachment (Akl and Baz ⁷⁷)	107
Figure 5.6: Finite element mesh of the engineered metamaterial cell (Akl and Baz ⁷⁷)	108
Figure 5.7: Finite element mesh of the engineered metamaterial cell coupled to the impedance tube and the finite element model of the impedance tube with microphone locations (Akl and Baz ⁷⁷).....	109
Figure 5.8: Finite element mesh of the engineered metamaterial cell coupled to the impedance tube with transmission loss attachment and the finite element model of the whole transmission loss measuring apparatus with microphone locations (Akl and Baz ⁷⁷).....	109
Figure 5.9: Real and imaginary components of the acoustic impedance in the uncontrolled case and comparison with the results obtained from the finite element model (Akl and Baz ⁷⁷).....	110
Figure 5.10: Real and imaginary components of the acoustic impedance in the positive feedback control case and comparison with the results obtained from the finite element model (Akl and Baz ⁷⁷)	110
Figure 5.11: Real and imaginary components of the acoustic impedance in the negative feedback control case and comparison with the results obtained from the finite element model (Akl and Baz ⁷⁷)	110
Figure 5.12: Transmission loss measurement of the developed cell and comparison with the results obtained from the finite element model for the uncontrolled case (Akl and Baz ⁷⁷)	111
Figure 5.13: Transmission loss measurement of the developed cell and comparison with the results obtained from the finite element model for the positive feedback case (Akl and Baz ⁷⁷)	112
Figure 5.14: Transmission loss measurement of the developed cell and comparison with the results obtained from the finite element model for the negative feedback case (Akl and Baz ⁷⁷)	112
Figure 5.15: (a) Transfer function between the reference microphone and the adjacent piezoelectric diaphragm, (b) Transfer function between the reference microphone and the farther piezoelectric diaphragm (Akl and Baz ⁷⁷)	113
Figure 6.1: Schematic of the developed cell for density and bulk modulus control.....	118
Figure 6.2: Electrical circuit analogous to the cavity with Helmholtz Resonator	122
Figure 6.3: Uncontrolled homogenized bulk modulus and density for a cavity with Helmholtz resonator.....	125
Figure 6.4: Electrical circuit analogous to the cavity with active Helmholtz resonator.....	127

Figure 6.5: (a,c) Stiffness and control voltage for Helmholtz resonator (b,d) Stiffness and control voltage for end-mounted panels. (e,f) resultant homogenized bulk modulus and density	128
Figure 6.6: (a,c) Stiffness and control voltage for Helmholtz resonator (b,d) Stiffness and control voltage for end-mounted panels. (e,f) resultant homogenized bulk modulus and density	129
Figure 6.7: Construction and dimensions of the proposed active acoustic metamaterial cell	130
Figure 6.8: Schematic of the operation mechanism of the proposed cell	132
Figure 6.9: Frequency response of face-mounted piezoelectric diaphragm	133
Figure 6.10: Frequency response of Helmholtz resonator mounted piezoelectric diaphragm	134
Figure 6.11: Frequency response of the pressure gradient in the uncontrolled and controlled cases	134
Figure 6.12: Frequency response of face-mounted piezoelectric diaphragm	135
Figure 6.13: Frequency response of Helmholtz resonator mounted piezoelectric diaphragm	136
Figure 6.14: Frequency response of the pressure gradient in the uncontrolled and controlled cases	136
Figure 7.1: Electric analog of the dually tunable system with added loss components	140
Figure 7.2: Resistances set to zero	143
Figure 7.3: Only viscous resistance in cavities	143
Figure 7.4: Only viscous resistance in Helmholtz neck	144
Figure 7.5: Only acoustic resistance from diaphragms	144
Figure 7.6: All inclusive resistances	145
Figure 7.7: Subtracted from baseline	145
Figure 8.1: Schematic for cascading cells (Akl and Baz^{92})	150
Figure 8.2: Electric Analog for cascading cells (Akl and Baz^{92})	150
Figure 8.3: Extension of metamaterial for cylindrical coordinates (a) Honeycomb layout for metamaterial A and B layers (b) Turning of the layers on side (c) Representation of layers for curved surface	151
Figure 8.4: Different configurations of A and B metamaterial layers relative to the thickness of the structure.	152

List of Symbols

A	area of cavity
a	area of Helmholtz resonator neck
C_C	compliance of cavity
C_D	open-loop compliance of diaphragm
C_{DC}	closed-loop compliance of diaphragm
C_P	capacitance of piezoelectric diaphragm
C_s	capacitance in series with piezoelectric diaphragm
C_T	closed-loop compliance of diaphragm
c_o	sound speed
D	electrical displacement
d	piezoelectric strain coefficient
d_A	effective Piezoelectric Coefficient ($d_A = d A$)
E	electrical field
G	feedback gain
k_D	diaphragm stiffness
L_C	inductance of cavity
l	length of cavity
l_H	length of Helmholtz resonator neck
M_D	mass of diaphragm
p	fluid pressure in the time domain
P	fluid pressure in the Laplace domain
Δp	pressure drop along cavity
Δp_P	pressure across piezoelectric diaphragm
Q	volumetric flow rate
q	electrical charge
R	radius of diaphragm
S	strain
s^E	piezoelectric compliance
s	Laplace complex number

T	stress
t	diaphragm thickness
u	flow velocity
V	volume of cavity
V_P	piezoelectric voltage
ΔVol	volume change of diaphragm
Z_P	Impedance of piezoelectric diaphragm and attachments

Greek Symbols

ε	permittivity
κ	bulk modulus of fluid
κ_0	bulk modulus in undeformed acoustical domain
κ'	dimensionless bulk modulus (κ / κ_0)
λ	wavelength
ρ	density of fluid
ρ_0	density in undeformed acoustical domain
ρ'	dimensionless density (ρ / ρ_0)
ϕ	electrical to acoustic domain transformer turn ratio
ω	frequency
μ	viscosity
ζ	damping coefficient

Subscripts

d	desired
o	ambient fluid
eff	effective
P	piezoelectric

Chapter 1 : Introduction

1.1: Motivation

The purpose of this work is to create an acoustic medium that reacts not as the average of the sum of its parts, but beyond. Metamaterials have been a popular topic for a while amongst the electromagnetic community, but has just recently started to gain grounds in the acoustic field. However, to this point, realized acoustic metamaterials remain very limited and only exist in very specific forms and applications. Recently, programmable acoustic metamaterial have been considered as a viable and practical alternative. Such a metamaterial could be adjusted for a variety of applications simply with programming rather than a complete rebuild of the structure. One important application for such a metamaterial is acoustic cloaking which can be used to treat critical objects in order to render them acoustically invisible.

The potential for cloaking technology has long been recognized in the modern era. The term “*cloaking*” was first coined by D.C. Fontana and has been popularized in science fiction media, but the developments in such technology have been, to a large degree, unfruitful in reality. References of cloaking technology are usually attributed to military purposes, as a way to conceal a person or object. Here, the term cloaking technology is often lumped with “*camouflage*”, *i.e.* the avoidance of observation. However, cloaking takes this a bit further allowing a signal to bypass an obstruction and continue onward whether object is a naval vessel or large pillar in a concert hall. A programmable metamaterial would be able to redirect a signal at will either continuing it

on as in the case of a cloak, or redirecting it in a desired manner such as an acoustic lens to magnify and focus acoustic signals.

1.2: Literature Review

This section has been broken into three subsections to detail the information leading to the theory necessary to create a programmable metamaterial which is essential for the realization of an acoustic cloak. The first is a literature review of metamaterials including a brief history and evolution of metamaterials. This includes the conceptualization of such materials before the term was coined or technology was available to produce a practical example to contemporary works and realizations, though technologies specific to cloaking will be left to the second subsection. This second subsection includes the early evolution of electromagnetic (EM) cloaks which set up the foundation for acoustic cloaks. The third subsection continues the timeline of cloak research but jumps into the acoustic realm.

1.2.1: Metamaterials

There has been a great deal of interest in the field of metamaterials in the past decade as a way of redirecting waves. Their unnatural characteristic has made them a perfect tool in the search for a means to cloak an object from incident waves. The term itself was only coined a little over decade ago by Rodger M. Walser¹. The prefix “*meta*” originates from the Greek word for “after” or “beyond” and it was then defined as a “*macroscopic composites having a manmade, three-dimensional, periodic cellular*

architecture designed to produce an optimized combination, not available in nature, of two or more responses to specific excitation.”

In an introductory article in the first issue of the journal *Metamaterials*, Shamonina and Solymar², in 2007, described interactions with metamaterials as "*phenomena associated somehow with wave propagation on resonant elements and with negative refraction*". At the time of the conception of that journal, the subject of metamaterials had mostly remained within the domain of electromagnetic, but has since expanded into multiple regions. To paraphrase a speaker from a Metamaterials conference in May of 2011, it seems today that the number of definitions for metamaterials varies with the number of researcher of metamaterials. Generally put, however, metamaterials are materials that gain their property not only from their composition, but also from their structure. This structural component is what distinguishes them from composite materials. These structures are most often sub-wavelength in size, but in certain cases, such as optical metamaterials dealing with phonic crystals, the structures are in the range of wavelength size. Since the structures are intrinsically tied to the wavelength it is important to note the requisite scale of the metamaterials structure. The chart below reveals how small electromagnetic metamaterials structures would have to be in the optical range leading to questions of production challenges.

Table 1.1: Common wave speeds and wavelengths

Seismic	Acoustic	Acoustic	Electromagnetic	Electromagnetic (Optical)
5km/s(In Granite)	343m/s(Air)	1,484m/s (Water)	3×10^8 m/s	3×10^8 m/s
5,000m@1Hz (P-wave)	0.343m@1kHz	1.5cm@100kHz	30 μ m@10THz (IR-C)	500nm@600THz (Green light)

As suggested by the chart above, research on metamaterials spans several domains of wave propagation. Initially, the focus of metamaterial was on the electromagnetic domain. The most dominant of these are those with negative refractive index i.e. materials that possess both negative permittivity (ϵ) and negative permeability (μ). These materials are sometimes referred to as left-handed media alluding in contrast to the “right-hand” rule memorization technique. Other names also include backward wave media, or double negative metamaterial. Though there are certain specific cases where a material with a negative permittivity can be found and a few rare cases when negative permeability occurs, the combination of the two has yet to be discovered naturally³. Victor Veselago was among the first to publish a detailed theoretical study of such a material in 1967 which was translated into English in 1968⁴. He suggested that the possibility of the existence of such a material with both negative ϵ and μ would fall into one of three categories. First he suggested that since the product of the two would be again positive, there would not be anything special about these materials. Secondly, it could be that such a material might violate some fundamental law of nature and therefore doesn’t exist. Finally, the case that Veselago realizes in his paper is the scenario where the double negative material can exist, and possesses some quality that is different to that of a double positive material. He extended the existing Snell law to reflect the “rightness” of the material.

$$\frac{\sin \varphi}{\sin \psi} = n_{1,2} = \sqrt{\frac{\epsilon_2 \mu_2}{\epsilon_1 \mu_1}} \quad \Rightarrow \quad \frac{\sin \varphi}{\sin \psi} = n_{1,2} = \frac{p_2}{p_1} \sqrt{\frac{\epsilon_2 \mu_2}{\epsilon_1 \mu_1}} \quad (1.1)$$

He also discusses what values of ϵ and μ are possible in principle such as the possibility of anisotropic values and the limitation what scenarios double negative material can occur. Veselago is often cited, in the last decade, as an early example of study into an

electromagnetic metamaterial^{5,6,7,3}. However, Sergei Tretyakov noted in 2005, on his historical paper on negative refraction and backward wave media⁸, that such left handed materials were suggested, at least in a cursory manner, by many others including but not limited to Mandelshtam (1940), Malyuzhinets (1951) and Silin (1959). Veselago, himself, references Pafomove (1959) when considering the reverse Doppler and Vavilov-Cerenkov effects for a “*substance with negative group velocity.*”

In 1999 Pendry and others⁹ were the first to show that split ring microstructures, built from non-magnetic conductors, could create the effect of a material with a permeability that doesn't exist in nature. Additionally, this effective permeability could be tuned to a desired value. This spurred a number of subsequent studies in negative index metamaterials. Many of these electromagnetic metamaterials were reviewed by Liu and Zhang¹⁰, Shalaev⁷, and also Ung¹¹ exploring chiral materials, single negative materials, photonic crystals as well as the aforementioned double negative materials.

More recently, metamaterials research has begun evolving in acoustic research as well. Sheng *et al.*¹², for example, have analyzed how a material with a certain average static density can have a completely different effective density in the dynamic case. Others have demonstrated metamaterial with specific properties such as the work of Lee *et al.*¹³ in creating a material with an effective negative density. Furthermore, acoustic metamaterial technology has been taken into the realm of application with metamaterials designed as acoustic lenses to focus sound waves^{14,15} or as in the case of this dissertation proposal, to redirect them around an object.

1.2.2: Electromagnetic Cloak

In 2006, Pendry *et al.*⁵ showed how Maxwell's equations basically held for a transformation of coordinates as displayed in Figure 1.1 such that a new coordinate system q_1, q_2, q_3 is a function of x, y, z . Thus:

$$\begin{aligned} \nabla \times \mathbf{E} &= -\mu\mu_0 \frac{\partial \mathbf{H}}{\partial t} \\ \nabla \times \mathbf{H} &= +\varepsilon\varepsilon_0 \frac{\partial \mathbf{E}}{\partial t} \end{aligned} \quad \Rightarrow \quad \begin{aligned} \nabla \times \hat{\mathbf{E}} &= -\mu_0 \hat{\mu} \frac{\partial \hat{\mathbf{H}}}{\partial t} \\ \nabla \times \hat{\mathbf{H}} &= +\varepsilon_0 \hat{\varepsilon} \frac{\partial \hat{\mathbf{E}}}{\partial t} \end{aligned} \quad (1.2)$$

where $\hat{\mu}, \hat{\varepsilon}$ are general tensors and $\hat{\mathbf{E}}, \hat{\mathbf{H}}$ are renormalized fields. In addition, when the new coordinate system is orthogonal, the permittivity and permeability terms simplify considerably.

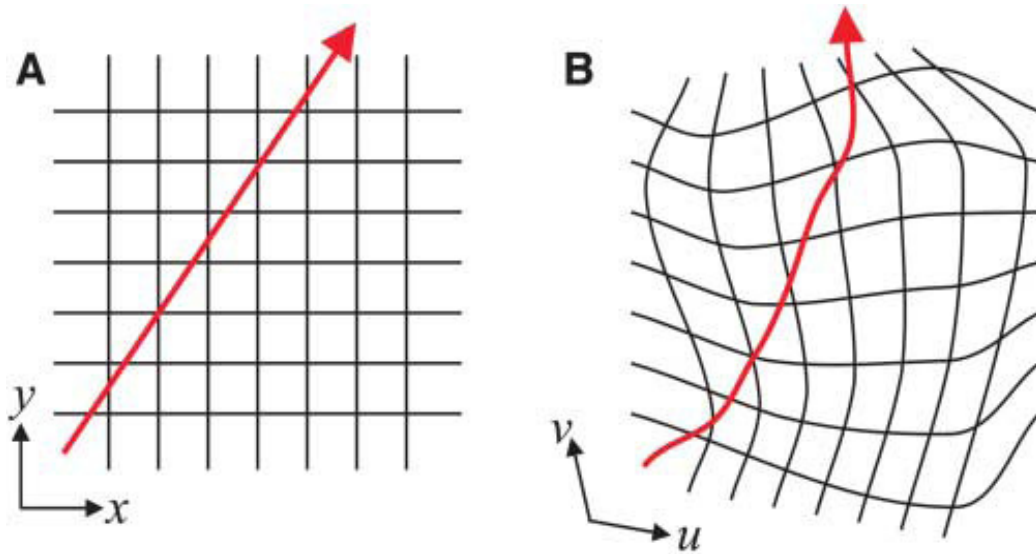


Figure 1.1: Arbitrary change of coordinate system (Pendry *et al.*⁵). (a) A field line with the background of a Cartesian coordinate system. (b) A distorted field line with the background of a similarly distorted coordinate system; the field line may be an electric displacement, magnetic induction or Poynting vector.

The article took the three dimensional example of an orthogonal coordinate transfer in the case of a sphere and gave the material properties for a transformation that corresponded to:

$$\begin{aligned}
 r' &= R_1 + \frac{r(R_2 - R_1)}{R_2} \\
 \theta' &= \theta \\
 \phi' &= \phi
 \end{aligned}
 \tag{1.3}$$

This transformation removes a portion of space ($r < R_1$) from the coordinate system, effectively hiding it as shown in Figure 1.2.

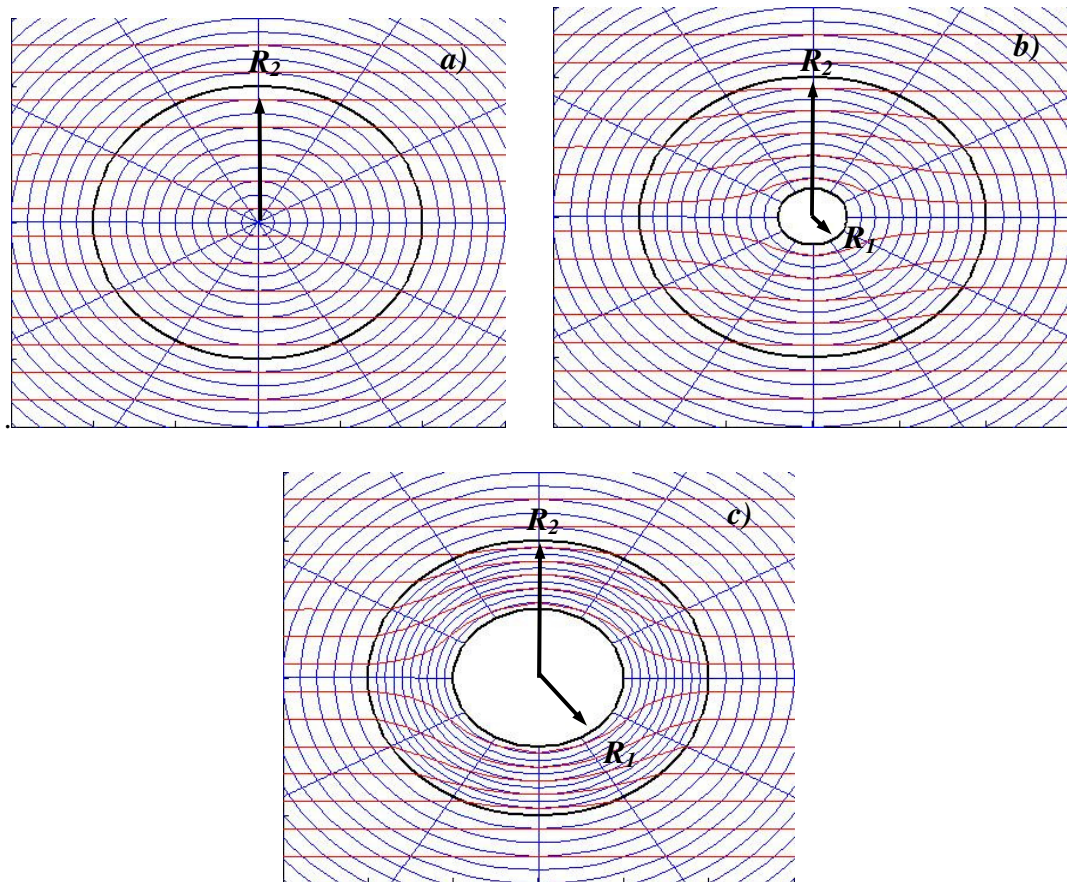


Figure 1.2: Change of coordinate system to exclude a void. (a) Normal Polar coordinates (b) Polar Coordinate with the beginnings of a small void exclusion (c) Polar coordinate with a large void exclusion in which R_1 is half of R_2

Detailed derivations for the material properties were published a few months later¹⁶. It included both the spherical coordinates printed in their June 2006 paper as well as a cylindrical coordinate transformation. With the mapping mentioned above, the original domain $0 < r < R_2$ was compressed into region $R_1 < r < R_2$ so that the origin was mapped to a fixed radius and the outer radius remained fixed such that it would blend with the material properties outside of R_2 which remained untransformed. They began the transformation by equating the unit vectors of the pre and post transformation space.

$$\frac{x^{i'}}{r'} = \frac{x^i}{r} \delta_i^{i'} \quad \Leftrightarrow \quad \begin{aligned} \frac{x'}{r'} &= \frac{x}{r} \\ \frac{y'}{r'} &= \frac{y}{r} \\ \frac{z'}{r'} &= \frac{z}{r} \end{aligned}$$

This was combined with the transformation from above to produce the components of the position vector as a function of only the components from the original space.

$$x^{i'} = a \frac{x^i}{r} \delta_i^{i'} + \frac{r(b-a)}{b} \frac{x^i}{r} \delta_i^{i'} \quad \Leftrightarrow \quad \begin{aligned} x' &= a \frac{x}{r} + \frac{(b-a)}{b} x \\ y' &= a \frac{y}{r} + \frac{(b-a)}{b} y \\ z' &= a \frac{z}{r} + \frac{(b-a)}{b} z \end{aligned} \quad (1.4)$$

Here the transformation matrix as defined by

$$\mathbf{T} = \frac{\partial x'_i}{\partial x_j} = \begin{bmatrix} \frac{\partial x'}{\partial x} & \frac{\partial x'}{\partial y} & \frac{\partial x'}{\partial z} \\ \frac{\partial y'}{\partial x} & \frac{\partial y'}{\partial y} & \frac{\partial y'}{\partial z} \\ \frac{\partial z'}{\partial x} & \frac{\partial z'}{\partial y} & \frac{\partial z'}{\partial z} \end{bmatrix} \quad (1.5)$$

could then be calculated using the position vectors resulting in the following.

$$\mathbf{T} = \begin{bmatrix} \frac{r'}{r} - \frac{ax^2}{r^3} & -\frac{axy}{r^3} & -\frac{axz}{r^3} \\ -\frac{ayx}{r^3} & \frac{r'}{r} - \frac{ay^2}{r^3} & -\frac{ayz}{r^3} \\ -\frac{azx}{r^3} & -\frac{azy}{r^3} & \frac{r'}{r} - \frac{az^2}{r^3} \end{bmatrix} \quad (1.6)$$

Since the coordinate system is symmetric, the matrix can be rotated such that $(x, y, z) = (r, 0, 0)$ to find the determinant of the transformation tensor.

$$\det \mathbf{T} = \frac{r' - R_1}{r} \left(\frac{r'}{r} \right)^2 \quad (1.7)$$

This transformation was then used to apply a tensor density transformation on the permittivity and permeability resulting in the following relations.

$$\epsilon^{i'j'} = \mu^{i'j'} = \frac{R_2}{R_2 - R_1} \left(\delta^{i'j'} - \frac{2R_1 r' - a^2}{r'^4} x^{i'} x^{j'} \right) \quad (1.8)$$

Which, written out, comes to:

$$\begin{aligned} \epsilon'_{r'} &= \mu'_{r'} = \frac{R_2}{R_2 - R_1} + \frac{(r' - R_1)}{r'} \\ \epsilon'_{\theta'} &= \mu'_{\theta'} = \frac{R_2}{R_2 - R_1} \\ \epsilon'_{\phi'} &= \mu'_{\phi'} = \frac{R_2}{R_2 - R_1} \end{aligned} \quad (1.9)$$

It is important to note that at the outer surface where $r = R_2$ the values become

$\mu'_{\theta'} = \mu'_{\phi'} = \frac{1}{\mu'_{r'}}$ and $\epsilon'_{\theta'} = \epsilon'_{\phi'} = \frac{1}{\epsilon'_{r'}}$. Also, since these transforms outside the outer radius

are no longer applied, the values of the transforms become $\epsilon'_{r'} = \epsilon'_{\theta'} = \epsilon'_{\phi'} = 1$ and

$\mu'_r = \mu'_\theta = \mu'_\phi = 1$ revealing that the outer layer of the transformed coordinate sphere is perfectly matched. Thus, the central region would exclude all outside fields and, conversely, no inner fields would escape. In addition, a ray exactly perpendicular to the tangent of the cloak would be a singularity where it “*does not know whether to deviate up or down, left or right.*” Schurig *et al.*¹⁶ acknowledged also that there may be issues attaining very small and very large values of permittivity and permeability, and that unless the surrounding medium had a very high refractive index where dispersion may be avoided, the cloak could only operate fully at a single frequency.

A few months after Pendry *et al.* published their paper, that Schurig and Smith from that group was joined by Cummer and Popa¹⁷ to publish a paper investigating the new electromagnetic cloak theory with simulations using a finite-element electromagnetic solver. The bulk of the simulations were based in a 2D cylindrical problem with a shell thickness normalized to the radius of the inner radius. Here they took four main scenarios. The first was the ideal cloak taken straight from the recently realized theory and was used mostly as a baseline for the subsequent scenarios. The second case introduced electric and magnetic losses which showed large amounts of forward scattering with a loss tangent of 0.1; however, backscattering actually reduced with the addition of the losses. They attributed this to some of the back scattering being lost within the cloaking layer before exiting the cloak. A smaller loss tangent of 0.01 was found to be almost imperceptible. The third scenario broke the cloak into 8 discrete layers as shown in Figure 1.3.

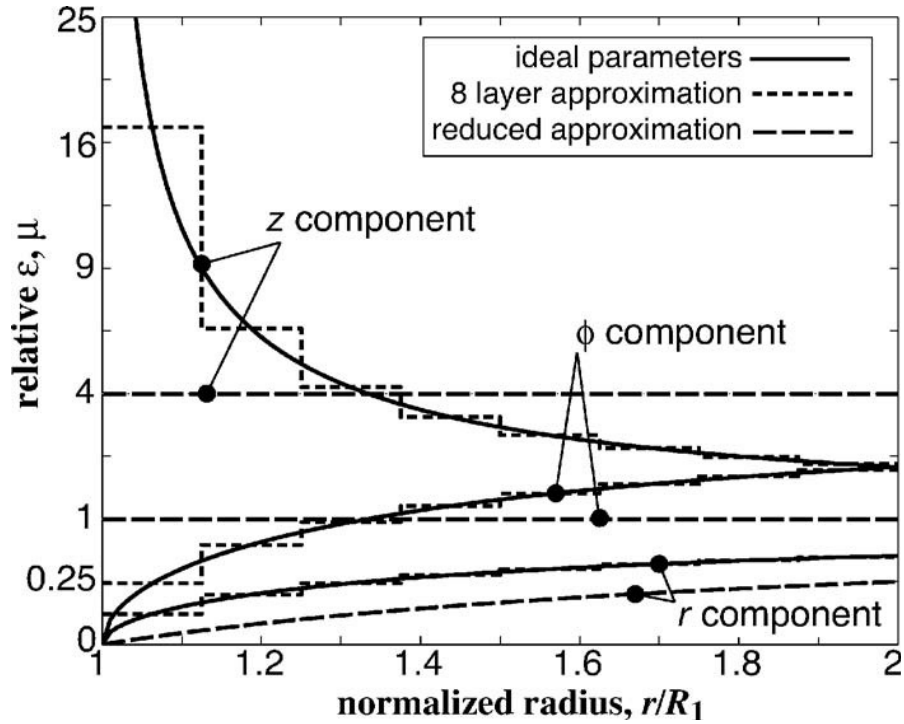


Figure 1.3: Descriptization of cloak layers (Cummer *et al.*¹⁷).

The result of the eight layer approximation showed more scattering than the ideal cloak, but still showed strong signs of the incident wave being redirected around the inner circle. The fourth case for the normalized cloaking thickness used a reduced approximation for the permittivity and permeability. Here, the only inhomogeneous property was the μ_r , while μ_ϕ remained at unity and ϵ_z was real and greater than one. This provided a more easily attainable example that could be achieved with an ordinary dielectric. While the scattering of the fourth case was worse than the previous three, it still showed significant improvement over the lack of a cloak altogether. Finally, there was a discussion of a cloak thickness that was only 25% of the inner radius. Here, the phase front of the ray would have to bend more radically than in the cases of the thicker cloak. Scattering in this case still remained fairly low, but the paper suggested that thinner cloaks would require more tightly controlled electromagnetic parameters.

Several of the members of the previous two groups were then joined by Mock, Justice, and Starr to bring the theory in to reality, as shown in Figure 1.4, using the aforementioned reduced approximation scenario¹⁸.

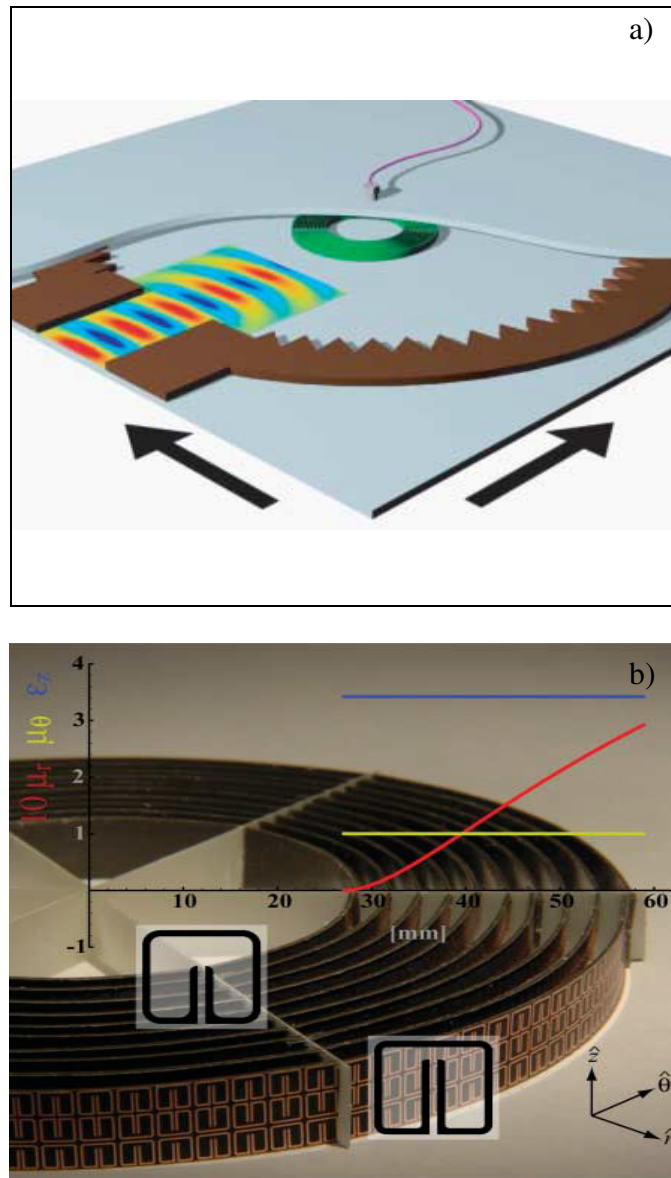


Figure 1.4: Electromagnetic cloak experiment (Schurig *et al.*¹⁸) (a) Experimental setup for the electromagnetic cloak for the X-band of microwaves. (b) Actual picture of the split ring cloak used in the experiment.

The cloak was composed of ten layers of split ring resonators (SRR) and imbedded in a waveguide as shown above with a saw-tooth microwave absorbing boundary. The setup was excited in the X-band of microwaves through the 8-12GHz range. The experimental measurements showed reduced scattering and bending of the wave plane within the cloaking region which was consistent with numerical simulations. Optimal cloaking was found at 8.5GHz in agreement with the design specifications of the cloak.

There are many more additional studies in electromagnetic cloaks but are not as pertinent to the evolution of the acoustic cloak.

1.2.3: Acoustic Cloaking Technology

One of the first appearances of acoustic cloaking by way of coordinate transformation was a paper by Milton *et al.* in 2006⁶. The often cited paper began with a history of invisibility laid out the general equation of motion for elastic media and showed that, in general, equations of motion were not invariant to coordinate transformations. For most cases, when the elastodynamic wave equation is transformed, additional terms appear where the terms for stress and momentum become coupled with velocity and strain respectively. The exception to this lack of invariance, aside from the introduction of a density matrix, was in cases of harmonic mappings. Milton began with the elastodynamic wave equation $\nabla C \nabla \mathbf{u} = -\omega^2 \rho \mathbf{u}$ and applied transformation which changed its form to $\nabla' C' \tilde{\mathbf{N}}' \mathbf{u}' + \nabla' S' \mathbf{u}' = \mathbf{D}' \nabla' \mathbf{u}' - \omega^2 \rho' \mathbf{u}'$ where S' and D' are third order tensors. The exception in harmonic mappings as satisfied by

$$\Delta x'_k = \frac{\partial^2 x'_k}{\partial x_i \partial x_i} = 0 \text{ for all } k \quad (1.10)$$

which occurs for the acoustic wave equation with zero shear modulus and zero shear viscosity in the absence of body forces.

The following year after the paper by Milton *et al.*, Schurig and Cummer¹⁹ extended their coordinate transformation theory for an electromagnetic cloak to acoustic cloak in 2D using the coordinate transformation special case and designing the cloak around an anisotropic material with a second rank density tensor. They showed the exact duality of the following variables from their respective equations.

$$\left(p, v_r, v_\phi, \rho_r, \rho_\phi, \lambda^{-1} \right) \Leftrightarrow \left(-E_z, H_\phi, H_r, \mu_\phi, \mu_r, \epsilon_z \right) \quad (1.11)$$

Cummer and Schurig realized a transformation from Cartesian coordinates to polar coordinates wherein permittivity in the electromagnetic case can be compared to density and bulk modulus in the acoustic case. This required that the bulk modulus and density be a function of their radial location and, as mentioned before, required material to be anisotropic as shown in Figure 1.5.

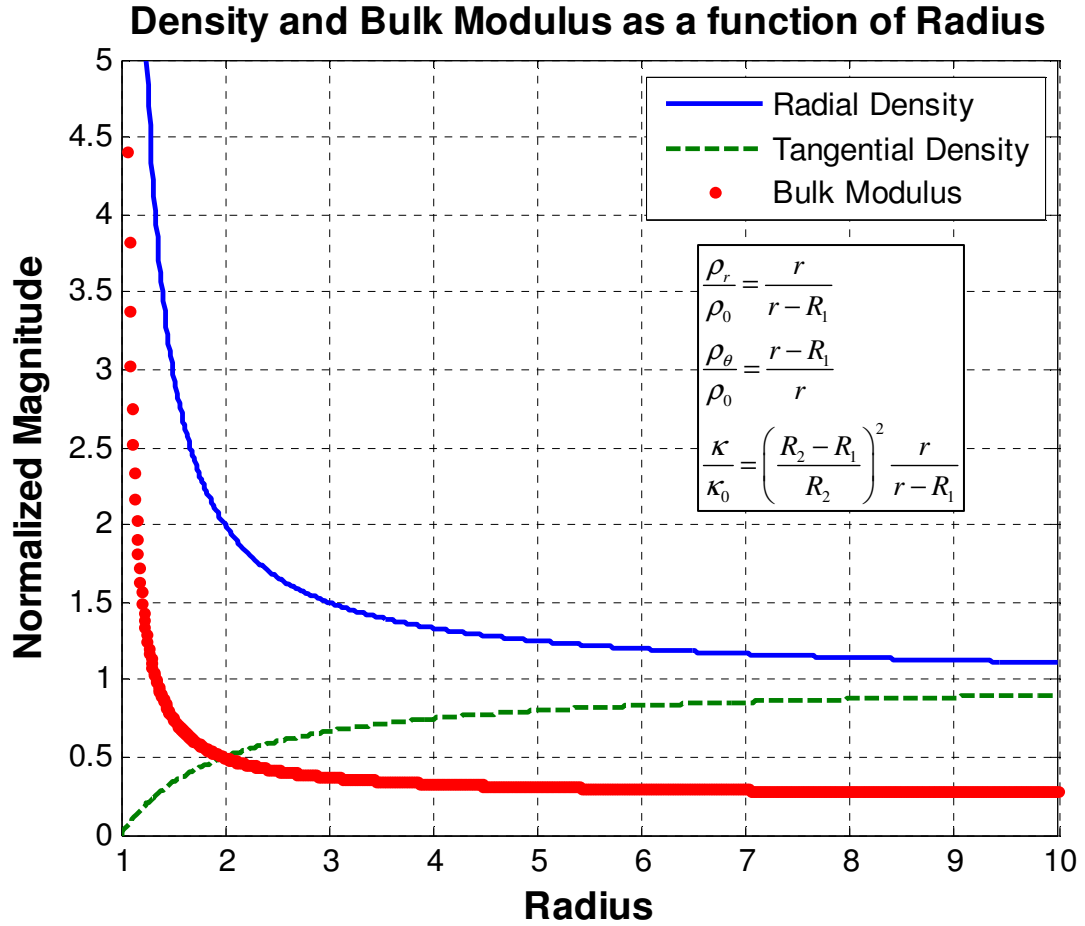
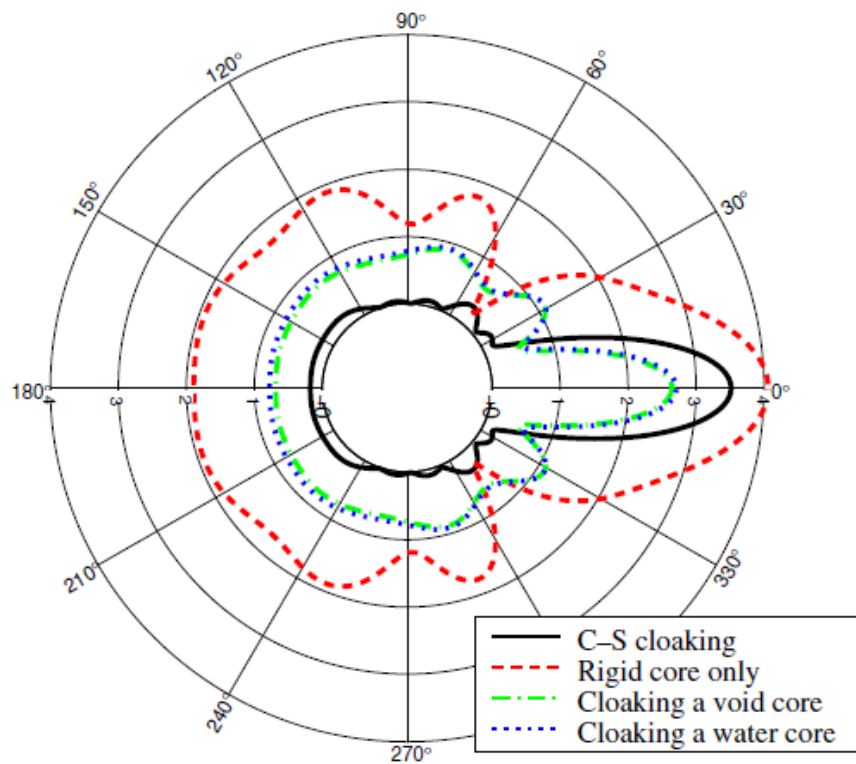


Figure 1.5: Acoustic cloak profile (Cummer and Schurig¹⁹)

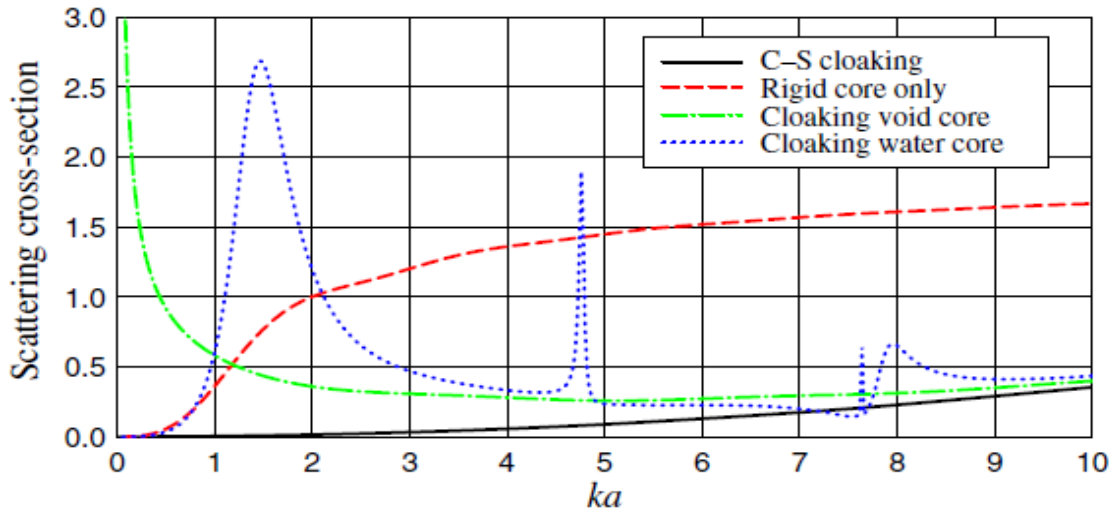
The paper continued by demonstrating the transformation using a finite difference code in Cartesian coordinates with normalized Gaussian wave. Three scenarios were shown to make visual comparisons between the cloaked scenario against an open field and a field with an uncloaked object. Cummer and Schurig noted that even with rough meshes, cloaking performances remained high implying insensitivity to imperfections. They also hinted that shifting the anisotropy from the density to the bulk modulus could be easier to realize.

An analysis of that paper by Cai and Sanchez-Dehesa²⁰ computationally compared results and showed the effectiveness of that cloak for planar and line source

waves. Comparisons were also made between a rigid core as in the original design, a cloaked void region and a cloaked region of water. They used scattering techniques which involves Bessel functions as solutions to the wave equation with 15 to 25 layers on the cloak. The analysis described that the effectiveness varied across the computed spatial frequency range, which was up to where the product of the wave number and outer radius of the cloaked shell equaled ten. It also showed in general that the rigid center produced the best results while a water medium produced the worst as seen on their scattering form factors from their paper below which show $ka=9.5$ as displayed in Figure 1.6.



(a)



(b)

Figure 1.6: Acoustic cloak scattering (Cai and Sanchez-Dehesa²⁰) (a) Scatter form factor and (b) scattering cross section as a function of ka for the original Cummer-Schurig cloak with rigid core, a rigid core only, a cloaked void core and a cloaked water core

Another finding was the total scattering cross section which is the total energy transmitted by a scattered wave. Again, the Cummer and Schurig cloak is shown to have the best result by having the scatter energy over the entire computed frequency band lower than the scattering energy from the rigid core alone. Cai and Sanchez-Dehesa noted that the cloaked water core shows resonant peaks. They looked at the scattering for the first peak at $ka = 1.5$ shown in Figure 1.7, and saw that the outline resembled that of a monopole resonance.

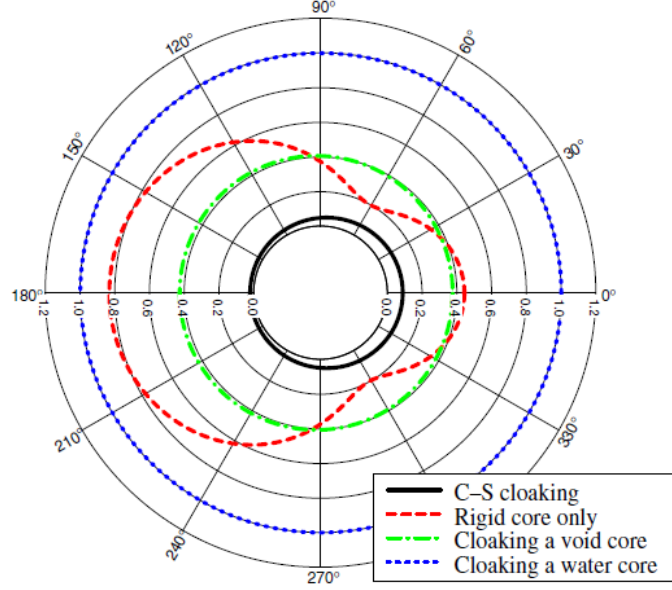


Figure 1.7: Scattering for $ka=1.5$ with resemblance of monopole resonance (Cai and Sanchez-Dehesa)

This resonance was also found at $ka=0$ for the void region. Though mathematically, this was found due to a peculiar property in the Bessel function, they reported that the physics behind the singularity was still unresolved.

At about the same time, Chen and Chan²¹ extended the acoustic cloaking theory to a 3D sphere using the linear radial transformation similar to that used by Schurig *et al.*¹⁶ for the electromagnetic case:

$$r' = a + \frac{r(b-a)}{b}, \quad \theta' = \theta, \quad \text{and } \phi' = \phi \quad (1.12)$$

The Jacobian transformation matrix is then applied to the wave equation.

$$\nabla' \left[\frac{1}{\rho'(x')} \right] \nabla' p'(x') = -\frac{\omega^2}{\kappa'(x')} p'(x') \quad \text{where} \quad \left[\frac{1}{\rho'(x')} \right] = \frac{\mathbf{T} \frac{1}{\rho(x)} \mathbf{T}^T}{\det \mathbf{T}} \quad (1.13)$$

$$\text{and } \frac{1}{\kappa'(x')} = \frac{1}{\kappa(x)} \frac{1}{\det \mathbf{T}}$$

which leads to the mass density and bulk modulus elements of

$$\begin{aligned}\frac{\rho_r}{\rho_0} &= \left(\frac{R_2 - R_1}{R_2} \right) \frac{r^2}{(r - R_1)^2} \\ \frac{\rho_\theta}{\rho_0} &= \frac{\rho_\phi}{\rho_0} = \left(\frac{R_2 - R_1}{R_2} \right) \\ \frac{\kappa}{\kappa_0} &= \left(\frac{R_2 - R_1}{R_2} \right)^3 \frac{r^2}{(r - R_1)^2}\end{aligned}\quad (1.14)$$

Cummer *et al.*²² did their own 3D derivation of a spherical shell, but began with the general second order wave equations, converted it to spherical coordinates, the used separation of variables to apply to apply the coordinate change to each variable via scattering techniques. Though their approach was different, their end result was the same as Chen and Chan. Cummer *et al.*¹⁹ also noted in their analysis that the parameters of a 3D acoustic cloak differentiates itself from its 3D electromagnetic counterpart in that it retains is singularity near the inner radius of the cloak.

An arXiv article by Norris²³ followed by its published version²⁴ in April 2008 analysis of the acoustic cloaks that had been derived even further by generalizing each of the material properties as a function of the special degree. He also related the anisotropic speed of sound through the cloak as a function of the coordinate transformation function and readdressed the material properties as function of the speed of sound the spatial dimensionality of the problem. Norris continues with demonstration that infinite mass is unavoidable in a perfect cloak by showing that the radial mass is described by

$$m_r = \frac{2}{R_2^2 - R_1^2} \left[R_2^2 \ln f(R_2) - R_1^2 \ln f(R_1) - 2 \int_{R_1}^{R_2} dr r \ln f(r) \right] \text{ for 2D} \quad (1.15)$$

$$\text{and } m_r = \frac{3}{R_2^3 - R_1^3} \left[\frac{R_1^4}{R_1} - \frac{R_2^4}{R_2} + 4 \int_{R_1}^{R_2} dr \frac{r^3}{f(r)} \right] \text{ for 3D.} \quad (1.16)$$

In his published paper, he continues by describing an alternate solution where the density is isotropic while the stiffness in the form of bulk modulus becomes anisotropic. This addresses the infinite mass problem by switching the singularity in the change of coordinates from the density as in all the previous inertial cloaks (IC) to the stiffness by way of pentamode (PM) material as initially described by Milton and Cherkaev²⁵ in 1995 and mentioned again by Milton in the context of cloaking in his paper in 2006. Norris continued down the PM cloak path²⁶ and inspired others like Scandrett *et al.*²⁷ to join in his direction as well.

Though the numerical simulations of 2D and 3D cloaks had become thoroughly analyzed, the reality of such an anisotropic material still needed to be addressed. In the first half of 2008, Cheng *et al.*²⁸ and independently Torrent and Sánchez-Dehesa²⁹ suggested a way to attain the anisotropic material through the use of alternating isotropic layers as demonstrated by Schoenberg and Sen³⁰ (Figure 1.8).

$$\begin{aligned}
 \rho_r &= \frac{\rho_A + \eta \rho_B}{1 - \eta} & \frac{\kappa}{\kappa_0} &= \frac{1}{1 + \eta} \left(\frac{1}{\kappa_A} + \frac{\eta}{\kappa_B} \right) \\
 \rho_\theta &= \frac{1}{1 + \eta} \left(\frac{1}{\rho_A} + \frac{\eta}{\rho_B} \right) & \text{where } \eta &= \frac{d_A}{d_B}
 \end{aligned} \tag{1.17}$$

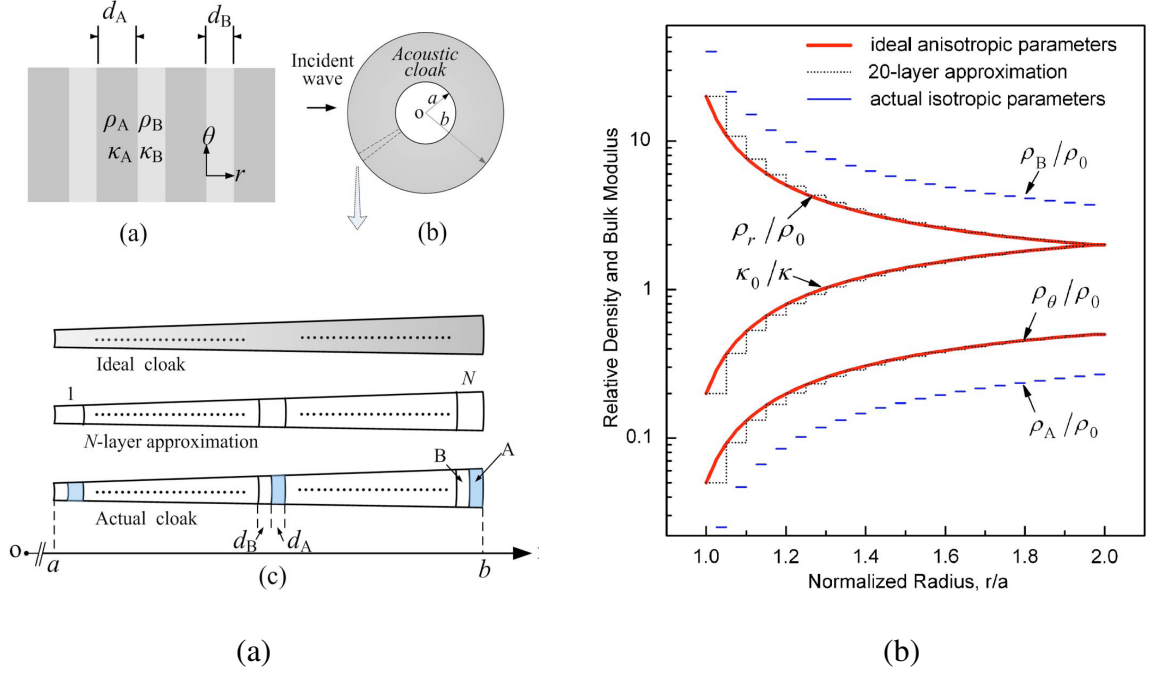


Figure 1.8: Layered isotropic parameters (Cheng *et al.*²⁸). (a) Idealized structure with layers for a 2D cloak. (b) Ideal and actual parameters necessary for the layers of a cloak for a 20 layer approximation

Also, Farhat *et al.*³¹ demonstrated a surface wave cloak, later that year solving for the Helmholtz equation:

$$\nabla^2 \Phi + \kappa^2 \Phi = 0 \quad (1.18)$$

where Φ is the potential, κ is the spectral parameter satisfied by

$$\omega^2 = g \kappa (1 + \kappa^2 d_c^2) \tanh(\kappa h) , \quad (1.19)$$

in which g is gravity and d_c is the capillarity length. Though it wasn't a pressure wave cloak, it was an interesting and successful demonstration on a non-EM wave.

The same month the surface wave paper by Farhat *et al.* was published, Pendry and Jensen³² suggested a metamaterial with a structure permeated by a fluid to satisfy the anisotropic parameters as displayed in Figure (1.9).

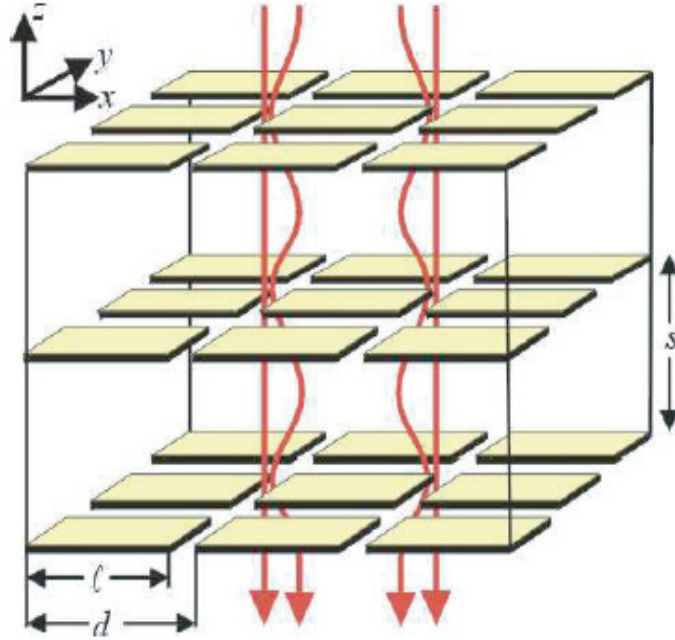


Figure 1.9: Possible metamaterial design (Pendry and Jensen³²)

Plates in the structure would affect the pressure gradient in the direction normal to the surface of the plate giving the effect of an anisotropic density. The bulk modulus of the metamaterial would be controlled with gas sacks upon the plate resulting in a weighted average bulk modulus of the fluid and the gas.

Many acoustic cloak researchers have turned to other aspects of the cloaks such as alternate methods of calculating material properties as in a generalized numerical method for designing cloaks of arbitrary shapes by Hu *et al.*³³, a cloak designed by conformal transformation by Ren *et al.*³⁴ or a cloak design based on optimization methods by Garcia-Chocano *et al.*³⁵ But from here, there's very little progress in producing a material with the parameters necessary to create a cloak which is the subject of this dissertation proposal.

1.3: Scope of Dissertation

Though the creation of a completely functional cylindrical cloak would be the ultimate accomplishment for a dissertation on an acoustic metamaterial, such an endeavor would prove infeasible. This dissertation shall focus on the creation of a modeling tool for metamaterials, a derivation of parameters for the control of directivity and dispersion of acoustic waves, an in depth investigation of a current theoretical model for a one dimensional metamaterial, a physical realization of that metamaterial model showing independently controlled density and bulk modulus, and the addition of loss components to aforementioned theoretical model. Subsequent investigation would be able to build on this dissertation as a result in the hopes that a fully realizable cloak may be built in the future.

1.4: Summary

This chapter has described the purpose of this proposal and the investigated various relevant literature. Though an absolutely exhaustive research may be unending through the constant maturation of new ideas and new technologies, this provides a solid bases and platform of understanding to proceed. As new literatures become available, pertinent one will always be analyzed carefully to add to this research.

Chapter 2 : Derivation for change of coordinate system

2.1: Generalized derivation for change of coordinate system in an acoustic medium

The foundation for all the material parameters is the change of coordinate system that creates the virtual void in space and shifts the space around it. Much of this follows the outline made by Ward and Pendry³⁶ and Cummer *et al.*³⁷ For this coordinate change we first declare the new coordinate system in terms of the old:

$$q_1(x^1, x^2, x^3) \quad q_2(x^1, x^2, x^3) \quad q_3(x^1, x^2, x^3)$$

With unit vectors $\hat{\mathbf{u}}_1$, $\hat{\mathbf{u}}_2$ and $\hat{\mathbf{u}}_3$ pointing in the corresponding axes respectively.

The length of a line segment in any orientation is described by

$$ds^2 = dx^i dx^j = Q_{ij} dq_i dq_j \quad (2.1)$$

where

$$Q_{ij} = \frac{(\partial x^1)^2}{\partial q_i \partial q_j} + \frac{(\partial x^2)^2}{\partial q_i \partial q_j} + \frac{(\partial x^3)^2}{\partial q_i \partial q_j}. \quad (2.2)$$

For a line lying along the direction of one of the new axes, the length can be given by

$$ds = Q_{ii} dq_i \quad (2.3)$$

For simplicity let:

$$Q_i^2 = \left(\frac{\partial x^1}{\partial q_i} \right)^2 + \left(\frac{\partial x^2}{\partial q_i} \right)^2 + \left(\frac{\partial x^3}{\partial q_i} \right)^2 = Q_{ii} \quad (2.4)$$

Let us now consider a parallelepiped described by the line segments of the new coordinate system as shown in Figure 2.1.

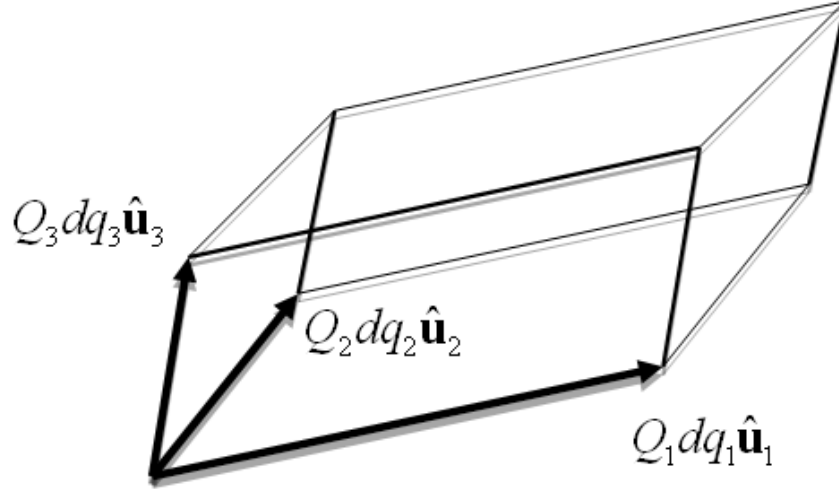


Figure 2.1: Parallelepiped

where $Q_1 dq_1 \hat{\mathbf{u}}_1$, $Q_2 dq_2 \hat{\mathbf{u}}_2$, and $Q_3 dq_3 \hat{\mathbf{u}}_3$ are all infinitesimal displacement vectors in direction of the unit vectors.

Applying the divergence theorem to the velocity vector field of this volume can be written as

$$\iiint_V (\nabla \cdot \mathbf{v}) dV = \iint (\mathbf{v} \cdot \mathbf{n}) dS \quad (2.5)$$

where the dV can be found by applying the triple scalar product of the displacement vectors

$$dV = Q_1 dq_1 Q_2 dq_2 Q_3 dq_3 |\hat{\mathbf{u}}_1 \times (\hat{\mathbf{u}}_2 \times \hat{\mathbf{u}}_3)| \quad (2.6)$$

Each surface and corresponding normal can be found with the following relations

$$\begin{aligned}
dS_1 &= Q_2 dq_2 Q_3 dq_3 |\hat{\mathbf{u}}_2 \times \hat{\mathbf{u}}_3|, & \mathbf{n}_1 &= \frac{\hat{\mathbf{u}}_2 \times \hat{\mathbf{u}}_3}{|\hat{\mathbf{u}}_2 \times \hat{\mathbf{u}}_3|} \\
dS_2 &= Q_1 dq_1 Q_3 dq_3 |\hat{\mathbf{u}}_3 \times \hat{\mathbf{u}}_1|, & \mathbf{n}_2 &= \frac{\hat{\mathbf{u}}_3 \times \hat{\mathbf{u}}_1}{|\hat{\mathbf{u}}_3 \times \hat{\mathbf{u}}_1|} \\
dS_3 &= Q_1 dq_1 Q_2 dq_2 |\hat{\mathbf{u}}_1 \times \hat{\mathbf{u}}_2|, & \mathbf{n}_3 &= \frac{\hat{\mathbf{u}}_1 \times \hat{\mathbf{u}}_2}{|\hat{\mathbf{u}}_1 \times \hat{\mathbf{u}}_2|}
\end{aligned} \tag{2.7}$$

Substituting into the divergence theorem and dividing through by $dq_1 dq_2 dq_3$ results in

$$\begin{aligned}
(\nabla \cdot \mathbf{v}) Q_1 Q_2 Q_3 |\hat{\mathbf{u}}_1 \times (\hat{\mathbf{u}}_2 \times \hat{\mathbf{u}}_3)| &= \\
\frac{\partial}{\partial q_1} Q_2 Q_3 (\mathbf{v} \cdot (\hat{\mathbf{u}}_2 \times \hat{\mathbf{u}}_3)) &+ \frac{\partial}{\partial q_2} Q_1 Q_3 (\mathbf{v} \cdot (\hat{\mathbf{u}}_3 \times \hat{\mathbf{u}}_1)) &+ \frac{\partial}{\partial q_3} Q_1 Q_2 (\mathbf{v} \cdot (\hat{\mathbf{u}}_1 \times \hat{\mathbf{u}}_2)) \tag{2.8}
\end{aligned}$$

Now let

$$V_{frac} = |\hat{\mathbf{u}}_1 \times (\hat{\mathbf{u}}_2 \times \hat{\mathbf{u}}_3)|. \tag{2.9}$$

which is the fraction in which the unit volume is compressed for nonorthogonal coordinate transformations. Note that

$$|\hat{\mathbf{u}}_1 \times (\hat{\mathbf{u}}_2 \times \hat{\mathbf{u}}_3)| = |\hat{\mathbf{u}}_2 \times (\hat{\mathbf{u}}_3 \times \hat{\mathbf{u}}_1)| = |\hat{\mathbf{u}}_3 \times (\hat{\mathbf{u}}_1 \times \hat{\mathbf{u}}_2)| \tag{2.10}$$

and

$$|\mathbf{v} \cdot (\hat{\mathbf{u}}_2 \times \hat{\mathbf{u}}_3)| = v^1 \hat{\mathbf{u}}_1 \cdot (\hat{\mathbf{u}}_2 \times \hat{\mathbf{u}}_3). \tag{2.11}$$

Making the above substitutions from (2.10) and (2.11) into the (2.8), we get

$$\begin{aligned}
(\nabla \cdot \mathbf{v}) Q_1 Q_2 Q_3 V_{frac} &= \\
\frac{\partial}{\partial q_1} (Q_2 Q_3 V_{frac} v^1) &+ \frac{\partial}{\partial q_2} (Q_1 Q_3 V_{frac} v^2) &+ \frac{\partial}{\partial q_3} (Q_1 Q_2 V_{frac} v^3) \tag{2.12}
\end{aligned}$$

Noting that the divergence of the velocity vector in the new coordinates is defined by

$$(\nabla_q \cdot \mathbf{v}) = \frac{\partial v^1}{\partial q_1} + \frac{\partial v^2}{\partial q_2} + \frac{\partial v^3}{\partial q_3} \quad (2.13)$$

we can write the rewrite (2.12) making the substitution to the right hand side

$$(\nabla \cdot \mathbf{v}) Q_1 Q_2 Q_3 V_{frac} = \nabla_q \cdot (V_{frac} \mathbf{Q} \mathbf{v}) = \nabla_q \cdot \hat{\mathbf{v}} \quad (2.14)$$

where

$$\mathbf{Q} = \begin{bmatrix} Q_{22} Q_{33} & 0 & 0 \\ 0 & Q_{11} Q_{33} & 0 \\ 0 & 0 & Q_{11} Q_{22} \end{bmatrix}. \quad (2.15)$$

By inspection it can be seen that

$$\hat{\mathbf{v}} = (V_{frac} \mathbf{Q} \mathbf{v}). \quad (2.16)$$

From here we can begin to make substitution to determine the necessary material parameters in the new coordinate system. Let us begin with Euler's mass conservation equation

$$\frac{\partial p}{\partial t} = \kappa_0 (\nabla \cdot \mathbf{v}). \quad (2.17)$$

First we multiply both sides by $Q_1 Q_2 Q_3 V_{frac}$ resulting in

$$\frac{\partial p}{\partial t} Q_1 Q_2 Q_3 V_{frac} = \kappa_0 (\nabla \cdot \mathbf{v}) Q_1 Q_2 Q_3 V_{frac} = \kappa_0 \nabla_q \cdot \hat{\mathbf{v}}. \quad (2.18)$$

We can already see that the right side of the equation can be written in terms of previously defined in the new coordinate system

$$\frac{\partial p}{\partial t} Q_1 Q_2 Q_3 V_{frac} = \kappa_0 \nabla_q \cdot \hat{\mathbf{v}}. \quad (2.19)$$

Finally setting

$$\frac{\partial p}{\partial t} = \kappa_q \nabla_q \cdot \hat{\mathbf{v}}, \quad (2.20)$$

we can define the new bulk modulus in terms of the old with

$$\kappa_q = (Q_1 Q_2 Q_3 V_{frac})^{-1} \kappa_0. \quad (2.21)$$

To get the density in the new coordinate system we start with Euler's momentum conservation equation

$$\nabla p = \rho_0 \frac{\partial \mathbf{v}}{\partial t}. \quad (2.22)$$

Let us recall the fundamental theorem of calculus

$$\int \nabla p \, ds_1 = \Delta p \quad (2.23)$$

where Δp is some change in p not the Laplace operator. For our change of coordinates we can set $ds_1 = Q_1 dq_1 \hat{u}_1$ so that (2.23) can be written as

$$\nabla p \cdot Q_1 \hat{u}_1 = \frac{\partial p}{\partial q_1}. \quad (2.24)$$

If we do the same for the other directions in the new coordinate system we can write the combination as

$$\mathbf{M} \cdot \mathbf{H} \cdot (\nabla p) = \nabla_q p \quad (2.25)$$

where

$$\mathbf{M} = \begin{bmatrix} Q_1 & 0 & 0 \\ 0 & Q_2 & 0 \\ 0 & 0 & Q_3 \end{bmatrix}, \quad \text{and} \quad \mathbf{H} = \begin{bmatrix} \hat{u}_1 \times \hat{u}_1 & \hat{u}_1 \times \hat{u}_2 & \hat{u}_1 \times \hat{u}_3 \\ \hat{u}_2 \times \hat{u}_1 & \hat{u}_2 \times \hat{u}_2 & \hat{u}_2 \times \hat{u}_3 \\ \hat{u}_3 \times \hat{u}_1 & \hat{u}_3 \times \hat{u}_2 & \hat{u}_3 \times \hat{u}_3 \end{bmatrix}. \quad (2.26)$$

Now if we multiply the original equation (2.22) by $\mathbf{M} \cdot \mathbf{H}$ and use (2.16) to substitute the velocity vector we would get

$$\mathbf{M} \cdot \mathbf{H} \cdot \nabla p = \nabla_q p = \mathbf{M} \cdot \mathbf{H} \cdot V_{frac}^{-1} \mathbf{Q}^{-1} \cdot \rho_0 \frac{\partial \hat{\mathbf{v}}}{\partial t} \quad (2.27)$$

It can be seen here that new density becomes:

$$\rho_q = \mathbf{M} \cdot \mathbf{H} \cdot V_{frac}^{-1} \mathbf{Q}^{-1} \rho_0 \quad (2.28)$$

At this point, a distinction needs to be made for the shape of the cloak and a simple metamaterial.

2.2: Coordinate Change Derivation for an Acoustic Cloak

The coordinate change necessary for an acoustic cloak places a “hole” in the new coordinate space as shown in Figure 2.2.

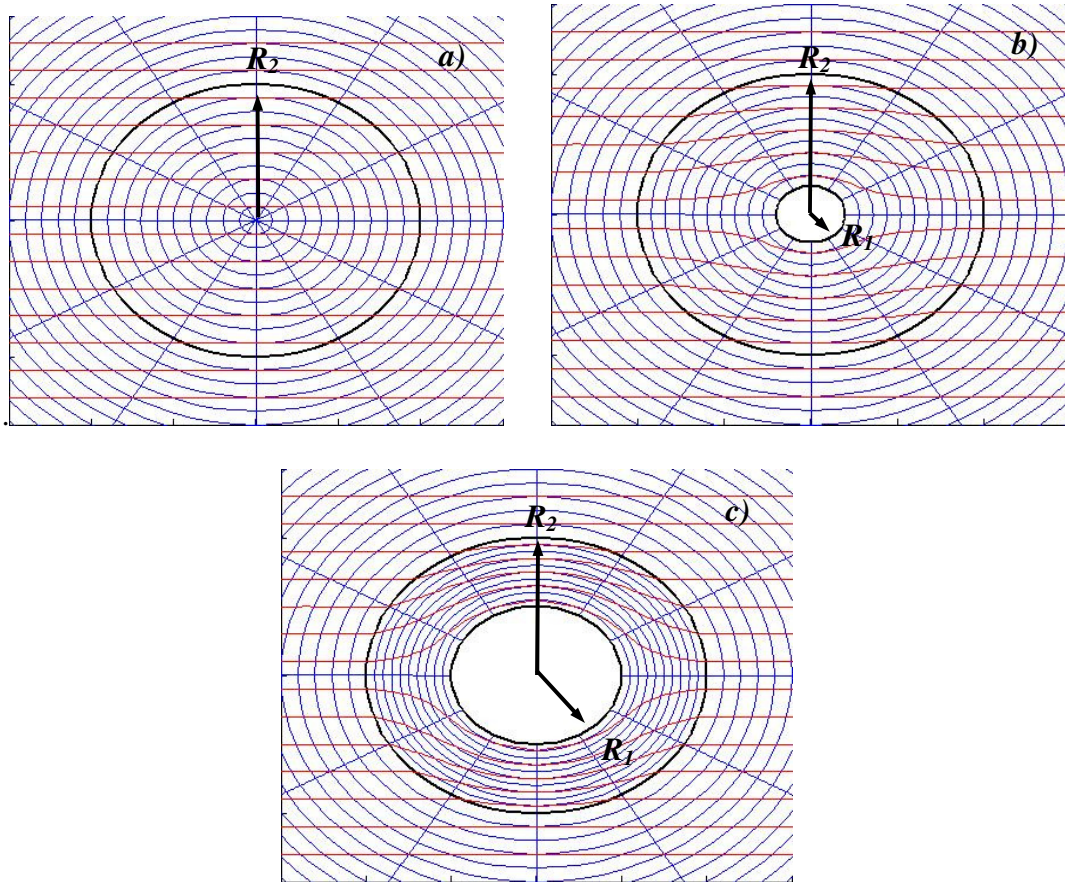


Figure 2.2: Change of polar coordinates (a) Normal polar coordinates (b) Polar Coordinate with the beginnings of a small void exclusion (c) Polar coordinate with a large void exclusion in which R_1 is half of R_2

This can be done in both cylindrical and spherical coordinates. Polar coordinates can also be easily derived from cylindrical coordinates by ignoring the third dimension.

For cylindrical coordinates we define the new coordinate system as:

$$r' = R_1 + r \left(\frac{R_2 - R_1}{R_2} \right), \quad \theta' = \theta, \text{ and } z' = z \quad (2.29)$$

where the length scaling factors are defined from equation (2.4) as

$$Q_r = \left(\frac{R_2}{R_2 - R_1} \right), \quad Q_\theta = \left(\frac{(r' - R_1)}{r'} \frac{R_2}{(R_2 - R_1)} \right), \text{ and } Q_\phi = 1 \quad (2.30)$$

Plugging into the previously defined matrices we get:

$$\mathbf{Q} = \begin{bmatrix} \left(\frac{(r' - R_1)}{r'} \frac{R_2}{(R_2 - R_1)} \right) & 0 & 0 \\ 0 & \left(\frac{R_2}{R_2 - R_1} \right) & 0 \\ 0 & 0 & \left(\frac{R_2}{R_2 - R_1} \right) \left(\frac{(r' - R_1)}{r'} \frac{R_2}{(R_2 - R_1)} \right) \end{bmatrix} \quad (2.31)$$

$$\mathbf{M} = \begin{bmatrix} \left(\frac{R_2}{R_2 - R_1} \right) & 0 & 0 \\ 0 & \left(\frac{(r' - R_1)}{r'} \frac{R_2}{(R_2 - R_1)} \right) & 0 \\ 0 & 0 & 1 \end{bmatrix} \quad \mathbf{H} = \begin{bmatrix} 1 & 0 & 0 \\ 0 & 1 & 0 \\ 0 & 0 & 1 \end{bmatrix} \quad V_{frac} = 1$$

where \mathbf{H} and V_{frac} are identity and unity respectively because of orthogonality.

Using equations (2.31) with (2.21) and (2.28) we solve for the bulk modulus and density as follows

$$\kappa_q = \left(\frac{R_2 - R_1}{R_2} \right)^2 \cdot \left(\frac{r'}{r' - R_1} \right) \kappa_0 \text{ and} \quad (2.32)$$

$$\rho_q = \begin{bmatrix} \frac{r'}{(r' - R_1)} & 0 & 0 \\ 0 & \frac{(r' - R_1)}{r'} & 0 \\ 0 & 0 & \frac{r'}{(r' - R_1)} \left(\frac{(R_2 - R_1)}{R_2} \right)^2 \end{bmatrix}.$$

Spherical coordinates are solved similarly with the third dimension replace by

$$\phi' = \phi \quad (2.33)$$

resulting in a different length scaling factor

$$Q_\phi = \left(\frac{(r' - R_1)}{r'} \frac{R_2}{(R_2 - R_1)} \right). \quad (2.34)$$

These result in the bulk modulus and density of

$$\kappa_q = \left(\frac{R_2 - R_1}{R_2} \right)^3 \cdot \left(\frac{r'}{r' - R_1} \right)^2 \kappa_0 \text{ and} \quad (2.35)$$

$$\rho_q = \begin{bmatrix} \left(\frac{(R_2 - R_1)}{R_2} \right) \left(\frac{r'}{(r' - R_1)} \right)^2 & 0 & 0 \\ 0 & \left(\frac{R_2 - R_1}{R_2} \right) & 0 \\ 0 & 0 & \left(\frac{R_2 - R_1}{R_2} \right) \end{bmatrix} \rho_0$$

2.3: Coordinate Change Derivation for Directivity and Dispersion

By coordinate change, as suggested in Figure 2.3, the material properties can also be produced to redirect and stretch a wave within the material domain.

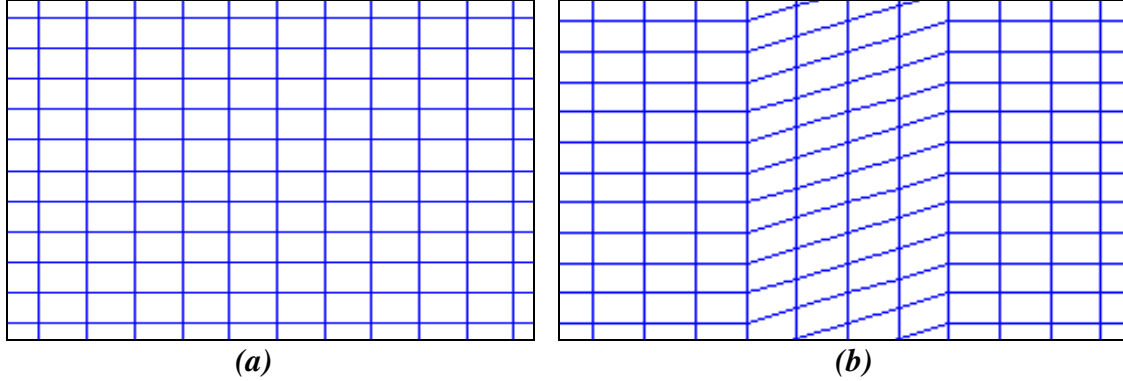


Figure 2.3: Change of Cartesian Coordinates (a) Normal Cartesian Coordinates (b) Cartesian Coordinates with change in directivity and dispersion

For this let us define a new coordinate system that rotates about the y direction as the following:

$$y' = y + ax \quad x' = x, \text{ and} \quad z' = z. \quad (2.36)$$

The corresponding length scaling factors are

$$Q_x = \sqrt{1+a^2}, \quad Q_y = 1, \text{ and} \quad Q_z = 1. \quad (2.37)$$

The resulting \mathbf{Q} and \mathbf{M} matrices are

$$\mathbf{Q} = \begin{bmatrix} 1 & 0 & 0 \\ 0 & \sqrt{1+a^2} & 0 \\ 0 & 0 & \sqrt{1+a^2} \end{bmatrix} \quad \text{and} \quad \mathbf{M} = \begin{bmatrix} \sqrt{1+a^2} & 0 & 0 \\ 0 & 1 & 0 \\ 0 & 0 & 1 \end{bmatrix}. \quad (2.38)$$

Using sine and cosine identities we rotate the $\hat{\mathbf{x}}$ unit vector of this non-orthogonal coordinate system

$$\hat{\mathbf{x}}' = \begin{bmatrix} b & 0 & 0 \\ 0 & 1 & 0 \\ 0 & 0 & 1 \end{bmatrix} \begin{bmatrix} \frac{x}{\sqrt{x^2+y^2}} & \frac{y}{\sqrt{x^2+y^2}} & 0 \\ \frac{-y}{\sqrt{x^2+y^2}} & \frac{x}{\sqrt{x^2+y^2}} & 0 \\ 0 & 0 & 1 \end{bmatrix} \begin{bmatrix} 1 \\ 0 \\ 0 \end{bmatrix} = \begin{bmatrix} \frac{b}{\sqrt{1+a^2}} \\ -a \\ \frac{b}{\sqrt{1+a^2}} \\ 0 \end{bmatrix} \quad (2.39)$$

Resulting in the following new unit vectors

$$\hat{\mathbf{x}}' = \frac{b}{\sqrt{1+a^2}} \hat{\mathbf{x}} + \frac{-a}{\sqrt{1+a^2}} \hat{\mathbf{y}}, \quad \hat{\mathbf{y}}' = \hat{\mathbf{y}}, \text{ and } \hat{\mathbf{z}}' = \hat{\mathbf{z}}. \quad (2.40)$$

The resulting \mathbf{H} and volume fraction are

$$\mathbf{H} = \begin{bmatrix} \frac{a^2+b^2}{1+a^2} & \frac{-a}{\sqrt{1+a^2}} & 0 \\ \frac{-a}{\sqrt{1+a^2}} & 1 & 0 \\ 0 & 0 & 1 \end{bmatrix} \quad \text{and} \quad V_{frac} = \frac{b}{\sqrt{1+a^2}}. \quad (2.41)$$

Plugging into (2.31) we get

$$\kappa_q = \frac{1}{b} \kappa_0 \quad \text{and} \quad \rho_q = \begin{bmatrix} \frac{a^2+b^2}{b} & \frac{-a}{b} & 0 \\ \frac{-a}{b} & \frac{1}{b} & 0 \\ 0 & 0 & \frac{1}{b} \end{bmatrix}. \quad (2.42)$$

However, practically, this matrix must be rotated to create a diagonal matrix to take advantage of diagonal anisotropic material design of Schoenberg and Sen³⁰ mentioned in the literature review.

For this, we select θ such that

$$\begin{aligned} & \begin{bmatrix} \rho_{xxn} & 0 & 0 \\ 0 & \rho_{yy n} & 0 \\ 0 & 0 & \rho_{zz} \end{bmatrix} \\ &= \begin{bmatrix} \cos(\theta) & -\sin(\theta) & 0 \\ \sin(\theta) & \cos(\theta) & 0 \\ 0 & 0 & 1 \end{bmatrix} \cdot \begin{bmatrix} \rho_{xxo} & \rho_{xyo} & 0 \\ \rho_{yxo} & \rho_{yyo} & 0 \\ 0 & 0 & \rho_{zz} \end{bmatrix} \cdot \begin{bmatrix} \cos(\theta) & \sin(\theta) & 0 \\ -\sin(\theta) & \cos(\theta) & 0 \\ 0 & 0 & 1 \end{bmatrix} \end{aligned} \quad (2.43)$$

And then set

$$\rho_{xyn} = 0 \quad (2.44)$$

This can be simplified and written as:

$$\rho_{xyo} (\cos(\theta)^2 - \sin(\theta)^2) + (\rho_{xxo} - \rho_{yyo}) \sin(\theta) \cos(\theta) = 0 \quad (2.45)$$

Using the double angle identity we get:

$$\rho_{xyo} \cos(2\theta) + \frac{(\rho_{xxo} - \rho_{yyo})}{2} \sin(2\theta) = 0, \quad (2.46)$$

finally resulting in:

$$\begin{aligned} \tan(2\theta) &= \frac{-2\rho_{xyo}}{(\rho_{xxo} - \rho_{yyo})} \\ &\Downarrow \\ \theta &= \frac{1}{2} \arctan\left(\frac{-2\rho_{xyo}}{\rho_{xxo} - \rho_{yyo}}\right) = \frac{1}{2} \arctan\left(\frac{2a}{(a^2 + b^2) - 1}\right) \end{aligned} \quad (2.47)$$

This theta can then be used to find the desired properties of the new diagonal matrix.

$$\begin{aligned} \rho_{xxn} &= \cos(\theta)(\rho_{xxo} \cos(\theta) - \rho_{xyo} \sin(\theta)) \\ &\quad - \sin(\theta)(\rho_{xyo} \cos(\theta) - \rho_{yyo} \sin(\theta)) \end{aligned} \quad (2.48)$$

$$\begin{aligned} \rho_{yy n} &= \sin(\theta)(\rho_{xyo} \cos(\theta) + \rho_{xxo} \sin(\theta)) \\ &\quad + \cos(\theta)(\rho_{yyo} \cos(\theta) + \rho_{xyo} \sin(\theta)) \end{aligned}$$

2.4: Summary

This chapter has described the coordinate system transformation that assists with defining the material parameters for a given need. This has been represented generally, as well as the two specific examples of a cylindrical cloak and a dispersion and directionality domain. It can clearly be seen that this same transformation can also be made for a number of other geometries at will as well. It has also been shown that a filled density matrix can easily be turned into a diagonal matrix as well for practical production.

Chapter 3 : Computer Modeling

3.1: Derivation of the second order acoustic wave equation

As shown in Chapter 2, the characteristics of the cloak are dependent in the radial direction; however, a Cartesian coordinate system is more easily programmable for a grid finite difference method and is more intuitive. Therefore the following will show the Cartesian implementation of the wave equation with the parameters of the cloak transformed into the Cartesian system in order facilitate numerical modeling of the metamaterials. The anisotropic wave equation can be described with a density tensor and a scalar bulk modulus as demonstrated below.

We can start with the transport equations for particle velocity vector v_k and particle pressure P as demonstrated by Torrent and Sanchez-Dehesa²⁹ where k is the indices for the x and y direction of the grid. Indicial notation is used for ease of manipulation then written out for clarity.

$$\begin{aligned}
 \frac{\partial P}{\partial x_i} + \sum_k \rho_{ik} \frac{\partial v_k}{\partial t} = 0 & \quad \Rightarrow \quad \begin{aligned} \frac{\partial P}{\partial x} + \rho_{xx} \frac{\partial v_x}{\partial t} + \rho_{xy} \frac{\partial v_y}{\partial t} &= 0 \\ \frac{\partial P}{\partial y} + \rho_{yx} \frac{\partial v_x}{\partial t} + \rho_{yy} \frac{\partial v_y}{\partial t} &= 0 \end{aligned} & \quad (3.1) \\
 \sum_i \frac{\partial v_i}{\partial x_i} + \frac{1}{\kappa} \frac{\partial P}{\partial t} = 0 & \quad \Rightarrow \quad \frac{\partial v_x}{\partial x} + \frac{\partial v_y}{\partial y} + \frac{1}{\kappa} \frac{\partial P}{\partial t}
 \end{aligned}$$

From equations (3.1) we can multiply through by the inverse of the density tensor and make the following transformations. Recall in this case the density of the cloak will be spatially dependent and thus the derivative must also be taken into consideration.

$$\sum_k \frac{\partial}{\partial x_k} \left\{ \sum_i \rho_{ki}^{-1} \frac{\partial P}{\partial x_i} + \frac{\partial v_k}{\partial t} \right\} = 0 \quad (3.3)$$

$$\Rightarrow \sum_k \sum_i \frac{\partial \rho_{ki}^{-1}}{\partial x_k} \frac{\partial P}{\partial x_i} + \sum_k \sum_i \rho_{ki}^{-1} \frac{\partial^2 P}{\partial x_k \partial x_i} + \frac{\partial}{\partial t} \sum_k \frac{\partial}{\partial x_k} v_k = 0$$

$$\Rightarrow \sum_k \sum_i \frac{\partial \rho_{ki}^{-1}}{\partial x_k} \frac{\partial P}{\partial x_i} + \sum_k \sum_i \rho_{ki}^{-1} \frac{\partial^2 P}{\partial x_k \partial x_i} - \frac{\partial^2 P}{\partial t^2} = 0$$

This can be written out as the following:

$$\Rightarrow \frac{\partial}{\partial x} \left[\rho_{xx}^{-1} \frac{\partial P}{\partial x} + \rho_{xy}^{-1} \frac{\partial P}{\partial y} \right] + \frac{\partial}{\partial y} \left[\rho_{yx}^{-1} \frac{\partial P}{\partial x} + \rho_{yy}^{-1} \frac{\partial P}{\partial y} \right] - \frac{1}{\kappa} \frac{\partial^2 P}{\partial t^2} = 0 \quad (3.4)$$

$$\Rightarrow \rho_{xx}^{-1} \frac{\partial^2 P}{\partial x^2} + \frac{\partial \rho_{xx}^{-1}}{\partial x} \frac{\partial P}{\partial x} + \rho_{xy}^{-1} \frac{\partial^2 P}{\partial x \partial y} + \frac{\partial \rho_{xy}^{-1}}{\partial x} \frac{\partial P}{\partial y} + \rho_{yx}^{-1} \frac{\partial^2 P}{\partial y \partial x} + \frac{\partial \rho_{yx}^{-1}}{\partial y} \frac{\partial P}{\partial x} + \rho_{yy}^{-1} \frac{\partial^2 P}{\partial y^2} + \frac{\partial \rho_{yy}^{-1}}{\partial y} \frac{\partial P}{\partial y} = \frac{1}{\kappa} \frac{\partial^2 P}{\partial t^2}$$

$$\Rightarrow \boxed{\rho_{xx}^{-1} \frac{\partial^2 P}{\partial x^2} + 2\rho_{xy}^{-1} \frac{\partial^2 P}{\partial x \partial y} + \rho_{yy}^{-1} \frac{\partial^2 P}{\partial y^2} + \left(\frac{\partial \rho_{xx}^{-1}}{\partial x} + \frac{\partial \rho_{yx}^{-1}}{\partial y} \right) \frac{\partial P}{\partial x} + \left(\frac{\partial \rho_{xy}^{-1}}{\partial x} + \frac{\partial \rho_{yy}^{-1}}{\partial y} \right) \frac{\partial P}{\partial y} = \frac{1}{\kappa} \frac{\partial^2 P}{\partial t^2}}$$

where ρ_{xx}^{-1} , ρ_{xy}^{-1} , ρ_{yx}^{-1} , and ρ_{yy}^{-1} are elements of matrix $\rho_{ki}^{-1} = \begin{bmatrix} \rho_{xx}^{-1} & \rho_{xy}^{-1} \\ \rho_{yx}^{-1} & \rho_{yy}^{-1} \end{bmatrix}$

This leads to the necessary transformation of the characteristic properties from polar to Cartesian coordinates. Auld³⁸ shows that a simple rotation of the density tensor can be utilized to accomplish this as displayed in Figure 3.1.

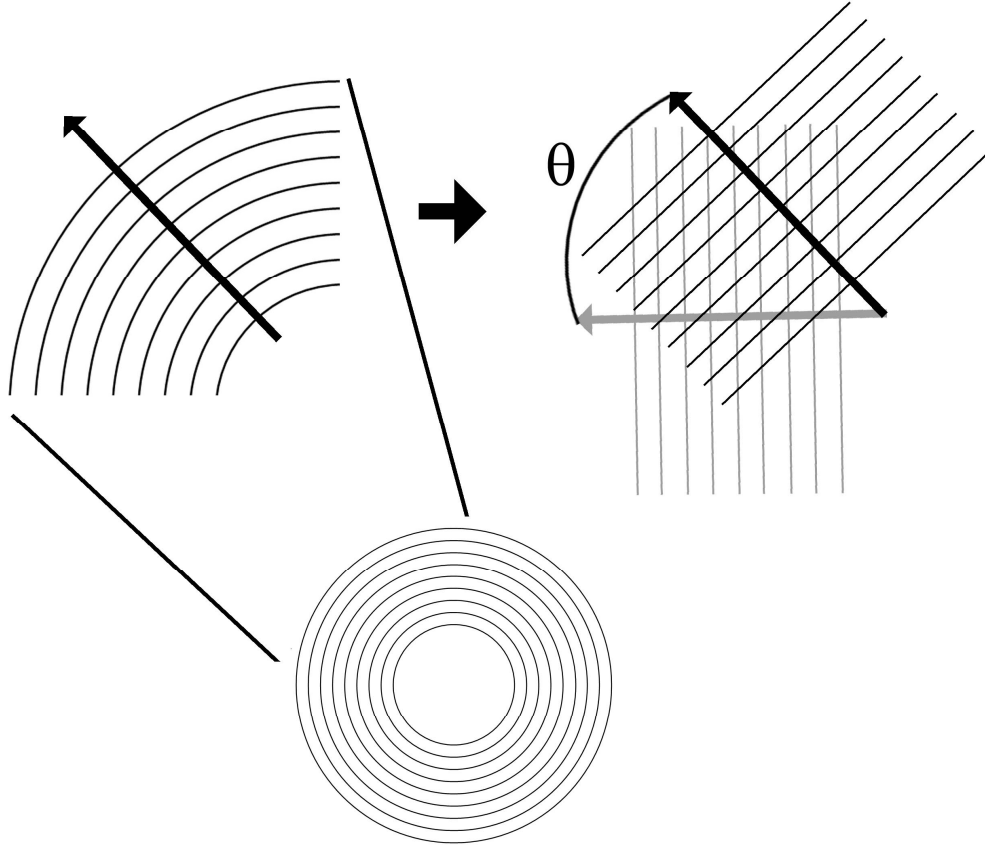


Figure 3.1: Conceptualization for a rotation of the density matrix to give equivalent values of polar properties in Cartesian coordinates.

For a counter clockwise rotation of the coordinate system (or clockwise rotation of the material), the transformation matrix in two dimensions can be described as:

$$\mathbf{R} = \begin{bmatrix} \cos(\theta) & -\sin(\theta) \\ \sin(\theta) & \cos(\theta) \end{bmatrix} \quad (3.4)$$

$$\text{The polar density matrix: } \boldsymbol{\rho} = \begin{bmatrix} \rho_r & 0 \\ 0 & \rho_\theta \end{bmatrix} \quad (3.5)$$

$$\text{and the rotated Cartesian density tensor: } \boldsymbol{\rho}' = \begin{bmatrix} \rho_{xx} & \rho_{xy} \\ \rho_{yx} & \rho_{yy} \end{bmatrix} \quad (3.6)$$

Therefore the coordinate rotation $\boldsymbol{\rho}' = \mathbf{R}\boldsymbol{\rho}\mathbf{R}^T$ is described as:

$$\begin{aligned}
\begin{bmatrix} \rho_{xx} & \rho_{xy} \\ \rho_{yx} & \rho_{yy} \end{bmatrix} &= \begin{bmatrix} \cos(\theta) & -\sin(\theta) \\ \sin(\theta) & \cos(\theta) \end{bmatrix} \cdot \begin{bmatrix} \rho_r & 0 \\ 0 & \rho_\theta \end{bmatrix} \cdot \begin{bmatrix} \cos(\theta) & \sin(\theta) \\ -\sin(\theta) & \cos(\theta) \end{bmatrix} \\
&= \begin{bmatrix} \rho_r \cos(\theta)^2 + \rho_\theta \sin(\theta)^2 & (\rho_r - \rho_\theta) \sin(\theta) \cos(\theta) \\ (\rho_r - \rho_\theta) \sin(\theta) \cos(\theta) & \rho_r \sin(\theta)^2 + \rho_\theta \cos(\theta)^2 \end{bmatrix}
\end{aligned} \tag{3.7}$$

Substituting the definitions for ρ_r and ρ_θ we get:

$$\rho_{xx}(x, y) = \rho_0 \frac{r}{r - R_1} \cos(\theta)^2 + \rho_0 \frac{r - R_1}{r} \sin(\theta)^2 \tag{3.8}$$

$$\rho_{yy}(x, y) = \rho_0 \frac{r}{r - R_1} \sin(\theta) + \rho_0 \frac{r - R_1}{r} \cos(\theta)^2$$

$$\rho_{xy}(x, y) = \left(\rho_0 \frac{r}{r - R_1} - \rho_0 \frac{r - R_1}{r} \right) \sin(\theta) \cos(\theta) = \rho_0 \left(\frac{r^2 - r^2 - rR_1 - R_1^2}{r^2 - rR_1} \right) \sin(\theta) \cos(\theta)$$

Where the coordinate transformation defines r and θ as:

$$r = \sqrt{x^2 + y^2} \quad \theta = \begin{cases} \arcsin \frac{y}{r} & \text{if } x \geq 0 \\ -\arcsin \frac{y}{r} + \pi & \text{if } x < 0 \end{cases} \tag{3.9}$$

The inverse can then be taken as:

$$\begin{bmatrix} \rho_{xx}^{-1} & \rho_{xy}^{-1} \\ \rho_{yx}^{-1} & \rho_{yy}^{-1} \end{bmatrix} = \begin{bmatrix} \frac{\rho_{yy}}{\det(\rho')} & \frac{-\rho_{xy}}{\det(\rho')} \\ \frac{-\rho_{yx}}{\det(\rho')} & \frac{\rho_{xx}}{\det(\rho')} \end{bmatrix} \tag{3.10}$$

3.1.1: Acoustic reflection to the cloak

As a sanity check one can look at possibility of reflection from the cloak. Acoustic reflection is a result of a mismatch of acoustic impedance and the acoustic impedance of a medium is defined as the product of the density and the speed of sound through the medium.

$$Z = \rho \cdot c \quad \text{where the speed of sound is:} \quad c = \sqrt{\frac{\kappa}{\rho}} \quad (3.11)$$

Here we can define the density and bulk modulus of the medium as κ_0 and ρ_0 respectively. Since any waves entering the cloak will be introduced in the radial direction, the pertinent properties of the cloak are defined as the following as previously described.

$$\rho_r = \frac{r}{r - R_1} \rho_0 \quad \kappa = \left(\frac{R_2 - R_1}{R_2} \right)^2 \frac{r}{r - R_1} \kappa_0 \quad (3.12)$$

The speed of sound for medium (m) and the outer boundary of the shell (obs) is calculated below

$$c_m = \sqrt{\frac{\kappa_0}{\rho_0}}, \quad c_{obs} = \sqrt{\kappa \frac{\rho_\theta}{\det \mathbf{p}}} = \sqrt{\frac{\left(\frac{R_2 - R_1}{R_2} \right)^2 \frac{r}{r - R_1} \kappa_0}{\frac{r}{r - R_1} \rho_0}} = \frac{R_2 - R_1}{R_2} \sqrt{\frac{\kappa_0}{\rho_0}} \quad (3.13)$$

Therefore, the impedances of the medium and outer boundary of the shell are

$$\begin{aligned}
Z_m &= \rho_0 \cdot c_m = \rho_0 \sqrt{\frac{\kappa_0}{\rho_0}} = \sqrt{\rho_0 \kappa_0} \\
Z_{obs} &= \frac{R_2}{R_2 - R_1} \rho_0 \cdot \frac{R_2 - R_1}{R_2} \sqrt{\frac{\kappa_0}{\rho_0}} = \sqrt{\rho_0 \kappa_0} = Z_m
\end{aligned}
\tag{3.13}$$

which are equal, thus avoiding reflections for the continuous form of the wave equation.

3.2: Implementation into Finite Difference

The Finite Difference Method (FDM) is a numerical method in which solutions to differential equations are approximated by discretizing a function space and using weighted sums of neighboring points to solve for the approximation. The finite difference method can be found in both the time domain (FDTD) and the frequency domain (FDFD).

One of the first papers to apply the finite difference method to the wave equation is Yee³⁹ in 1966. His paper based on Maxwell's equations spurred a number of others in the same field of electromagnetic (EM) waves. Taflove and Brodwin⁴⁰ in 1975 defined numerical stability for Yee's algorithm. Taflove first coined the term "Finite Difference Time Domain" in their paper in 1980⁴¹. In 2000 Sullivan published a book on EM simulation using FDTD⁴².

3.2.1: Stability

Courant-Friedrichs-Lewy (CFL) condition is a popular stability condition used in finite difference implementation of partial differential equations. Richard Courant, Kurt Friedrichs, and Hans Lewy first introduced this condition in their paper⁴³ in 1928. The condition presented is a *necessary* condition which basically point out that the information propagation in finite difference cannot be faster than the physical speed of the information in reality.

The CFL condition is defined as $\frac{c\Delta t}{h} \leq N$ where c is the speed (of sound for the acoustic case), Δt is the time step, h is spatial interval, and N is a number dependent on the dimensionality of the equation. In this 2D wave equation where $h = \Delta x = \Delta y$, the CFL condition is

$$\max\left(\frac{c\Delta t}{h}\right) \leq \frac{1}{\sqrt{3}} \text{ since } c \text{ varies spatially.} \quad (3.14)$$

Von Neumann stability uses the Fourier transform of numerical error to determine if the error from each iteration will compound to cause the finite difference method to become unstable. Like the CFL method, the stability analysis is necessary but it can additionally be a sufficient condition as well for certain circumstances. The Von Neumann method is often used even when its application is not “*fully justified*”, in the words of Smith⁴⁴, because it’s simplicity and useful results.

The condition for Von Neumann stability requires that the absolute value of the growth factor G for the finite difference equation to be less than or equal to one ($|G| \leq 1$).

From the second order wave equation we get $G = \frac{b \pm \sqrt{b^2 - 4}}{2}$ (3.14)

where

$$b = -2 + \kappa \Delta t^2 \left(\frac{4\rho_{xx}^{-1}}{\Delta x^2} \sin^2\left(\frac{k\Delta x}{2}\right) + \frac{4\rho_{yy}^{-1}}{\Delta y^2} \sin^2\left(\frac{l\Delta y}{2}\right) + \frac{2\rho_{xy}^{-1}}{\Delta x \Delta y} \sin(k\Delta x) \sin(l\Delta y) \right. \\ \left. - \left(\frac{\partial \rho_{xx}^{-1}}{\partial x} + \frac{\partial \rho_{yx}^{-1}}{\partial y} \right) \frac{i \sin(k\Delta x)}{\Delta x} - \left(\frac{\partial \rho_{xy}^{-1}}{\partial x} + \frac{\partial \rho_{yy}^{-1}}{\partial y} \right) \frac{i \sin(l\Delta y)}{\Delta y} \right) \quad (3.15)$$

and where stability occurs if $0 \leq |b| \leq 2$. See Appendix II for derivation and details.

3.2.2: Boundary Conditions

Because computer memory and ability is finite, it is necessary to create a boundary condition on the finite discrete domain to emulate infinite medium. This is often referred to as an absorbing boundary condition (ABC) as a reflection to it ability to absorb energy in boundary bound wave and prevent reflection back into the pertinent region of the medium. The difficulty in this is that any change in medium properties causes reflection in itself. Earliest attempts at ABCs required large regions for the ABC layers so that their absorbing properties could be ramped up slowly. Engquist and Majda⁴⁵ and Clayton and Engquist^{46,47} are noted papers of ABCs in acoustic and elastic waves using paraxial approximations to separate the outward moving wave field from the inward moving one and thus reduce reflections. A paper by Mur⁴⁸ described the first numerically stable absorbing boundary condition for finite difference simulation of EM waves as shown in Figure 3.2.

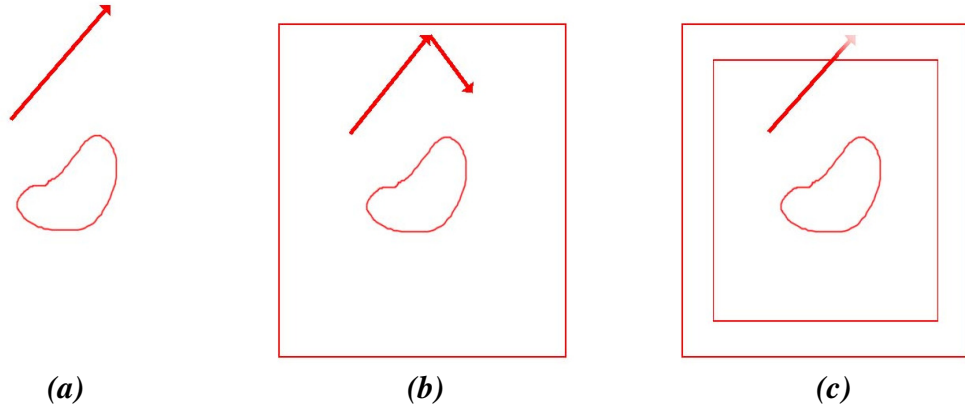


Figure 3.2: Boundary Conditions for (a) Infinite Medium (b) Finite Medium with no defined boundary conditions (c) Finite medium with absorbing boundary conditions

The above methods all looked at conditions necessary to create a transparent boundary, however, Jean-Pierre Berenger^{49,50} took a different approach to create a perfectly matched layers (PML) for electromagnetic waves which match impedance with the medium to avoid reflectance, but dissipate energy in the imaginary domain. Taking that the solution to the wave equation can be written in the form of

$$p(x) = p_0 e^{-ikx} . \quad (3.16)$$

Redefining solution to

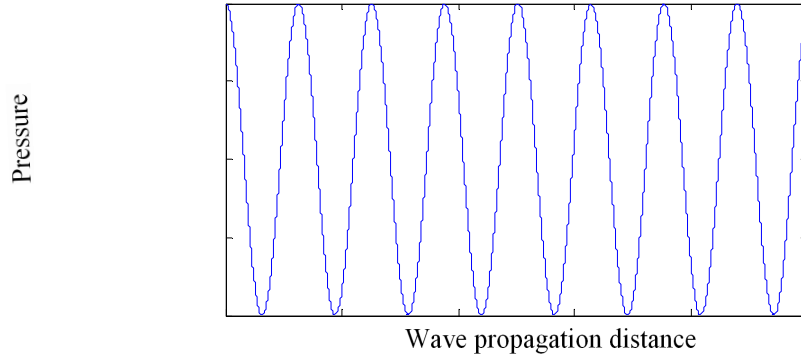
$$p(x) = p_0 e^{-ikx} e^{-\frac{k}{\omega}\Gamma(x)} \quad (3.17)$$

would result in a decaying wave. This, in turn, can be written as

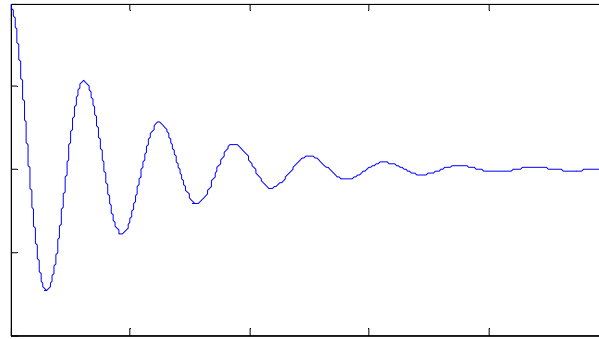
$$p(x) = p_0 e^{-ik(x + \frac{\Gamma(x)}{i\omega})} . \quad (3.18)$$

Comparing this to the original solution, Figure 3.3 shows that implementing this into the wave equations becomes simply a matter of a change in coordinate systems where the new

$$\tilde{x} = x + \frac{\Gamma(x)}{i\omega} \quad \text{or} \quad \frac{d\tilde{x}}{dx} = 1 + \frac{1}{i\omega} \frac{d\Gamma(x)}{dx} = 1 + \frac{\sigma(x)}{i\omega}. \quad (3.19)$$



(a)



Wave propagation distance

(b)

Figure 3.3: Effect of PML boundary condition on wave (a) propagation cross section through a normal system (b) propagation cross section showing absorption through a perfectly matched layer

Other papers following Berenger's expanded the application of the PML to acoustic and elastic waves Chew and Liu⁵¹ and Hu⁵², Liu and Tao⁵³, Li⁵⁴, Zheng and Huang⁵⁵, and Komatitsch, D. and Tromp⁵⁶, of which Chew and Liu and Hu are among the earliest. Variations on PML were also developed such as the convolution PML (CPML) Roden and Gedney⁵⁷ and the nearly perfectly matched layer NPML Cumber⁵⁸. Papers

by Berenger⁵⁹, Hu and Cummer⁶⁰, Chen and Bording⁶¹, and Chen, Zheng, and Bording⁶² are a few examples that give comparisons between the variations of the layers.

The approach taken here is based on a paper by Xing Li⁵⁴ who treated the derivation of the PML as a stretch of the coordinate system. This was done by a change of coordinates such that $\tilde{x} = x - i\gamma$ and $\tilde{y} = y - i\gamma$ where γ must be differentiable.

Defining $\gamma = \frac{1}{\omega} \int_0^{x_i} \sigma(s) ds$ the change of coordinates becomes:

$$\tilde{x}_i = x_i - \frac{i}{\omega} \int_0^{x_i} \sigma(s) ds \quad (3.20)$$

where $x_i = x$ and y for two dimensions and σ is some weight profile for the damping across the PML layer which gradually increases to reduce numeric reflection.

After differentiating, the coordinate transformation can be written as:

$$\frac{\partial}{\partial \tilde{x}_i} = \frac{i\omega}{i\omega + \sigma(x_i)} \frac{\partial}{\partial x_i} \quad \text{or} \quad \frac{\partial}{\partial \tilde{x}_i} = \frac{1}{\xi_i} \frac{\partial}{\partial x_i} \quad \text{where} \quad \xi_i = 1 + \frac{\sigma(x_i)}{i\omega} \quad (3.21)$$

The analytical coordinate transformation is made in both direction but the application of the weight profile only occurs on the edges of the map as needed. In a Cartesian coordinate system, the PML layer is divided into eight regions of three distinct types as displayed in Figure 3.4. The areas on the limits in the x direction with no overlap with the y limits, which we'll call region 1, only have the x coordinates transformed. The opposite applied for the limits of the y direction, region 2. The corners of the map, region 3, have both coordinates transformed. Areas where the coordinate transformation is not applied have the respective σ weight set to zero returning the coordinate stretching in that dimension back to normal.

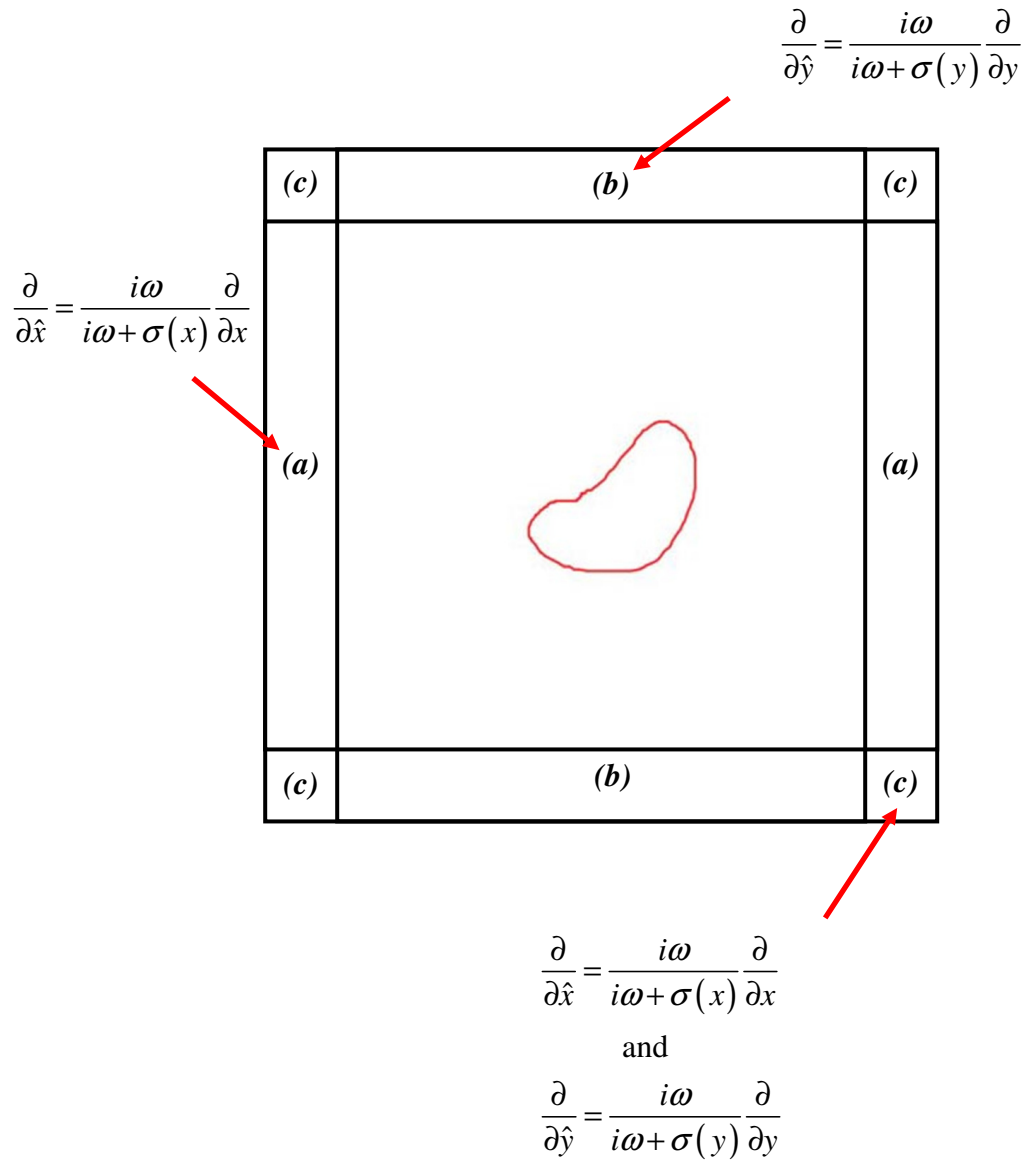


Figure 3.4: PML boundary conditions on field where domains (a), (b), and (c) represent changes in coordinate systems in the x direction, y direction, and both the x and y directions respectively

For the coordinate transformation we'll start with the wave equation with variable density written in the frequency domain. Since the PML layer exists only in the scalar fluid medium, off axis terms will be eliminated and $\rho_{xx}^{-1} = \rho_{yy}^{-1}$.

$$\begin{aligned} \rho_{xx}^{-1} \frac{\partial}{\partial \tilde{x}} \frac{\partial}{\partial \tilde{x}} P + 2\rho_{xy}^{-1} \frac{\partial}{\partial \tilde{x}} \frac{\partial}{\partial \tilde{y}} P + \rho_{yy}^{-1} \frac{\partial}{\partial \tilde{y}} \frac{\partial}{\partial \tilde{y}} P \\ + \left(\frac{\partial}{\partial \tilde{x}} \rho_{xx}^{-1} + \frac{\partial}{\partial \tilde{y}} \rho_{yx}^{-1} \right) \frac{\partial}{\partial \tilde{x}} P + \left(\frac{\partial}{\partial \tilde{x}} \rho_{xy}^{-1} + \frac{\partial}{\partial \tilde{y}} \rho_{yy}^{-1} \right) \frac{\partial}{\partial \tilde{y}} P = \frac{(i\omega)^2}{\kappa} P \end{aligned} \quad (3.22)$$

Now we introduce the change of coordinates which results in the following:

$$\frac{(i\omega)^2}{\kappa} P = \rho_{xx}^{-1} \frac{1}{\xi_x} \frac{\partial}{\partial x} \left(\frac{1}{\xi_x} \frac{\partial}{\partial x} \right) P + \rho_{yy}^{-1} \frac{1}{\xi_y} \frac{\partial}{\partial y} \left(\frac{1}{\xi_y} \frac{\partial}{\partial y} \right) P \quad (3.24)$$

Using the product rule of differentiation, we get:

$$\frac{(i\omega)^2}{\kappa} P = \rho_{xx}^{-1} \frac{1}{\xi_x^2} \frac{\partial}{\partial x^2} P + \rho_{xx}^{-1} \frac{1}{\xi_x} \frac{\partial \xi_x^{-1}}{\partial x} \frac{\partial}{\partial x} P + \rho_{yy}^{-1} \frac{1}{\xi_y^2} \frac{\partial}{\partial y^2} P + \rho_{yy}^{-1} \frac{1}{\xi_y} \frac{\partial \xi_y^{-1}}{\partial y} \frac{\partial}{\partial y} P \quad (3.25)$$

Now let $P = P_1 + P_2 + P_3 + P_4$ such that

$$\begin{aligned} \frac{(i\omega)^2}{\kappa} (P_1 + P_2 + P_3 + P_4) = \\ \rho_{xx}^{-1} \frac{1}{\xi_x^2} \frac{\partial}{\partial x^2} P + \rho_{xx}^{-1} \frac{1}{\xi_x} \frac{\partial \xi_x^{-1}}{\partial x} \frac{\partial}{\partial x} P + \rho_{yy}^{-1} \frac{1}{\xi_y^2} \frac{\partial}{\partial y^2} P + \rho_{yy}^{-1} \frac{1}{\xi_y} \frac{\partial \xi_y^{-1}}{\partial y} \frac{\partial}{\partial y} P \end{aligned} \quad (3.26)$$

From here on, the derivation will be done in the x direction, but the same is done in the y direction as well. Let P_1 and P_2 correspond to the first to x terms so that:

$$\begin{aligned} \frac{-\omega^2}{\kappa} P_1 = \rho_{xx}^{-1} \frac{1}{\left(1 + \frac{\sigma(x)}{i\omega}\right)^2} \frac{\partial P}{\partial x^2} \\ \frac{-\omega^2}{\kappa} P_2 = \rho_{xx}^{-1} \frac{1}{\left(1 + \frac{\sigma(x)}{i\omega}\right)} \frac{-\frac{1}{i\omega} \sigma'(x)}{\left(1 + \frac{\sigma(x)}{i\omega}\right)^2} \frac{\partial P}{\partial x} \end{aligned} \quad (3.27)$$

This can be rewritten as:

$$\left(1 + \frac{\sigma(x)}{i\omega}\right)^2 \frac{-\omega^2}{\kappa} P_1 = \rho_{xx}^{-1} \frac{\partial P}{\partial x^2}$$

and

$$\left(1 + \frac{\sigma(x)}{i\omega}\right)^3 \frac{(i\omega)^3}{\kappa} P_2 = \rho_{xx}^{-1} \sigma'(x) \frac{\partial P}{\partial x}$$
(3.28)

Taking the inverse Laplace transform results in:

$$\left(\frac{\partial}{\partial t} + \sigma(x)\right)^2 P_1 = \kappa \rho_{xx}^{-1} \frac{\partial P}{\partial x^2}$$
(3.29)

$$\left(\frac{\partial}{\partial t} + \sigma(x)\right)^3 P_2 = -\kappa \rho_{xx}^{-1} \sigma'(x) \frac{\partial P}{\partial x}$$

Since the second equation above will result in a third order time term, we'll make a substitution of variables $\zeta_1 = \left(\frac{\partial}{\partial t} + \sigma(x)\right) P_2$ resulting in the following.

$$\left(\frac{\partial}{\partial t} + \sigma(x)\right)^2 \zeta_2 = -\kappa \rho_{xx}^{-1} \sigma'(x) \frac{\partial P}{\partial x}$$
(3.30)

Now let us define the dampening profile

$$\sigma(x) = \frac{\kappa}{\rho\tau} \log\left(\frac{1}{R}\right) \left(\frac{x}{\tau}\right)^2$$

where R is the reflectance and τ is the thickness of the PML layer. The only remaining step is to do the same for the variables in the y direction and discretize the equation for use with the FDTD method. The discretization can be found in Appendix III.

3.3: Numeric Results

The initial numerical model made was created using the commercial finite element package, COMSOL Multiphysics Finite Element Analysis Software as used by Cummer *et al.*¹⁷ in simulations exploring electromagnetic cloaks. This formed the initial basis of comparison for results when creating the FDTD model from scratch. Using a normalized density and bulk modulus and setting the R_1 and R_2 values to 1.5 and 3 respectively, values were taken along the x direction at $y=0$ such that the properties in the x and y direction are equal to those in the radial and tangential respectively and off-diagonal values are zero. The density values for this cross section are as shown in Figure 3.5.

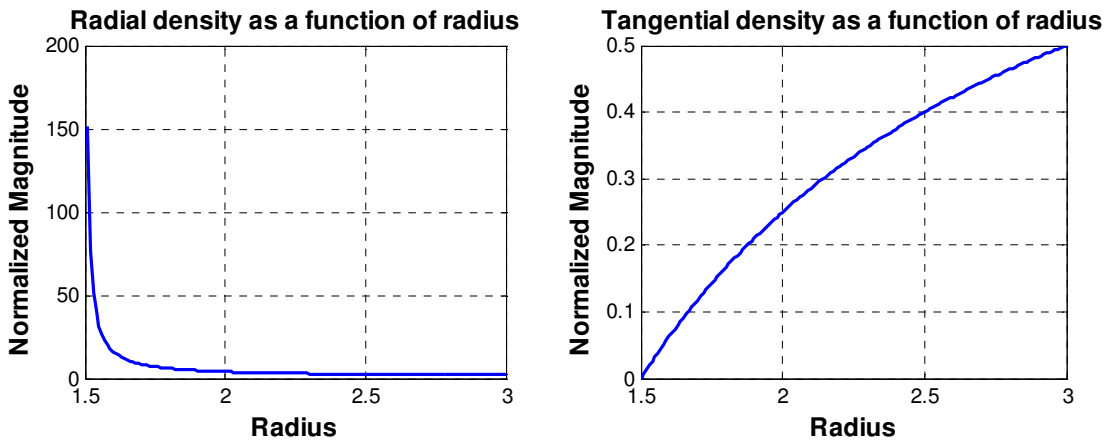


Figure 3.5: Density cross section

and the resulting bulk modulus profile is as shown in Figure 3.6.

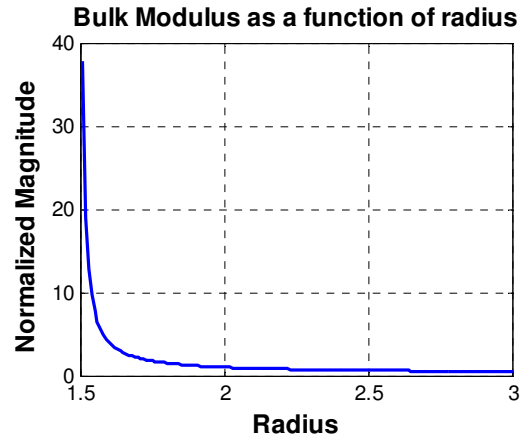


Figure 3.6: Bulk modulus cross section

This results in the anisotropic speeds of sound shown in Figure 3.7.

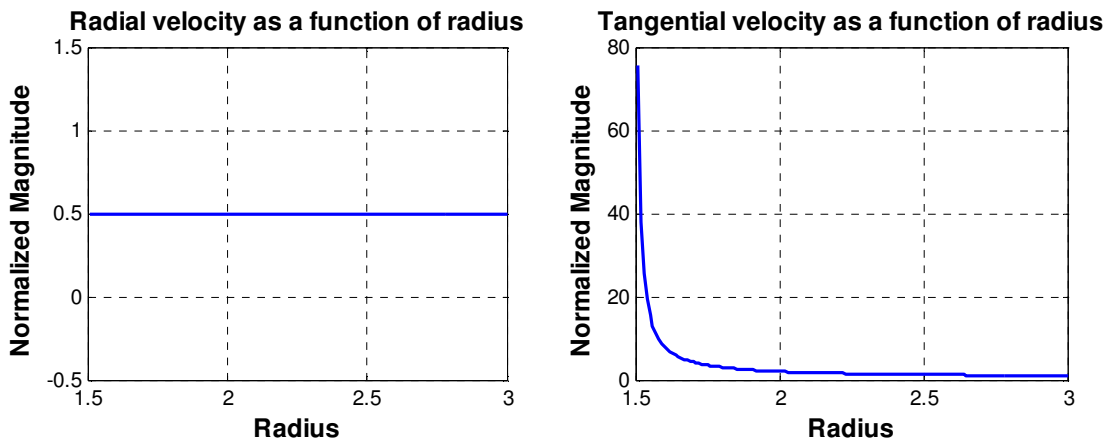
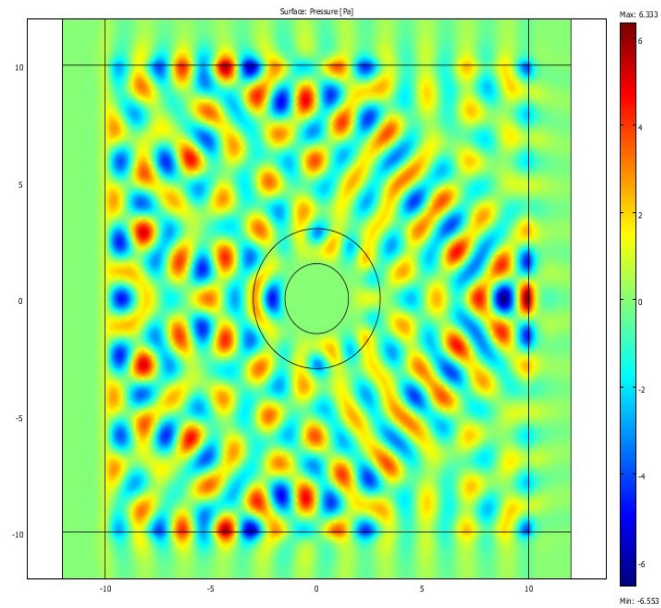


Figure 3.7: Anisotropic speed of sound: radial (left) and tangential (right)

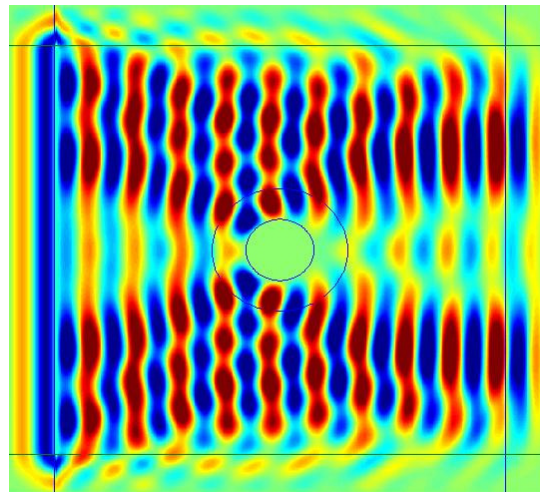
With material properties of the custom made FDTD model agreeing with the commercial FEM model we continue to compare pressure output. However, the asymptotically increasing material values are chopped off in the FDTD model to satisfy the aforementioned stability requirements while still retaining two orders of magnitude of change.

3.3.1: Cloak with Line Source

The first scenario is a repetition of the popular plane wave source used in a number of the previously cited papers. The amplitude used in the model is 1 and frequency is 0.5Hz.



(a)

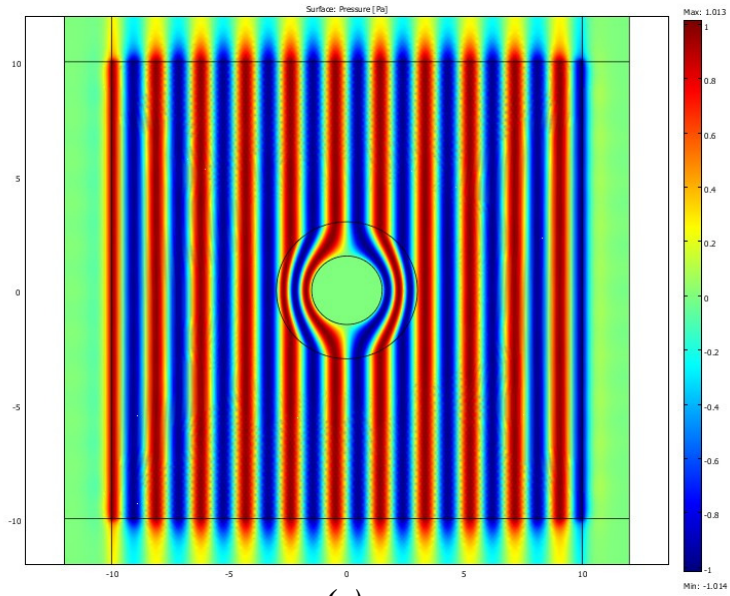


(b)

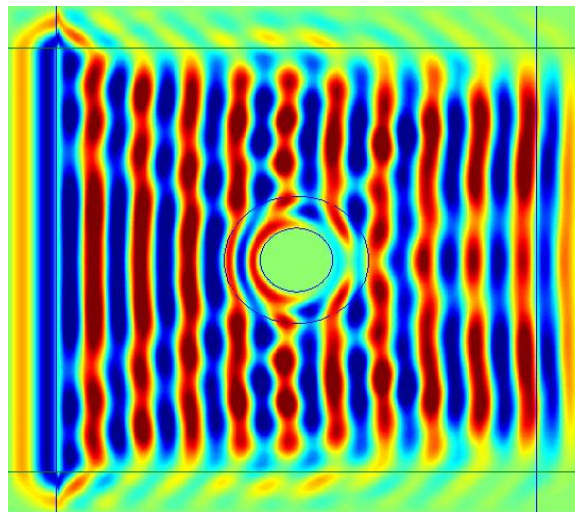
Figure 3.8: Line source from left on a cylinder with Dirichelet boundary conditions for (a) COMSOL FEM and (b) the Custom FDTD model

Above lies one of the advantages of the FDTD method. The COMSOL results are shown in Figure 3.8. On the left is shown what almost looks like a random scattering of pressures throughout the field. Though the only still image can be presented in this paper, the FDTD image on the right is only the last frame of the progression of the wave through the field domain. This progression can be viewed in its entirety to study how the wave moves through this field.

The next set of images however, shown in Figure 3.9 emphasize the disadvantage of FDTD. COMSOL uses variable meshes to calculate the field. This allows a very fine mesh at the boundaries as well as allowing nodes to occur on the boundary itself. The FDTD used in the model, however, has a set grid mesh throughout the system. This causes the material parameters exactly at the boundary to be often skipped over. The result is that the acoustic impedances near the boundary don't exactly match, which results in reflections. This can be diminished with a finer mesh, but a finer meshed is practically limited by memory and computation time.



(a)



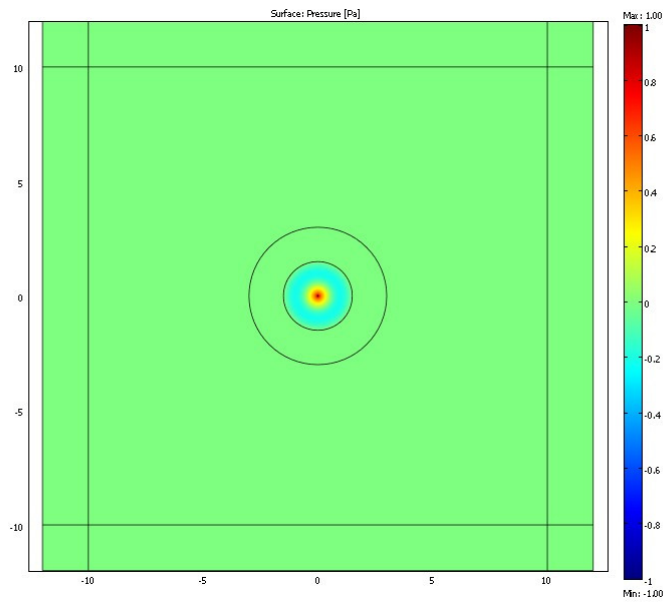
(b)

Figure 3.9: Line source from left on above cylinder with addition of cloak layer for (a) COMSOL FEM and (b) the Custom FDTD model

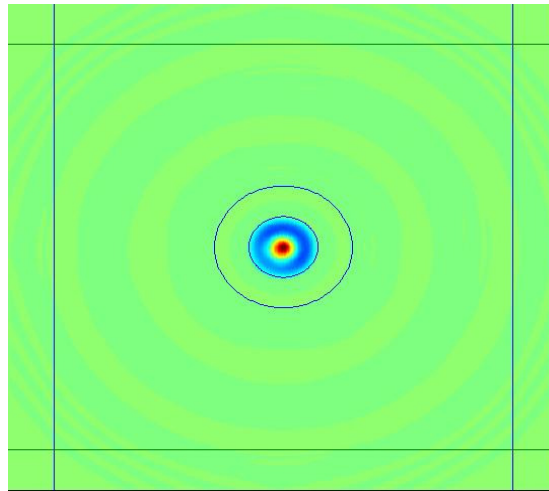
Aside from the slight reflection at the boundary on the cloak, one can still see the benefit of the cloak on both the forward scatter and back scatter as compared to the shell without the cloak.

3.3.2: Cloak with Internal Source

The design of this cloak was based on a transformation of coordinates to omit part of the original space from the new coordinate system. This was verified in the numerical simulation as well by bringing the source inside the cylinder in the form of a point source as displayed in Figure 3.10.



(a)



(b)

Figure 3.10: Internal point source for (a) COMSOL FEM and (b) the Custom FDTD model

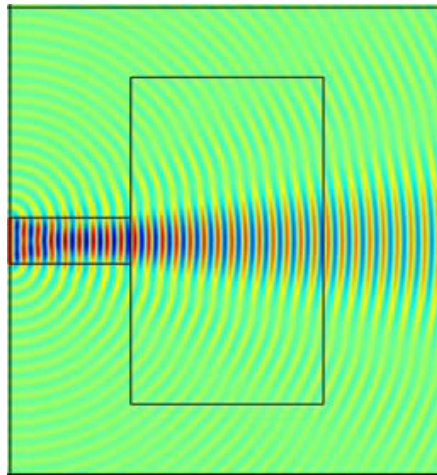
Again, the two models show a good level of agreement. It's important to note that since the sound within the cylinder has nowhere to escape, that energy will need to be dissipated through some other method not covered in this paper.

3.3.3: Directivity and Dispersion Metamaterial

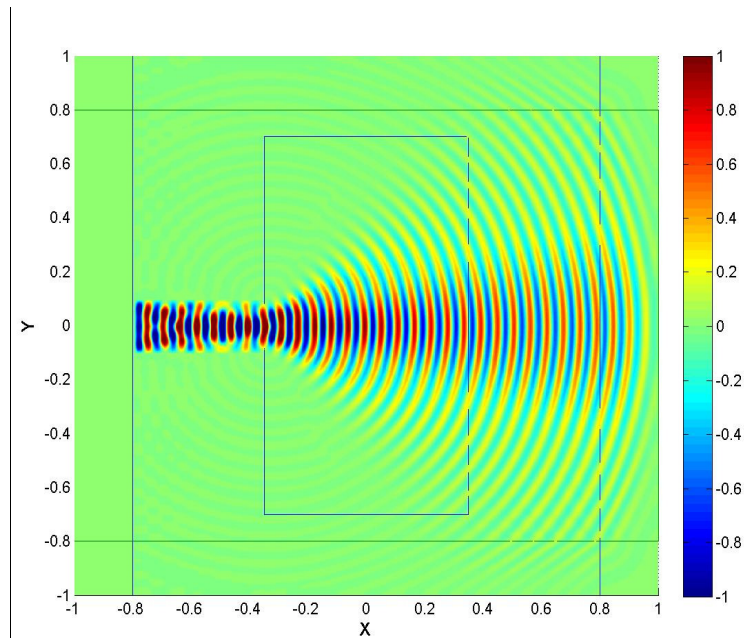
As mentioned in section (2.3), using a change of coordinate systems, a metamaterial can be designed for desired directivity and dispersion. The following are a series of results for directivity and dispersion for a set of permutations of the aforementioned “*a*” and “*b*” coefficients. The metamaterial domain is 0.7 x 1.4 with a 0.2 length line source. The input frequency of 6000Hz relative to a 343m/s speed of sound in the fluid domain for the COMSOL model which corresponds to 17.5Hz

frequency the normalized speed of sound used in the used for the nominal fluid domain in the FDTD model.

The first example shown in Figure 3.11 depicts the normal scattering through material properties that are equivalent to the surrounding media.



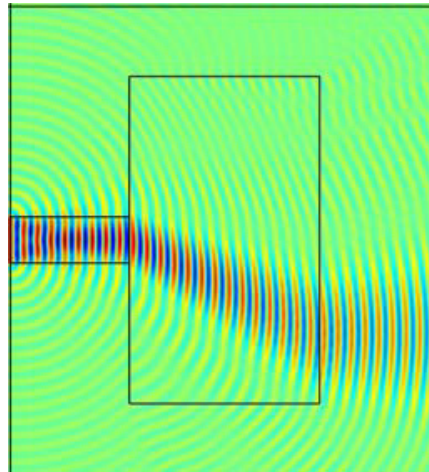
(a)



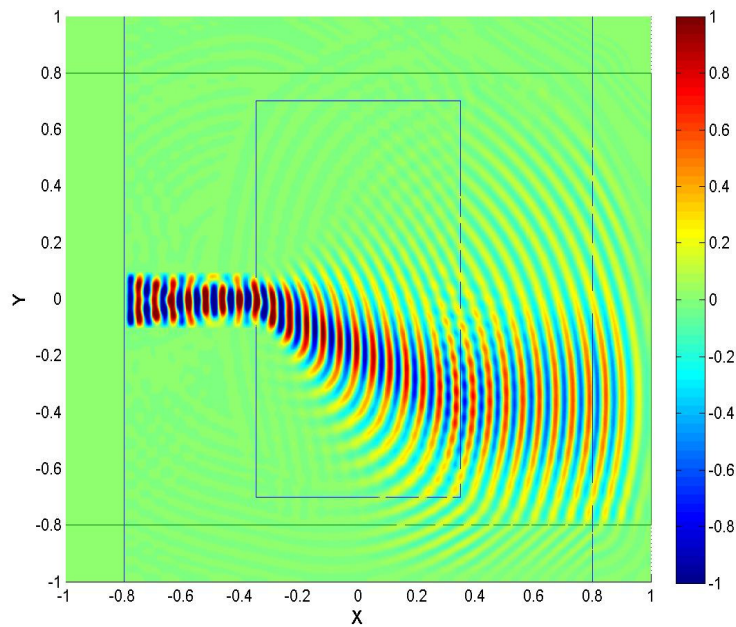
(b)

Figure 3.11: $a=0, b=1$ for (a) COMSOL FEM and (b) the Custom FDTD model

The two examples shown in Figures 3.12 and 3.13 illustrate the change in directivity by adjusting the first parameter from -0.5 to 0.5 and leaving the second parameter at 1.

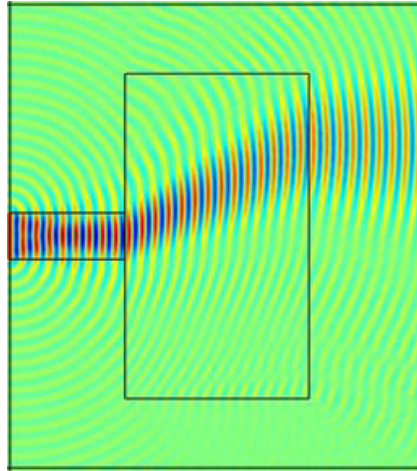


(a)

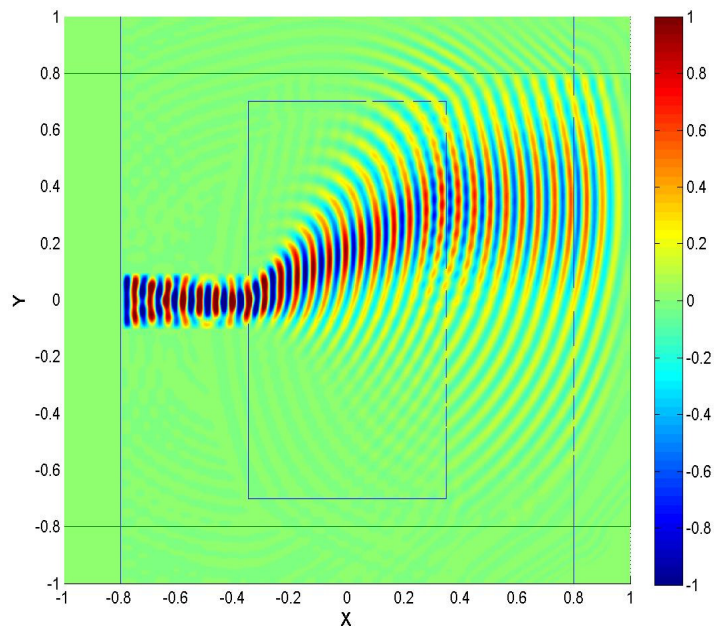


(b)

Figure 3.12: $a=-0.5$, $b=1$ for (a) COMSOL FEM and (b) the Custom FDTD model



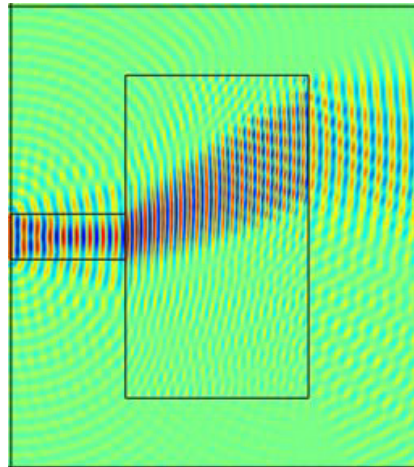
(a)



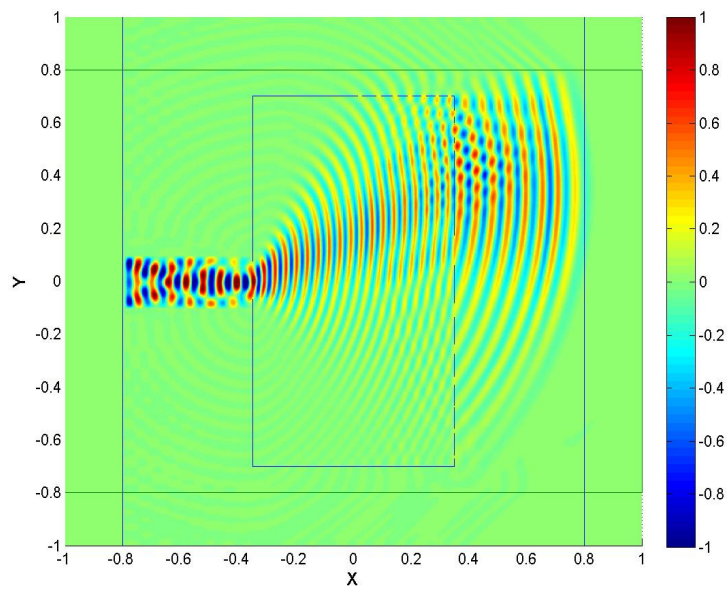
(b)

Figure 3.13: $a=0.5$, $b=1$ for (a) COMSOL FEM and (b) the Custom FDTD model

Figures 3.14 and 3.15 demonstrate the ability to change the dispersion of the wave by changing the second parameter from 0.5 to 1.5 while holding the first parameter constant.

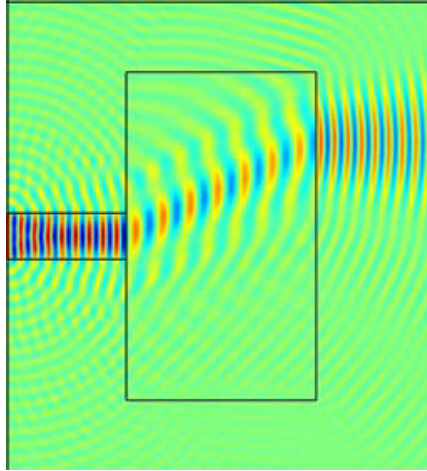


(a)

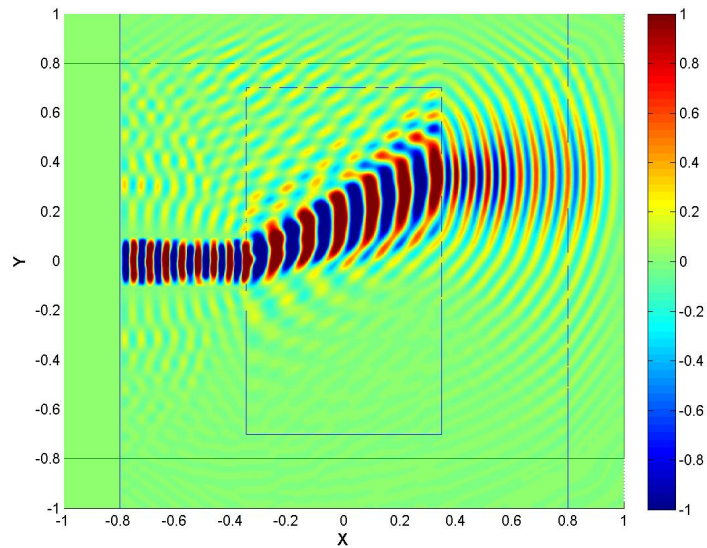


(b)

Figure 3.14: $a=0.5$, $b=1.5$ for (a) COMSOL FEM and (b) the Custom FDTD model



(a)



(b)

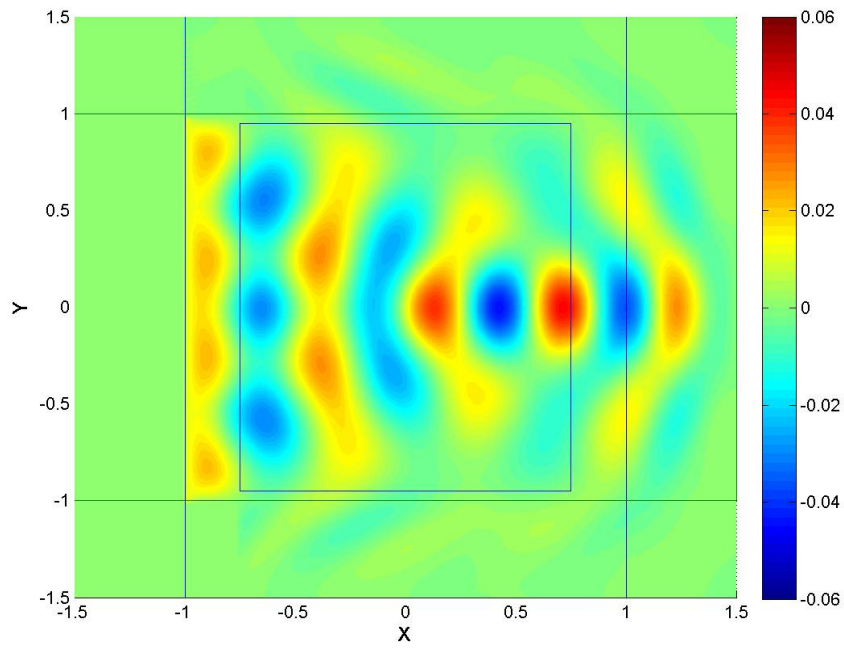
Figure 3.15: $a=0.5$, $b=0.5$ for (a) COMSOL FEM and (b) the Custom FDTD model

Now that the FDTD model has been demonstrated to hold fairly well to a commercial finite difference model, we proceed in the future just using only the custom FDTD model.

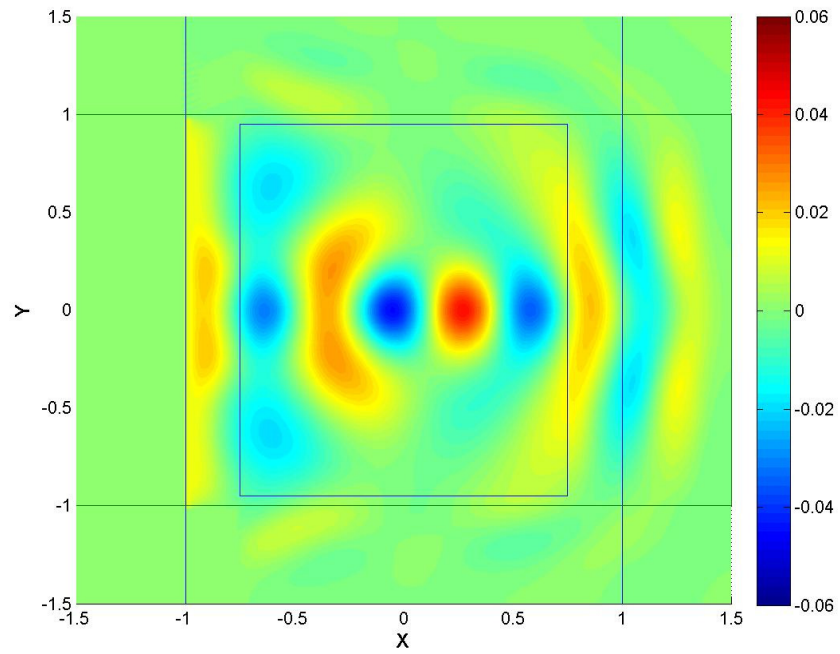
3.3.4: Velocities for Focusing Waves

Velocities in the material domain of the FDTD can also be adjusted in such a way as to focus a plane wave. Below are several examples of plane waves being focused with a varying sound velocity field which could be realized with a metamaterial. Faster sound velocities on the outside of the field turn the wave toward some point in the center of the field. Some important parameters that effect focus of the wave include the rate of increase of the sound velocity, the length of the material, and the shape of the increase in velocity. These will be changed in the following examples for comparison. As with the first cloak examples, the source is a line source from the left.

The first two set of examples, shown in Figures 3.16 and 3.17, use a linear increase in sound speed, which creates basically a “V” shaped profile. Each set of three correspond to a 1, 3, and 5 meter per second per meter increase in sound speed starting with ambient. In other words, the vertical center has ambient sound speed in all cases and linearly increases such that the sound speed one meter away in either direction, above or below, will be 1, 3, or 5 meters per second faster than the ambient. The first set has a wide material domain of 1.5x1.9.



a)



b)

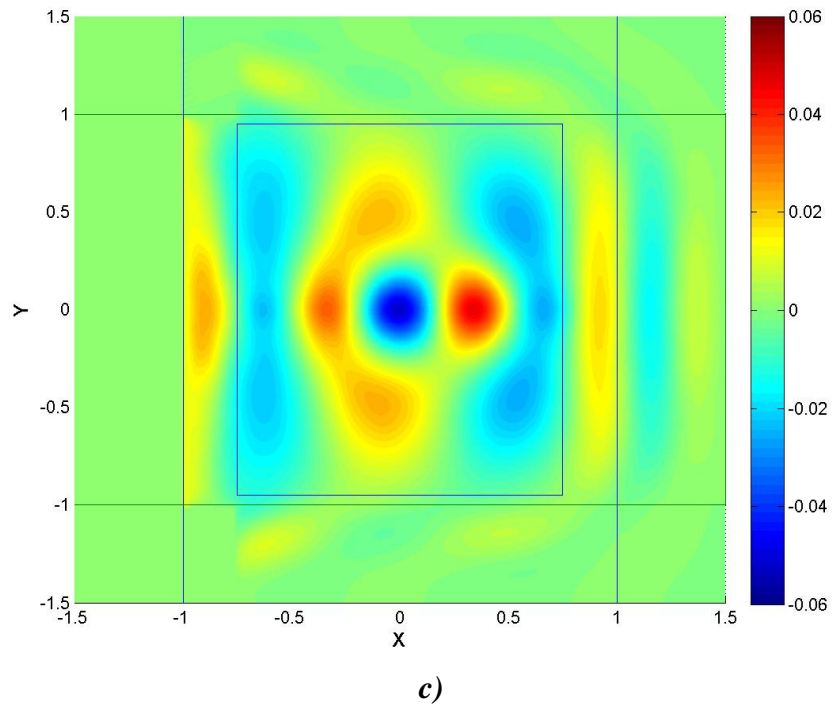
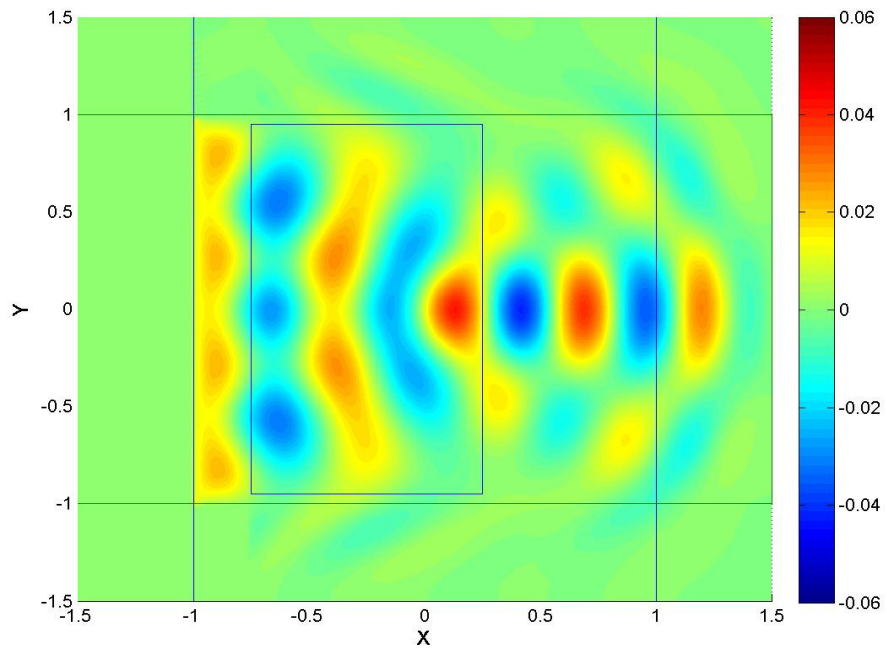
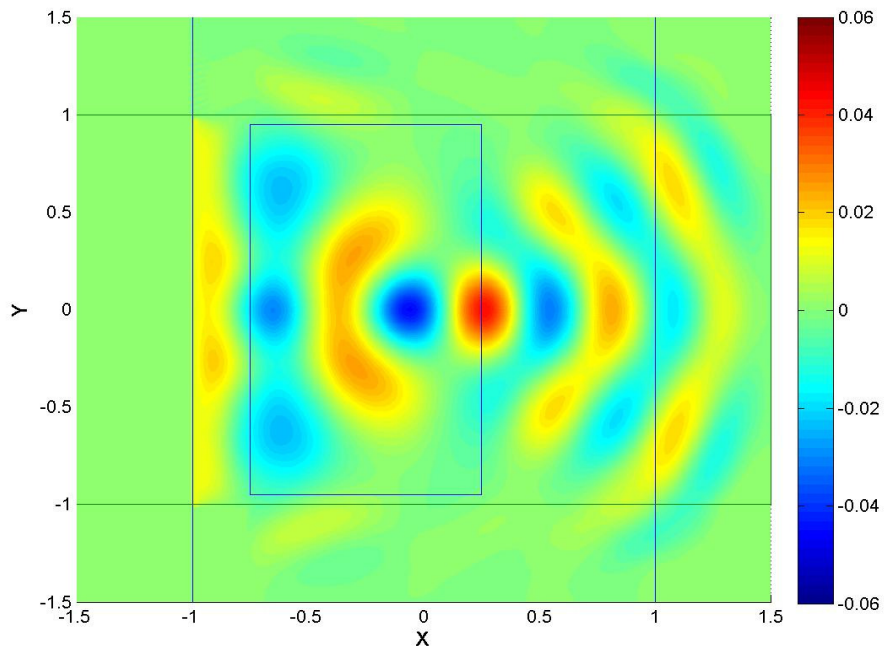


Figure 3.16: Linear increase in sound speed in a wide domain with (a), (b), and (c) corresponding to 1, 3 and 5 meters per second increase per meter respectively.

It can be seen that even in the first case, the focus point occurs well within the material domain. It can also be observed that the wave leaving the material becomes more spread out the further in the domain the focus point occurs. The next set shortens the domain to 1.0x1.9 but keeps the linear profile.



a)



b)

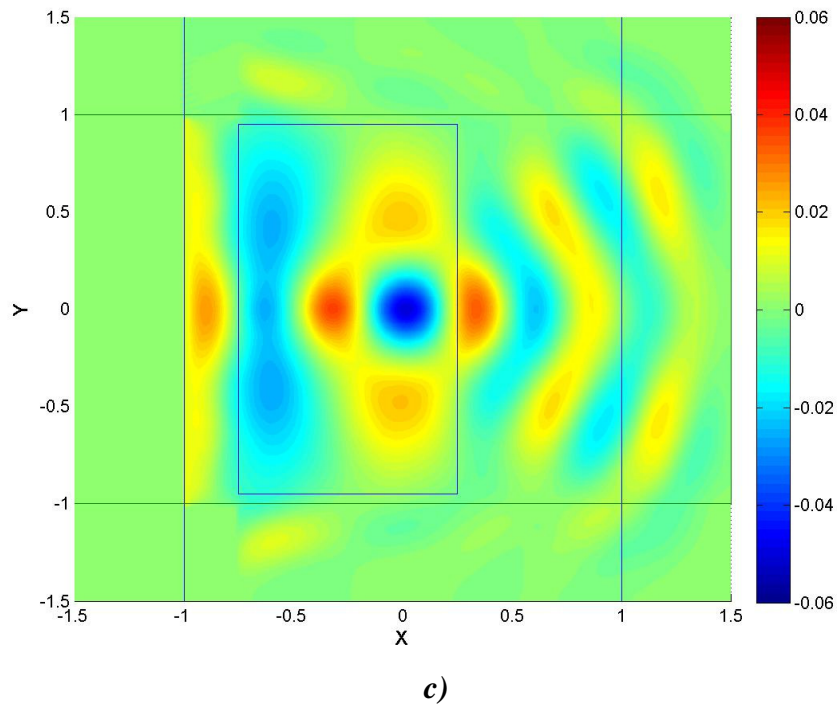
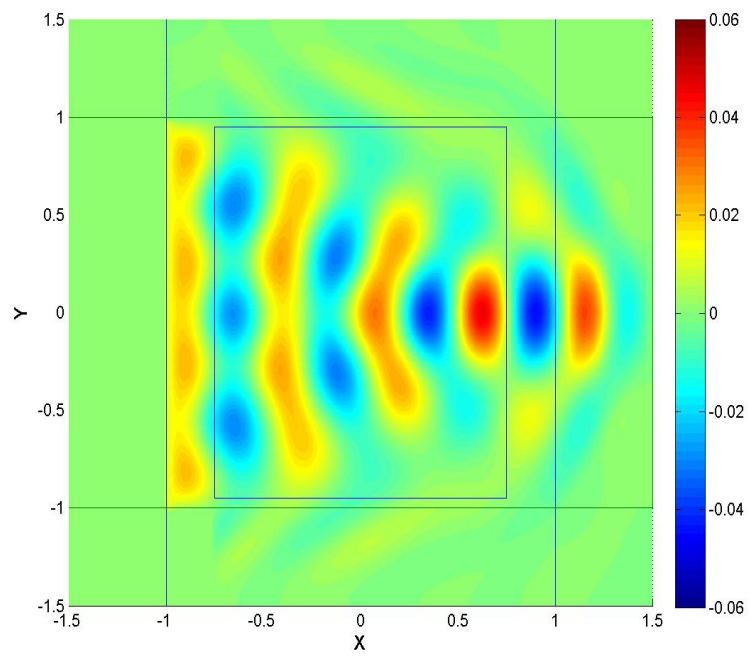


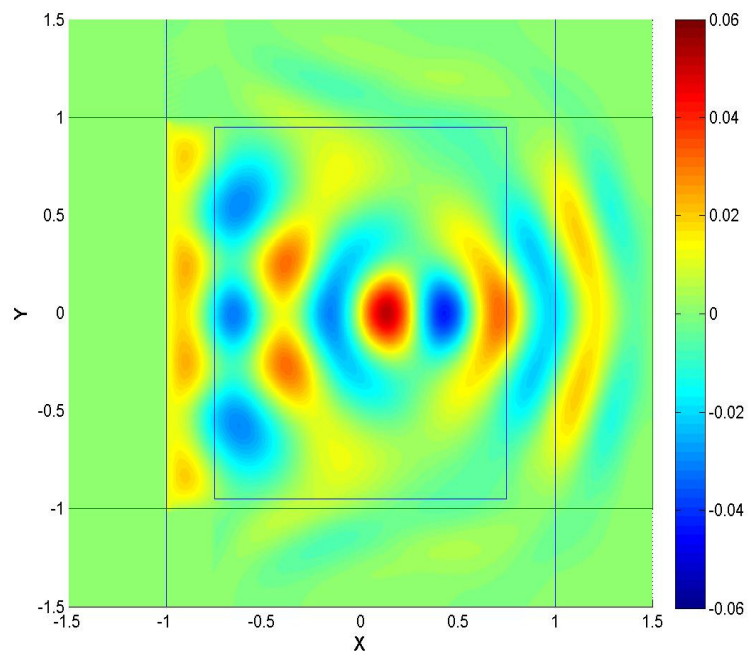
Figure 3.17: Linear increase in sound speed in a short domain with (a), (b), and (c) corresponding to 1, 3 and 5 meters per second increase per meter respectively.

The first example in Figure 3.17 shows a focus point very near the edge of the material domain if not slightly past. Once leaving the material domain the point only remains fairly focused for the first one as well.

The next two sets of examples, shown in Figures 3.18 and 3.19, use a quadratic increase in sound speed such that each set corresponds to 1, 9 and 25 meters per second increase at one meter from the center.



a)



b)

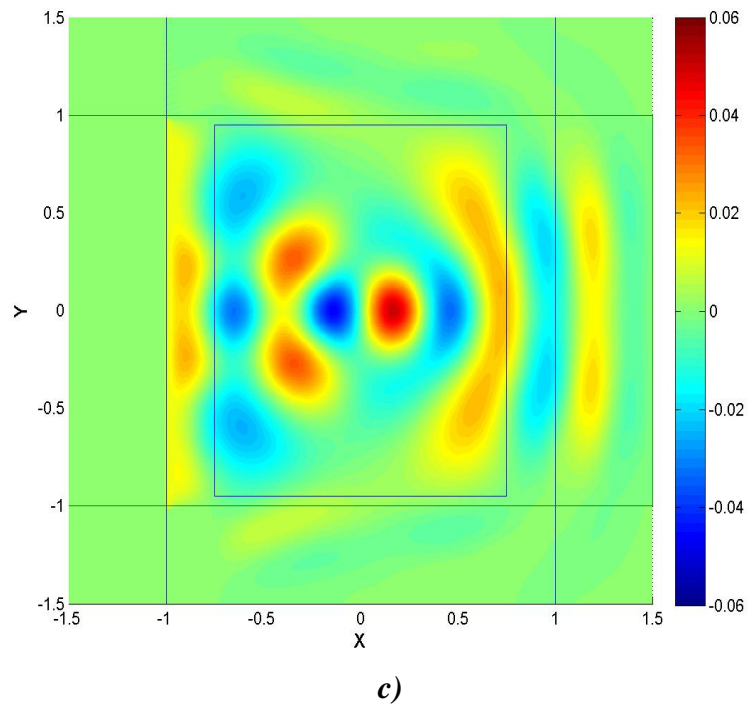
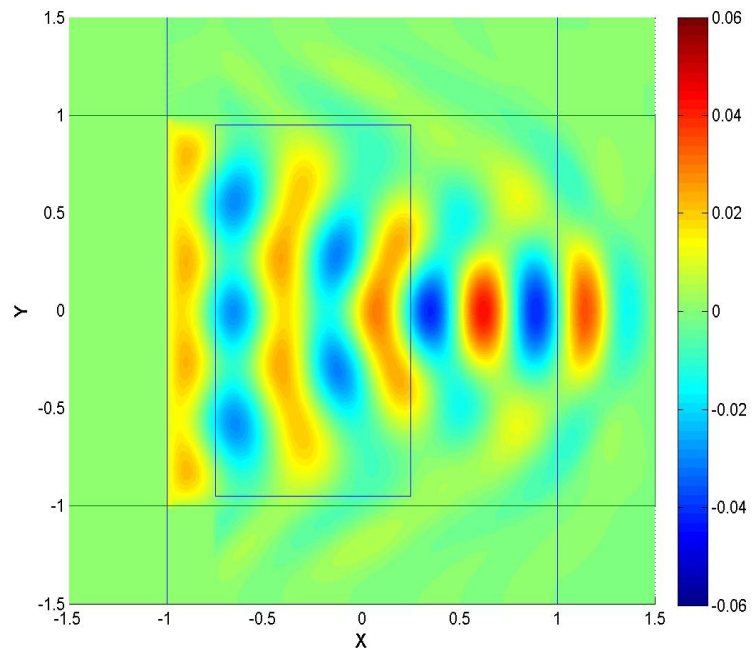
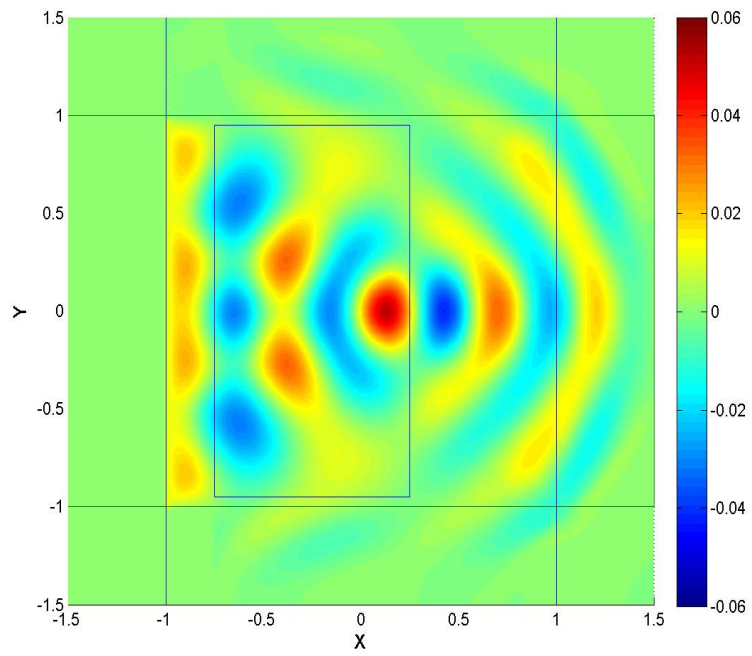


Figure 3.18: Quadratic increase in sound speed in a wide domain with (a), (b), and (c) corresponding to 1, 9 and 25 meters per second increase at one meter from the center.

The second example in Figure 3.18 clearly shows a higher pressure than its corresponding example in Figure 3.16.



a)



b)

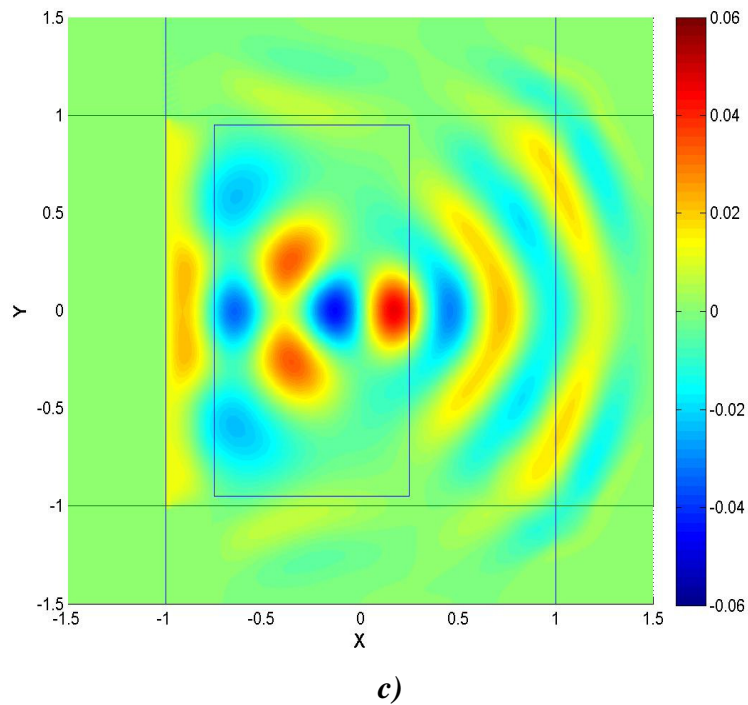


Figure 3.19: Quadratic increase in sound speed in a short domain with (a), (b), and (c) corresponding to 1, 9 and 25 meters per second increase at one meter from the center.

Examples in Figure 3.19 also show higher pressures than the corresponding ones in Figure 3.17. Looking at the entire domain, the wave appears to turn sooner such that there is less general dispersion before the focus occurs.

Taking this concept to its next step would involve creating a metamaterial with substructures that would increase the effective sound speed. A more useful material would allow sound speeds to be changed at will so to achieve an arbitrary focus. This again is the goal of this dissertation.

3.4: Summary

This chapter has described the steps for the creation of a Finite Difference Time Domain (FDTD) model which was created using MATLAB software. Both stability and boundary conditions have been addressed in this chapter and detailed in the appendix. Models have been shown to have good agreement with the commercial finite element software COMSOL Multiphysics and has been used iteratively to study a focusing field. However, the square grid nature of the Finite Difference Method (FDM) does create a limitation for curved geometries where properties become very important such as that of matching impedances. Here, finer grids are necessary to better approximate the values near the boundary. Mesh refinement cannot continue ad infinitum, though, as memory and run time becomes large factors. Additionally, solutions to the FDTD model can take anywhere from minutes to hours depending on the mesh size and time step. This is in comparison with Finite Element Method (FEM) which can get a frequency domain result in less than a minute for a moderate mesh. Because of this the FEM is utilized in future sections of this dissertation

This program, however, can be easily manipulated to handle future models due to its very intuitive nature. This is one strong point of FDMs. Adjustments necessitate only a description of the model geometry with values for density and bulk modulus.

It should be noted that mesh size is important for both the FDTD method as well as the FEM as structures within the metamaterial must be less than that of the wavelength. This fact is vital to the design of the metamaterial and is emphasized throughout this dissertation.

Chapter 4 : Active Acoustic Metamaterial (AAMM) with Tunable Effective Density

4.1: Overview

As detailed in the previous literature review section, there have been many approaches taken to address the issue of creating a metamaterial to control the propagation of acoustical wave energy. However, these approaches have been passive in nature and rely material properties that are fixed. The application of such passive metamaterial designs to designs such as the cloak has lead to problems of practically achieving such material properties, such as those problems of infinite mass described by Norris^{23,24}.

This chapter investigates, in detail, a one dimensional metamaterial presented by Baz⁶³ with a tunable effective density which allows for easy adaptation of the material for different purposes. The modeling method and investigation of the model design demonstrated in this chapter will be directly built upon in chapters 6 and 7 in the dissertation. The fundamentals of the electric-acoustic analog are the basis of which tie the components of this metamaterial together. Thus it is important to understand the basic methodology used to create the model to forward those same concepts into more complex cases such as those in chapters 6 and 7.

The paper described in this chapter outlines model used to tune the effective density, specifically, a method that gives access to densities both above and below that of the surrounding medium and can be tuned independently across the volume of the

metamaterial. This allows the material properties to vary spatially across the material leading to such designs as the acoustic cloak which would render an object acoustically invisible. The model itself is based on a sub-wavelength acoustic cylindrical cavity ended by piezoelectric diaphragms which puts the entirety of model into acoustic, mechanical and electrical domains. Control of the end mounted piezo diaphragm adjusts the overall stiffness of the cavity which determines the dynamic density of the overall cavity cell. The following sections follow the paper by Baz in the analysis of the theoretical model including the theoretical predictions. The various control strategies offered by Baz are also described which is closely related to the extension of this model into the control of bulk modulus.

The review of Baz work indicates that the lumped-parameter model used is non-dissipative. Therefore, special effort will be exerted in this dissertation to investigate the effect of adding realistic dissipation on the performance of the metamaterial. This is carried out in details in Chapter 7.

4.2: Motivation for the Active Acoustic Metamaterial

Baz begins by addressing the driving motivation for the metamaterial with tunable density in the introduction. As described in the literature review section, many achievements have been made in the area of metamaterials in the last decade and evidence of popularity of metamaterials can be found in overviews of authors such as the aforementioned Shamonina and Solymar² as well as the synopses given by Lapine⁶⁴, and Gil et al⁶⁵. The landmark paper of Cummer and Schurig¹⁹ comes as one of the most important in the acoustic metamaterial field as it defines the necessary density and bulk modulus for the acoustic metamaterial cloak. Subsequent authors such as Popa and

Cummer⁶⁶, Cheng *et al.*²⁸, and Cheng and Liu⁶⁷ further defined the requirements for the 2 and 3 dimensional acoustic cloak based off the original approach by Cummer and Schurig. Others such as Chen *et al.*⁶⁸ took a different approach to try to avoid the infinite mass problem described by Norris^{23,24}. Additionally, papers by Pendry and Li³² and Norris⁶⁹ theorize the use of composite layers to achieve anisotropic properties. Many of these works, however, have been fruitless when considering practical applications due to problems of physical realization of the design or limitations in achievable parameters.

Works much closer in concept to that of Baz include that of Lee *et al.*^{13,70} and Yao *et al.*⁷¹ who have also taken the approach of cavities terminated with membranes to produce metamaterials with negative density. These too, however, lack the range necessary for the acoustic cloak. It is the addition of the active component suggested by Baz that drastically increases the range material properties achievable by the cloak while at the same time allowing the static design of the metamaterial structure to be physically the same regardless of tuned effective density and the location of the individual structure.

The subsequent sections follow the paper of Baz with an additional section expanding on history of the circuit analog prior to the section which models the metamaterial.

4.3: Description of the Active Acoustic Metamaterial

4.3.1: Using an active acoustic metamaterial for the purpose of a cloak

Figure 4.1 shows the layout of the acoustic cloak in the 2 dimensional configuration.

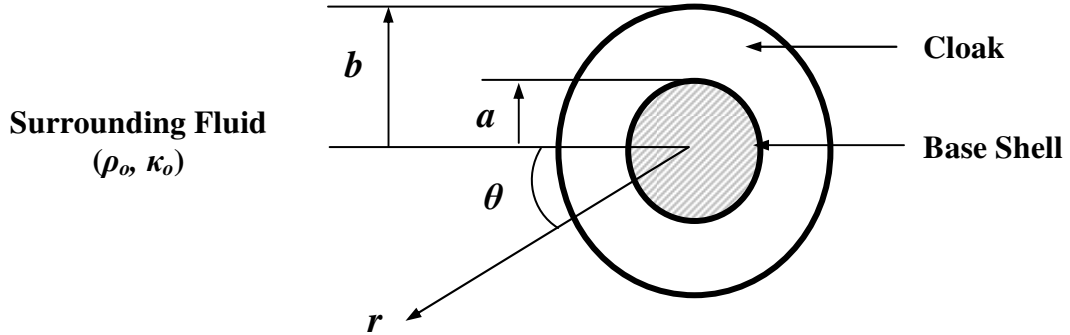


Figure 4.1: Layout of the acoustic cloak (Baz⁶³)

The properties of the ideal cloak as described by Cummer and Schurig¹⁹ require an anisotropic density matrix with ρ_r and ρ_θ corresponding with the densities in the radial and tangential directions and bulk modulus, κ , as described by equation 4.1 respectively.

$$\frac{\rho_r}{\rho_o} = \frac{r}{r-a}, \quad \frac{\rho_\theta}{\rho_o} = \frac{r-a}{r}, \quad \text{and} \quad \frac{\kappa_o}{\kappa} = \left(\frac{b}{b-a}\right)^2 \frac{r-a}{r} \quad (4.1)$$

Since no homogeneous material exists that can reflect these properties, Cheng *et al.*²⁸ and Torrent and Sanchez-Dehesa¹ suggested a manor to achieve such properties using composite layers of materials to perform the function of such an idea anisotropic materis. Figure 4.2 depicts the layered cloak as described with alternating layers of materials which draw from the work of Schoenberg and Sen³⁰.

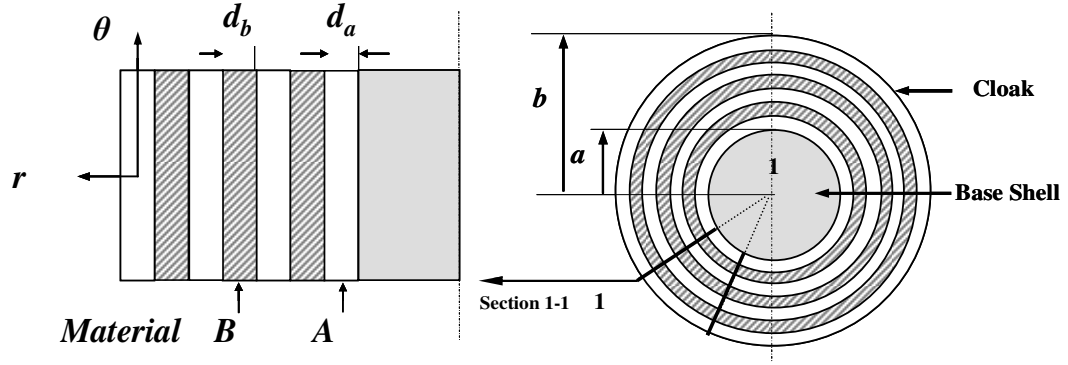


Figure 4.2: Multi-layered acoustic cloak (Baz⁶³)

In the case when the thickness of the different layers is equal and outer radius is twice that of the inner. The property values of the density and bulk modulus of can be found as a function of materials A and B can be described equations in (4.2) as found by Cheng *et al.*²⁸:

$$\rho'_r = \frac{1}{2}(\rho'_A + \rho'_B), \quad \rho'_\theta = 2 \frac{\rho'_A \rho'_B}{(\rho'_A + \rho'_B)}, \quad \text{and} \quad \kappa' = 2 \frac{\kappa'_A \kappa'_B}{(\kappa'_A + \kappa'_B)} \quad (4.2)$$

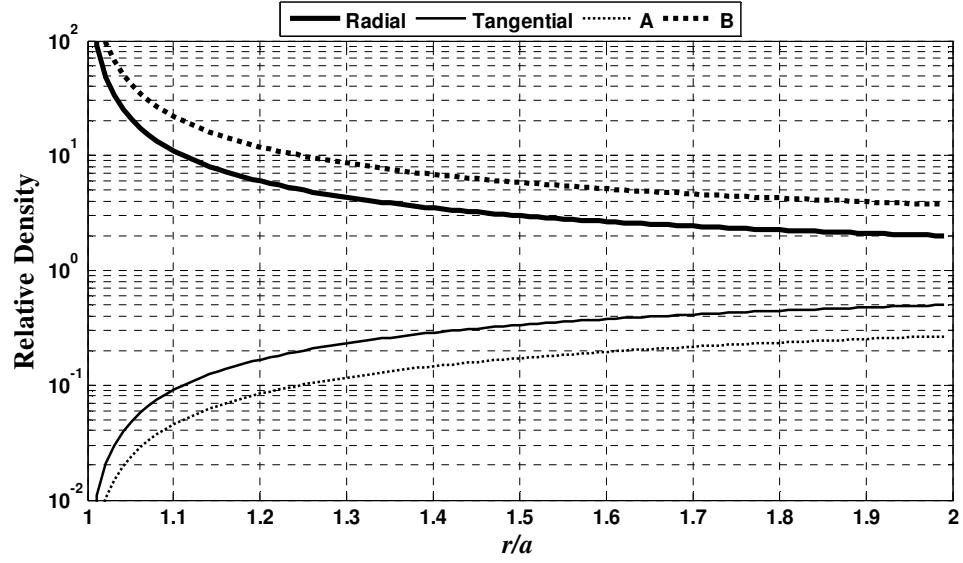
where ρ'_i and κ'_i are normalized values to the surrounding medium.

The density values for ρ'_A and ρ'_B , by solving for them from equation (4.2) simultaneously to find the values that need to be achieved as described in equation (4.3) as a function of the ideal values.

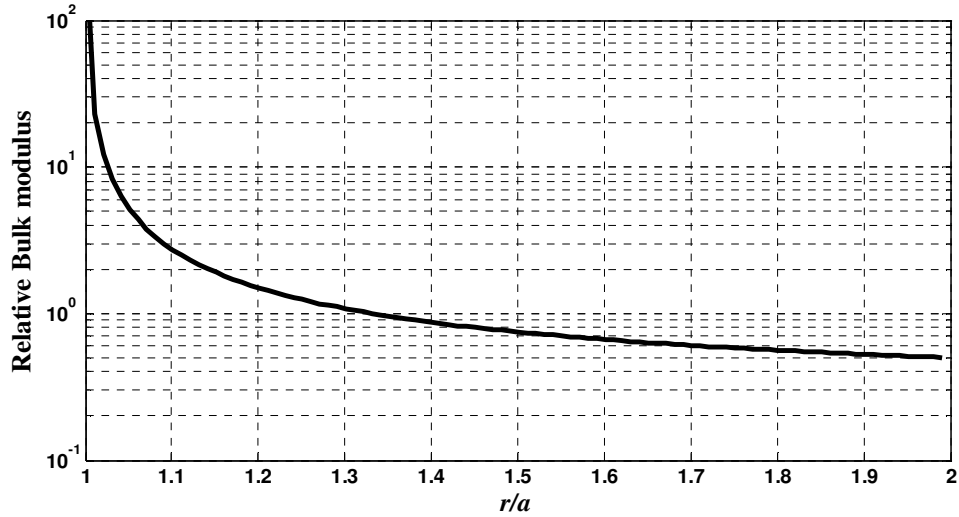
$$\rho'_A = \rho'_r - \sqrt{\rho_r'^2 - 1}, \quad \text{and} \quad \rho'_B = \rho'_r + \sqrt{\rho_r'^2 - 1}. \quad (4.3)$$

From Figure 4.3 it can be seen that the relative density and bulk modulus for the ideal cloak vary several orders of magnitude. Even further, the constituent materials for the composite layers require even more extreme values than that of the ideal case. Prior to the study of metamaterials, acquisition of such materials that vary to such a degree even in separate isotropic forms would be difficult if not impossible. And even with the

advent of metamaterials, accomplishing such dramatic changes is still a difficult challenge. This is the prime reason for taking the active approach to this problem.



(a)



(b)

Figure 4.3: Density (Baz⁶³) (a) and bulk modulus (b) distributions

4.3.2: The configuration of the active acoustic metamaterial

The array of cell cavities in Figure 4.4 displays a cross section of the layers of an acoustic cloak divided by piezoelectric boundaries. This cross section can be considered a “slice” denoted by “section 1-1” on Figure 4.2. As previously mentioned, each of these cells are mechanically identical to each other which increases the ease of manufacture. Each of the cells, however, will be controlled separately to be tuned to the necessary parameters outlined in the previous section with increasing and decreasing densities depending on the layer.

The author makes a note that this configuration is solely for the control of the effective density with future studies in plan for control of bulk modulus as well. Furthermore the metamaterial is to be analyzed in its passive form to delineate the limitations of a passive form and the need for the metamaterial to active.

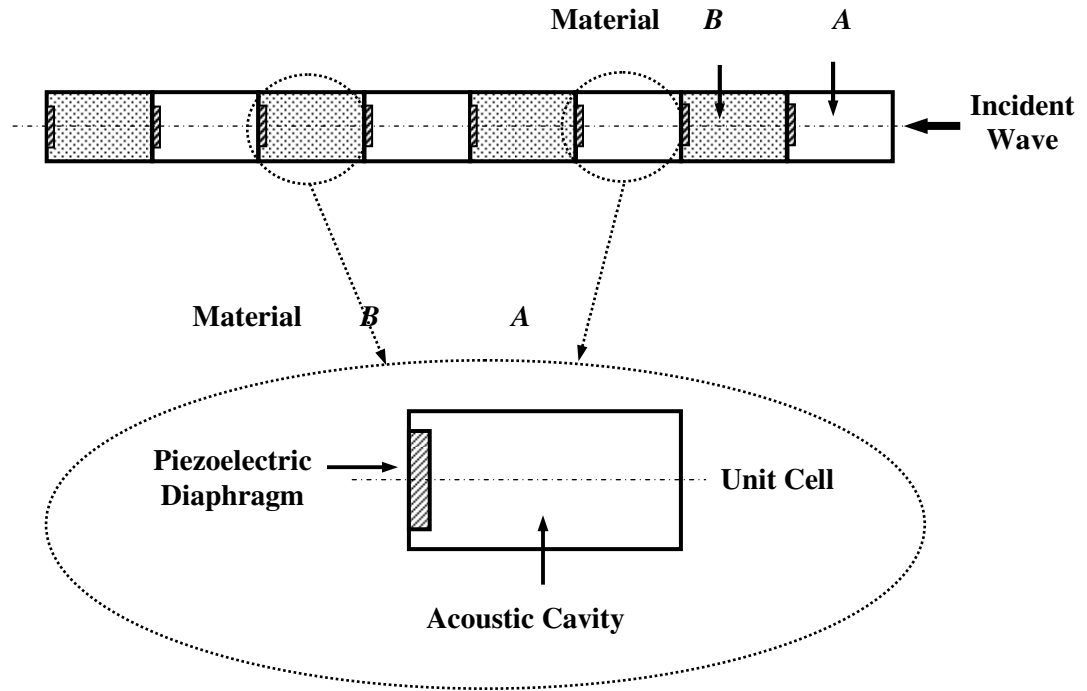


Figure 4.4: Configuration of active acoustic metamaterial (Baz⁶³)

4.4: Circuit Analog

In some complex, multi domain systems, it is easier to consolidate the domains of the system into a single domain analog. The use of analogs has been noted by Bauer to extend back to at least Volta and Ohm, around the 1800s, in equating the still infant concepts of electricity to more familiar and developed domains such as hydraulics, mechanics and heat⁷². In 1933, Firestone⁷³ drew in depth analogs between the behaviors of electrical and mechanical systems.

Over the years Firestone and others found multiple analogies between the acoustic, mechanical and electrical domains. Bauer drew from these and attempted to consolidate the information. The chart below is an adaptation from that paper.

Table 4.1: Analogs adapted from Bauer⁷²

Acoustical Quantity	Mechanical Quantity	Electrical Quantity	
		EFP Analogy	IFP Analogy
Sound Pressure(p) N/m ²	Force(F) N	Voltage (E) Volt	Current (I) Ampere
Volume Velocity (U) m ³ /s	Velocity (V) m/s	Current (I) Ampere	Voltage (E) Volt
Volume Displacement (V) m ³	Displacement (D) m	Charge (I) Coulomb	Impulse Volt-s
Acoustic Resistance (R _A) N-s/m ⁵	Mech. Resistance (R _M) N-s/m	Resistance (R) Ohm	Conductance (G) Ohm
Inertance (M _A) kg/m ⁴	Mass (M) kg	Inductance (L) Henry	Capacitance (C) Farad
Acoustic Compliance (C _A) m ⁵ /N	Mech Compliance (C _M) m/N	Capacitance (C) Farad	Inductance (L) Henry
Acoustic Impedance (Z _A) Z _A =p/U	Mech. Impedance (Z _M) Z _M =F/v	Impedance (Z) Z = E/I	Admittance (Y) Y=I/E

4.5: Plain Acoustic Cavity

Using the circuit analogy from the previous section a simple cavity can be described by as a equivalent circuit as in Figure 4.5.

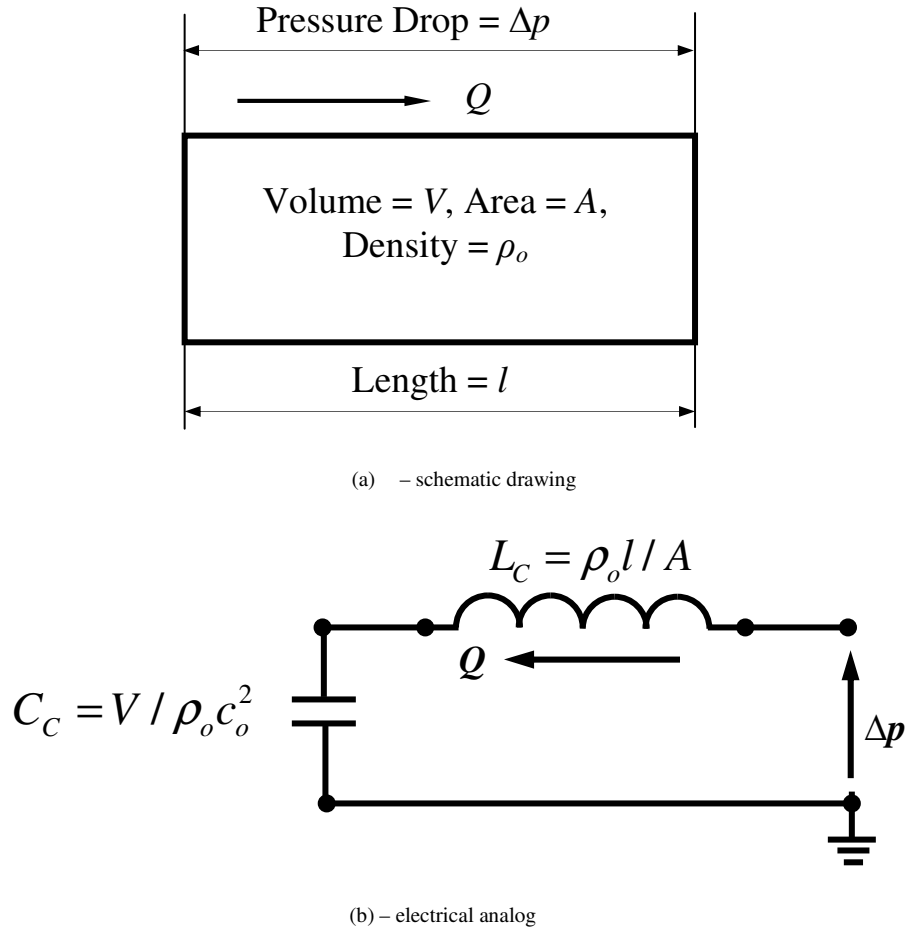


Figure 4.5: Plain acoustic cavity (Baz⁶³) (a) schematic (b) electric analog

Using Kirchoff's voltage law, the dynamics of the cavity can be described by solving for the difference in pressure across the cavity to give:

$$\frac{\rho_o l}{A} \frac{dQ}{dt} + \frac{\rho_o c_o^2}{V} \int Q dt = -\Delta p \quad (4.4)$$

which can be rewritten in the Laplace domain as:

$$\left(\frac{\rho_o l}{A} s + \frac{\rho_o c_o^2}{V} \frac{1}{s} \right) Q = -\Delta P \quad (4.5)$$

Equation (4.5) can be rewritten in the form of Euler's equation.

$$\Delta P / l = -\rho_o \left(1 + \frac{c_o^2}{l^2} \frac{1}{s^2} \right) s u \quad (4.6)$$

where $u=Q/A$ is the fluid velocity. Equation (4.6) can then be rewritten as in *Kinsler et al*⁷⁴ as:

$$\rho_{eff} / \rho_o = \left(1 + \frac{c_o^2}{l^2} \frac{1}{s^2} \right) \quad (4.7)$$

For sinusoidal excitation, equation (4.7) can be rewritten as:

$$\rho_{eff} / \rho_o = \left(1 - \frac{c_o^2}{l^2} \frac{1}{\omega^2} \right) \quad (4.8)$$

From equation (4.8) the author points out that as frequency increases from 0 to ∞ , the effective normalized density ρ_{eff} / ρ_o can only vary from $-\infty$ to a maximum value of 1. Therefore, effective densities which are greater than that of the surrounding medium cannot be achieved in this form.

4.6: Acoustic Cavity with Flexible Diaphragm

Baz then takes the case of the acoustic cavity with a flexible diaphragm as depicted in Figure 4.6 which is similar to the experimental set-up conceived by Lee *et al.*¹³.

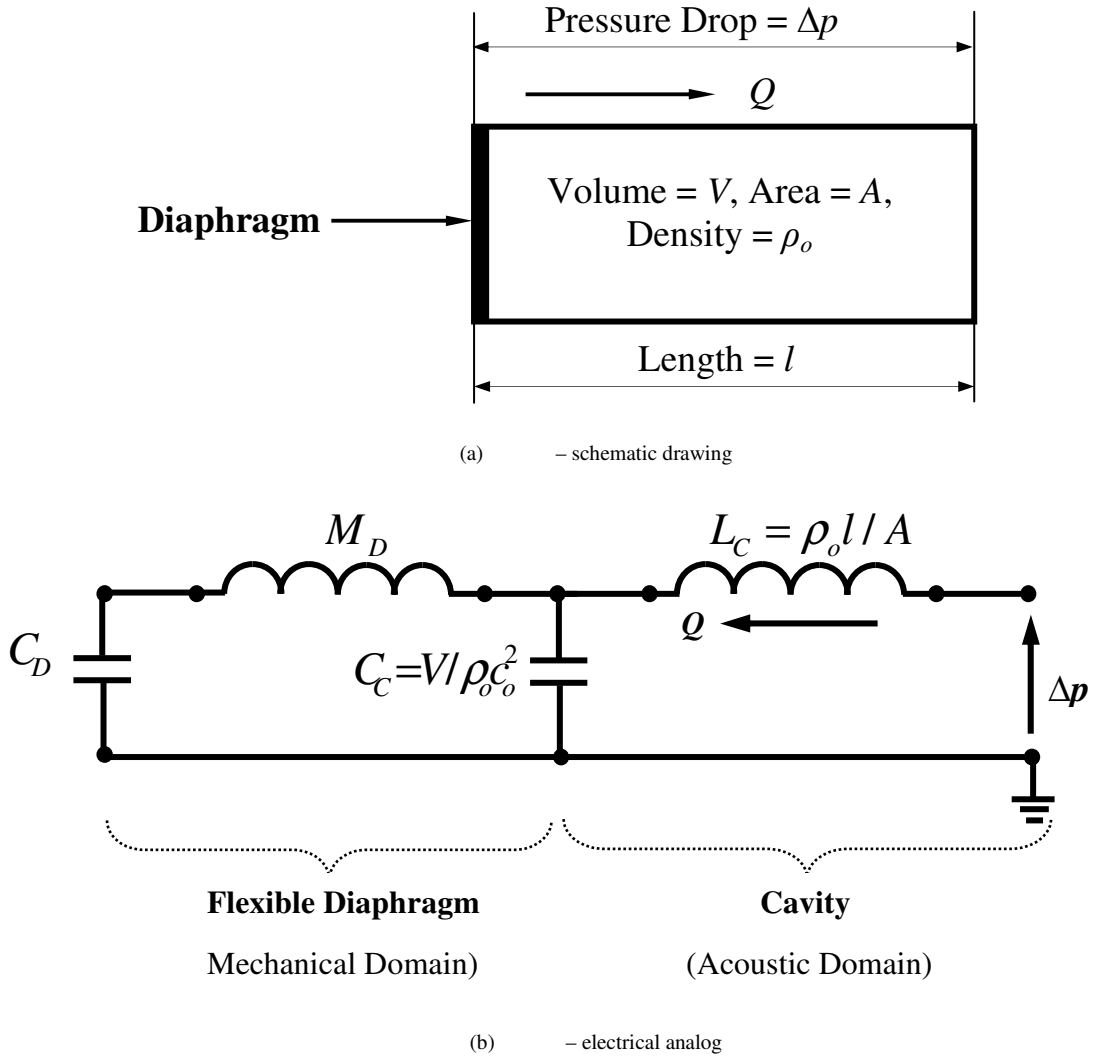


Figure 4.6: Acoustic cavity with flexible diaphragm cavity (Baz⁶³) (a) schematic (b) electric analog

Again, Kirchhoff's law is applied and the equation for the system is found as a solution for the difference in density:

$$\left(\frac{\rho_o l}{A} s + \frac{1}{C_D} \frac{1}{s} \right) Q = -\Delta P \quad (4.9)$$

Being a metamaterial it is assumed that the cavity is much smaller than the wavelength of the incoming wave or $l \ll \lambda$.

Equation (4.9) can then be written as the Euler equation form:

$$\Delta P / l = -\rho_o \left(1 + \frac{A}{l \rho_o C_D} \frac{1}{s^2} \right) s u \quad (4.10)$$

Resulting in an effective density of:

$$\rho_{eff} / \rho_o = 1 + \frac{A}{l \rho_o C_D} \frac{1}{s^2} = 1 + \frac{k_D}{\rho_o s^2} \quad (4.11)$$

where $k_D = \frac{A}{l C_D}$ = diaphragm stiffness.

Analyzing equation (4.11), it can be seen that ρ_{eff} is a function of both the diaphragm stiffness k_D as well as the frequency ω . Therefore, the desired effective density may be set by the stiffness of the diaphragm for a single frequency, but will be dramatically changed for other operating frequency. Furthermore, as with the previous case, density values above that of the ambient medium cannot be attained.

4.7: Acoustic Cavity with Piezoelectric Diaphragm

4.7.1: Basic Equations

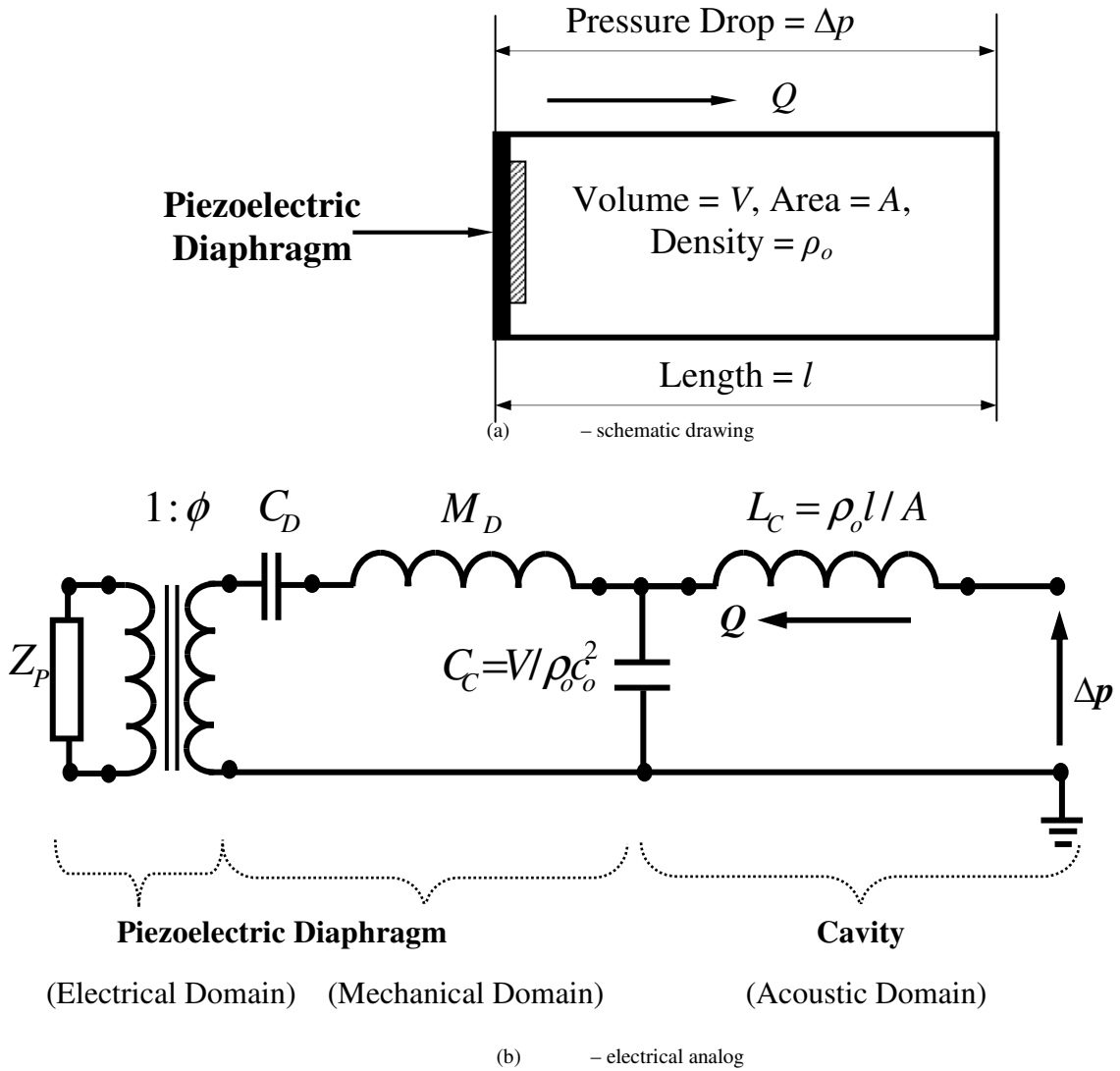


Figure 4.7: Acoustic cavity with open-loop piezoelectric diaphragm cavity (Baz⁶³) (a) schematic (b) electric analog

The final configuration to be analyzed is the acoustic cavity with the piezoelectric diaphragm as shown in Figure 4.7. Note the lumped impedance Z_p which will be described later.

Baz first takes the basic constitutive equations as presented by (ANSI/IEEE STD 176-1987)⁷⁵:

$$\begin{Bmatrix} S \\ D \end{Bmatrix} = \begin{bmatrix} s^E & d \\ d & \epsilon \end{bmatrix} \begin{Bmatrix} T \\ E \end{Bmatrix} \quad (4.12)$$

where S is the strain, D is the electrical displacement, T is the stress, E is the electrical field, s^E is the compliance, d is the piezoelectric strain coefficient, and ϵ is the permittivity and rewrites it in the form used by Prasad *et al.*⁷⁶:

$$\begin{Bmatrix} \Delta Vol \\ q \end{Bmatrix} = \begin{bmatrix} C_D & d_A \\ d_A & 1/Z_p s \end{bmatrix} \begin{Bmatrix} \Delta p_p \\ V_p \end{Bmatrix} \quad (4.13)$$

Here ΔVol is the change in diaphragm volume, q is the electrical charge, Δp_p is the pressure across piezoelectric diaphragm, V_p is the voltage, C_D is the diaphragm compliance, and Z_p is the impedance of piezoelectric diaphragm with attached elements.

This lumped impedance can be described by:

$$Z_p = [(L_p s) / \{1 + L_p C_p C_s s^2 / (C_p + C_s)\}] \quad (4.14)$$

where C_p = capacitance of piezoelectric diaphragm, L_p is a shunted inductance *in-parallel* with the piezoelectric diaphragm, and C_s is a capacitance *in-series* with the piezoelectric diaphragm.

This piezo diaphragm can then be used as a self-sensing actuator. In this case, the second row of equation 4.13 can give the charge as a function of the change in pressure across the piezo diaphragm:

$$q = d_A \Delta p_P \quad (4.15)$$

The necessary voltage applied to the piezoelectric diaphragm can then be found as a function of the sensed charge and a feedback gain G .

$$V_P = -G d_A \Delta p_P \quad (4.16)$$

With this we can rewrite the first row of equation (4.13) to yield:

$$\Delta Vol = (C_D - d_A^2 G) \Delta p_P = C_{DC} \Delta p_P \quad (4.17)$$

where C_{DC} is the closed-loop compliance of piezoelectric diaphragm.

With the closed-loop compliance the circuit diagram can be redrawn as in Figure 4.8.

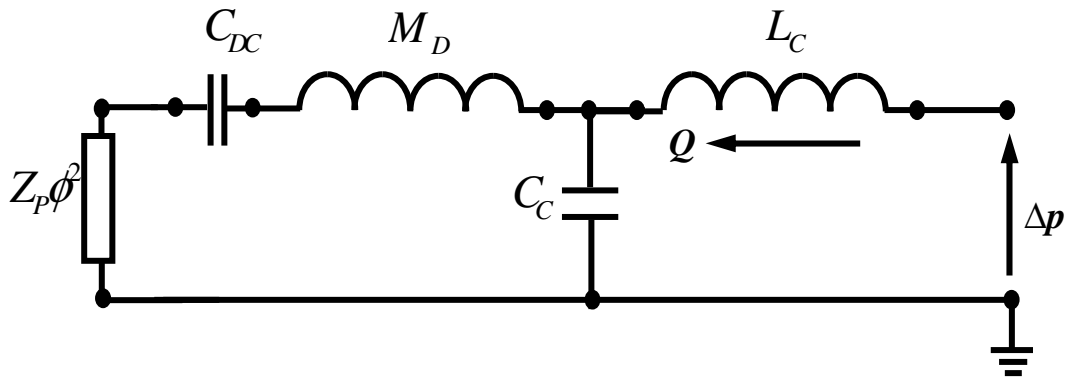


Figure 4.8: Acoustic cavity with closed-loop piezoelectric diaphragm cavity (Baz⁶³)

In a similar manner as the prior cases the effective density of the case of the acoustic cavity with the piezoelectric diaphragm end can be written as:

$$\rho_{eff} = \rho_0 \left[1 + \frac{C_{DC}T + 1}{L_C s^2 (C_{DC} + C_C [C_{DC}T + 1])} \right] \quad (4.18)$$

where $T = M_D s^2 + Z'_p s$ (4.19)

with $Z'_p = Z_p \phi^2$ (4.20)

4.7.2: Analysis of the effective density

Baz next considers several cases to analyze the possible performance metamaterial cell. He first considers if the mass of the diaphragm is negligible:

i. **If $M_D \approx 0$,** In this case the equation (4.18) reduces to:

$$\rho_{eff} / \rho_o \cong \left[1 + \frac{C_{DC} Z'_p s + 1}{L_C s^2 [C_{DC} + C_C (C_{DC} Z'_p s + 1)]} \right] \quad (4.21)$$

From this point, two sub-cases can be identified:

Subcase A: $C_{DC} \rightarrow 0$, In the first subcase, if the diaphragm is rigid, the equation becomes the same as equation 4.7:

$$\rho_{eff} / \rho_o \cong \left[1 + \frac{1}{L_C C_C s^2} \right] = \left[1 + \frac{c_o^2}{l^2 s^2} \right] \quad (4.22)$$

Subcase B: $C_C \rightarrow 0$, In the second subcase, if the fluid within the cavity is incompressible, the equations becomes the same as equation (4.11) when there is no piezoelectric effect.

$$\rho_{eff} / \rho_o \cong \left[1 + \frac{1}{L_C C_D s^2} \right] = \left[1 + \frac{k_D}{\rho s^2} \right] \quad (4.23)$$

And with piezoelectric effect, equation (4.18) yields:

$$\rho_{eff} / \rho_o \cong \left[1 + \frac{C_{DC} Z_{PS}' + 1}{L_C C_{DC} s^2} \right] \quad (4.24)$$

Now if we set the effective density ρ_{eff} / ρ_o to the desired density ρ_d' then we can use equation (4.24) to solve for the feedback gain to result in:

$$G = \frac{(\rho_d' - 1)L_C C_D s^2 - C_D Z_{PS}' - 1}{d_A^2 \left[(\rho_d' - 1)L_C s^2 - Z_{PS}' \right]} \quad (4.25)$$

ii. If $M_D \gg 0$ In this second case where the mass of diaphragm is not negligible, the equation for the feedback gain can be similarly found as:

$$G = \frac{(\rho_d' - 1)L_C s^2 (C_C + C_D + C_C C_D T) - C_D T - 1}{d_A^2 \left[(\rho_d' - 1)L_C s^2 (1 + C_C T) - T \right]} \quad (4.26)$$

The author notes here that the gain in equation (4.26) gives a fourth order characteristics equation; however, the gain reduces to a third order equation when $M_D \approx 0$ as given by equation (4.25). The accuracy of the reduced-order feedback gain equation later described by the author in the subsequent section of his paper.

4.8: Numerical Performance of an Acoustic Cavity with Piezoelectric Diaphragm

In the next section of the paper by Baz, he models the performance of the offered metamaterial cavity with the characteristics listed in Table 4.2⁷⁶.

Table 4.2: Parameters of acoustic cavity and piezoelectric diaphragm system cavity (adapted from Baz⁶³)

PARAMETER	VALUE
l	$0.01m$
ρ_o	$1,000 \text{ kg/m}^3$
c_o	$1,500 \text{ m/s}$
ϕ	138.3 Pa/V
C_D	$1.5243 \times 10^{-13} \text{ m}^4 \text{ s}^2/\text{kg}$
M_D	13456 kg/m^4
d_A	$-2.1080 \times 10^{-11} \text{ m}^3/\text{V}$
C_P	18.239 nF
C_C	$1.8466 \times 10^{-15} \text{ m}^4 \text{ s}^2/\text{kg}$
L_C	24069 kg/m^4

In Figure 4.9 the frequency response of the passive cavity is compared with that of the active with controlled density of. The passive cavity begins with a negative density in the low frequency range and converges towards $\rho'_d = 1$ as $\omega \rightarrow \infty$ which agrees with the results by Lee *et al*¹³. This reemphasizes the inability of the passive cavity to reach a desired density above that of the ambient fluid. Alternatively, the active cavity does hold at $\rho'_d = 20$ over the frequency spectrum. The author notes that the control voltage required to hold the density at lower frequencies is very high, but decreases significantly for higher frequencies. Additionally, the closed loop compliance C_{DC} is held positive through a large frequency range only with the addition of the attached $L_P=50 \text{ H}$ and $C_S=0.2\text{pF}$.

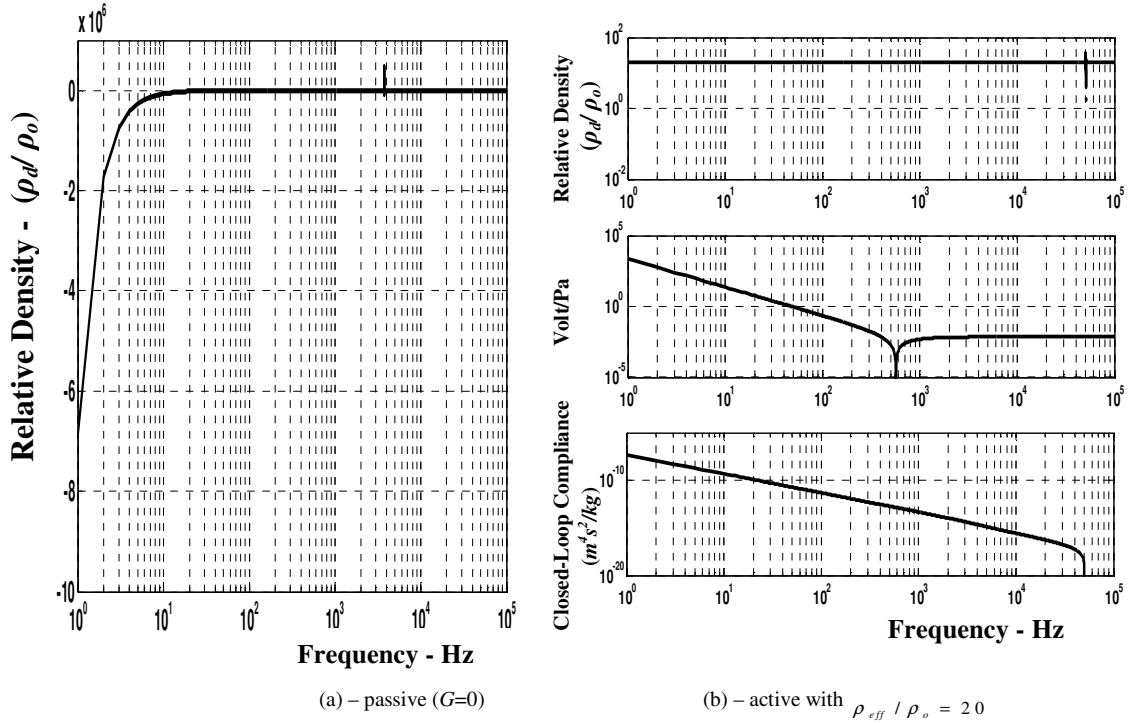


Figure 4.9: Comparison between passive and active cavities cavity (Baz⁶³) (a) passive (b) active

Extending this to application purposes, eight of these metamaterial cells could be attached in an array as in Figure 4.4. Four of these could have densities decreasing towards the inner radius such as those in Figure 4.10 and the other four could have densities increasing such as those in Figure 4.11. These eight is just given as an example but a true scenario would require much higher numbers to accurately recreate the required material characteristics for the cloak.

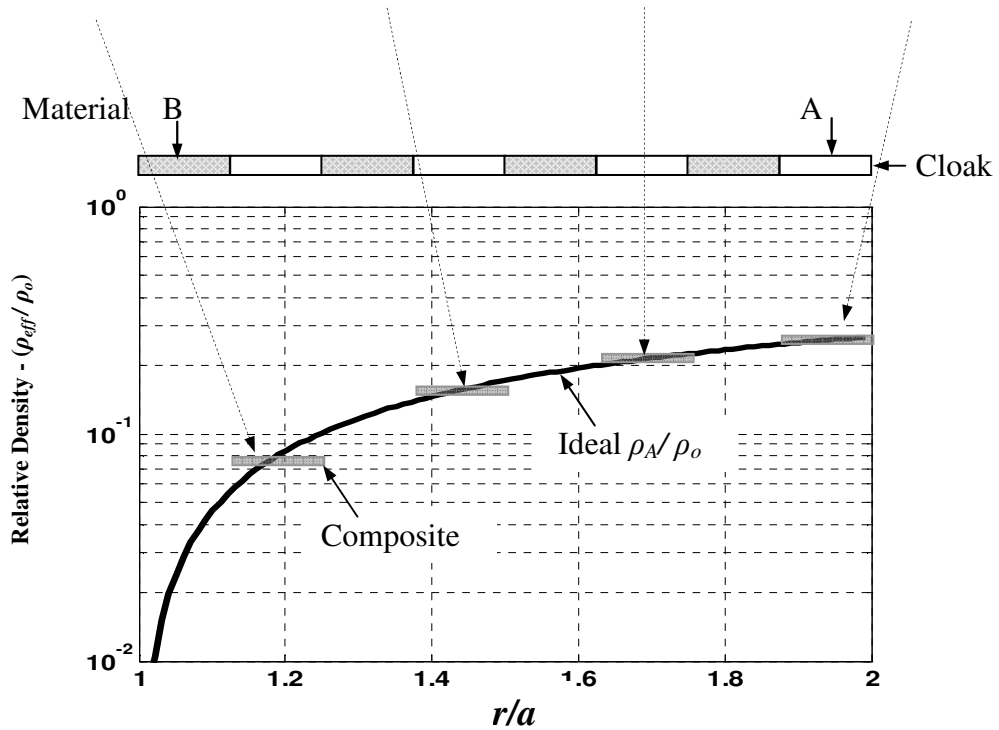
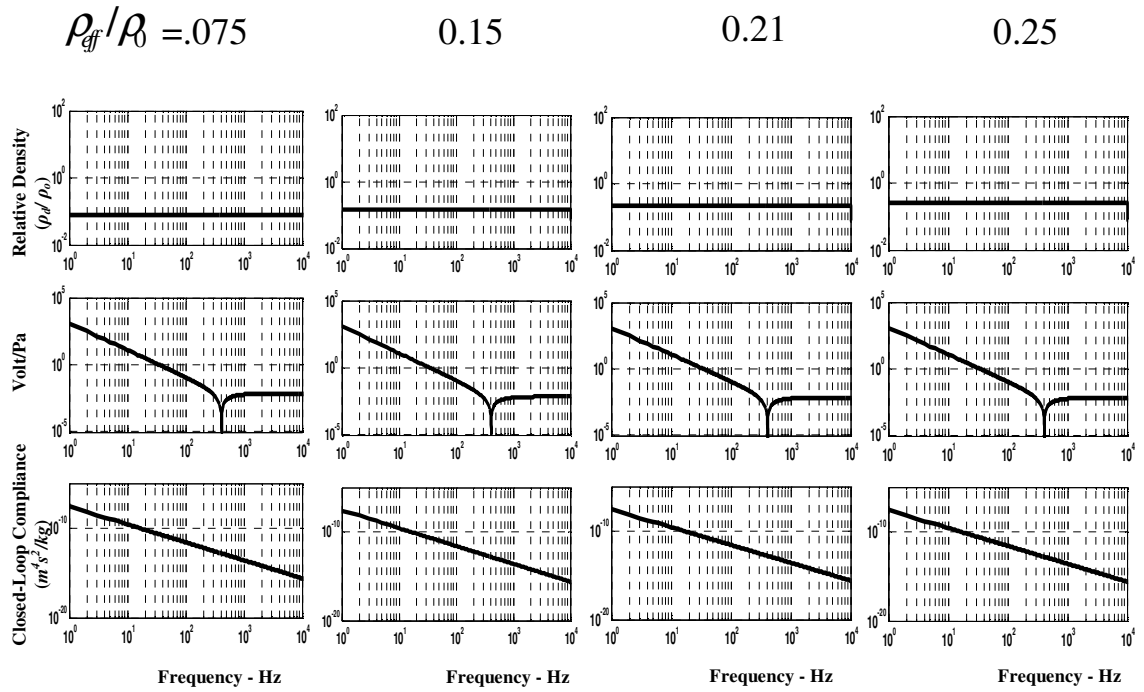


Figure 4.10: Active acoustic metamaterial (A) with increasing density distribution cavity (Baz⁶³)
 (a) passive (b) active

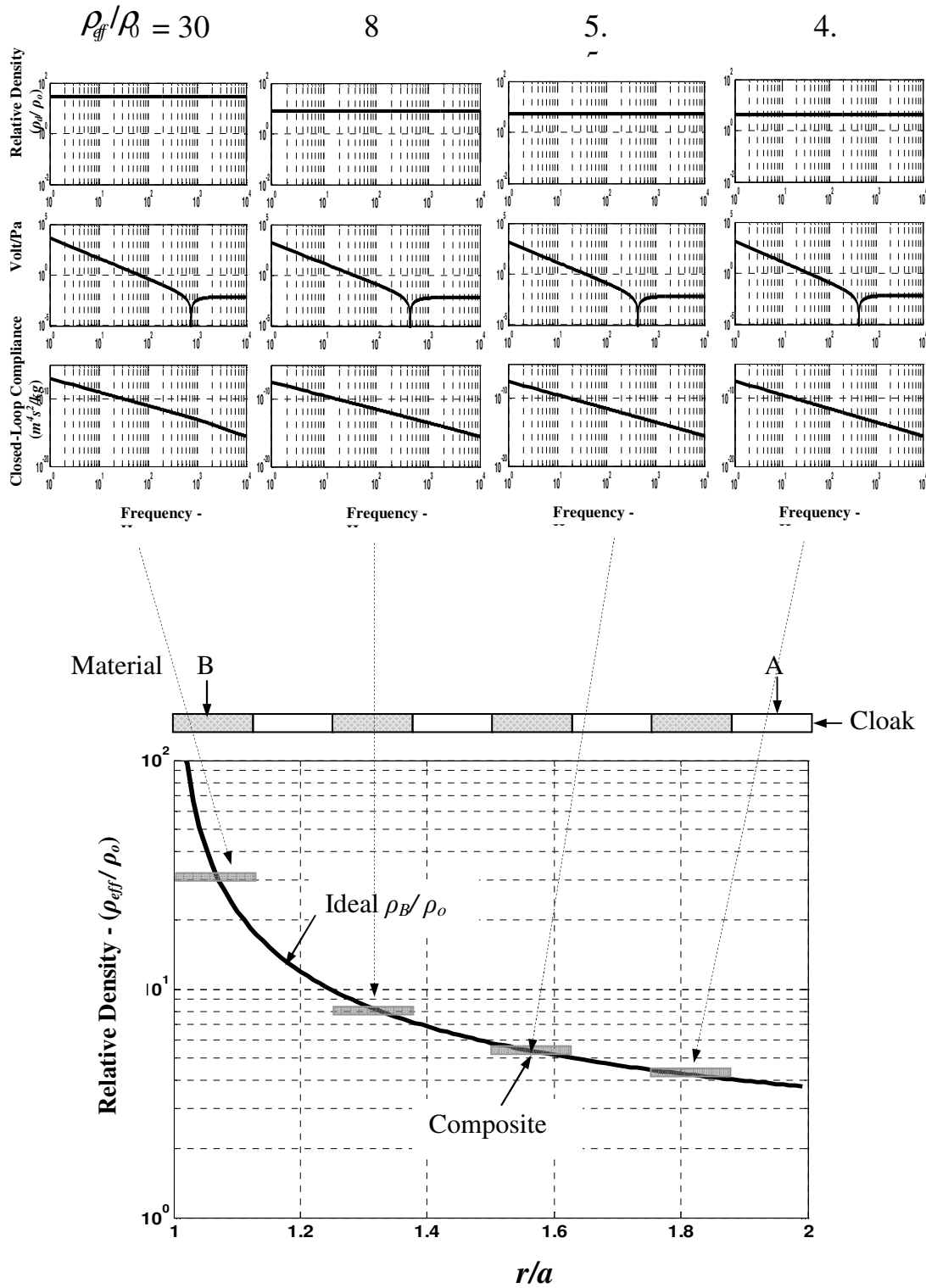


Figure 4.11: Active acoustic metamaterial (B) with decreasing density distribution cavity (Baz⁶³)
 (a) passive (b) active

Finally, the author makes comparisons between the full and reduced order feedback gain solutions shown below in Figure 4.12 for values of ρ_{eff} / ρ_o of 30 and 0.075. The reduced order models fit fairly well with that of the exact models for this active acoustic cell and significantly reduces the complexity of the solution.

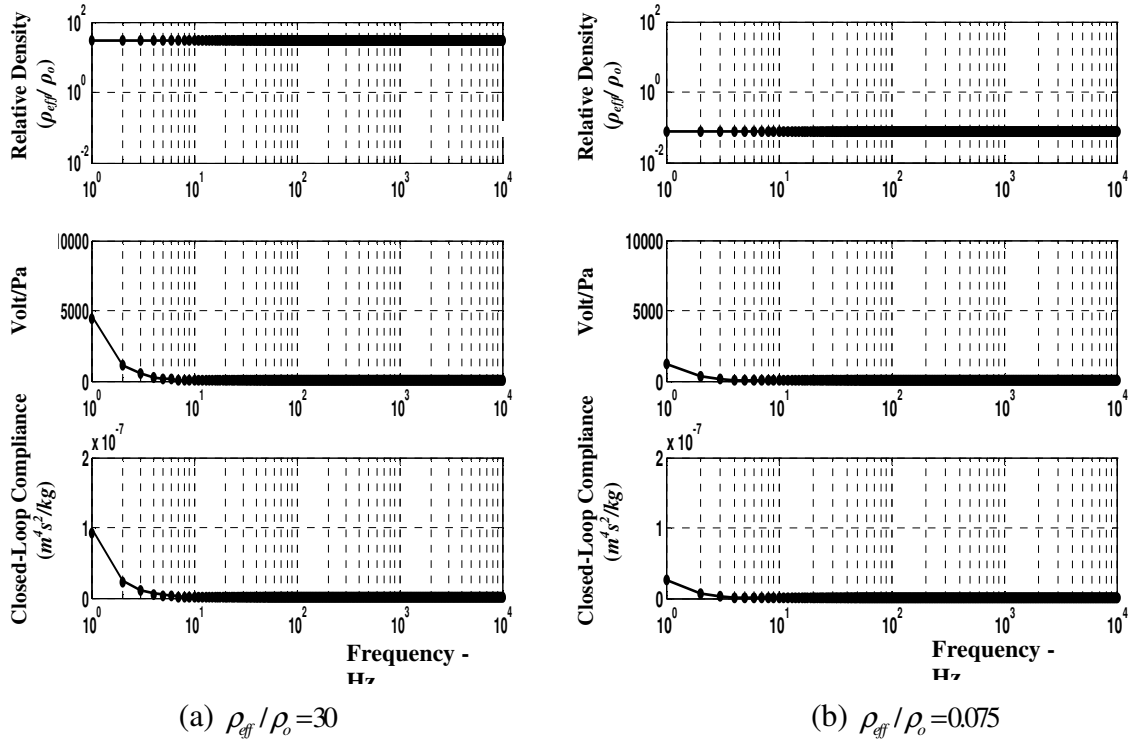


Figure 4.12: Comparison between the predictions of the full (exact) and reduced (approximate) order feedback gain models (— exact , • approximate) cavity (Baz⁶³)

4.9: Summary

This chapter has described a class of one-dimensional acoustic metamaterials as presented by Baz⁶³. The active component of this metamaterial allows for *programmable* densities which can be tuned to be both below and above that of the ambient medium.

The metamaterial, which is made up of acoustic cavities separated by piezoelectric diaphragms has been analyzed using a lumped parameter approach. Control strategies for the metamaterial have been presented and compared with the passive form of this same metamaterial. The metamaterial has shown to be mechanically independent of its tunable effective density allowing for ease of production.

The author notes that results from this study are for a single cell and the addition of multiple cells in an array would need to be studied in a future for cross effects. Also, the addition of bulk modulus control is the natural extension for this study.

This model is extended into the experimental domain in the following chapter in a review of the work of Akl and Baz⁷⁷. Furthermore, it is important to note here that Baz work⁶³ indicates that the lumped-parameter model used is non-dissipative. Therefore, special effort will be exerted in this dissertation to investigate the effect of adding realistic dissipation on the performance of the Metamaterial. This is carried out in details in Chapter 7.

Chapter 5 : Experimental Demonstration of an Active Acoustic Metamaterial with Tunable Effective Density

5.1: Overview

As the previous chapter pertained to the theoretical design of an active acoustic metamaterial (AAMM), this chapter will follow a paper by Akl and Baz⁷⁷. The experimental demonstration and characterization of the one dimensional active acoustic metamaterial model presented from the previous chapter will be detailed citing comparisons to finite element modeled prepared to the specifications of those of the physical cavity. Again, it is important to thoroughly understand the methodology presented in the above cited paper to extend it to the works presented in chapters 6 and 7. The results of this paper demonstrate the reaction to excitation as a homogenous system which is a vital attribute for this metamaterial. The setup described in this chapter is important for demonstrating such a attribute lending to the importance of this description of the paper.

The design of this individual active metamaterial cell is based on the need for a large bandwidth which has been shown to be a lacking feature of passive counterparts. Additionally, the importance of the characterization of this single metamaterial cell extends into the need to use this cell as a building block for multi arrayed arrangements. The prototype described in the following sections is composed of a cylindrical cavity terminated by piezo bimorphs on either end. Characterization of the cell includes acoustic impedance and transmission loss measurements. Characterizations are then compared with predictions made by the finite element model which will be shown to be

of good agreement. Additionally, the transfer function between a reference microphone in the impedance tube and the end mounted piezoelectric element will show the coupled nature of the metamaterial cell reflecting the model's performance as an equivalent single degree for freedom system.

This prototype may be useful for future demonstrations of metamaterials such as the ones with programmable dispersion and directivity characteristics such as that of Akl, Smoker and Baz⁷⁸.

5.2. Introduction

The introduction section of the paper presented by Akl and Baz delineates the interest in acoustic metamaterials and various associated uses. One of which is the control of wave propagation through directivity and dispersion control of the metamaterial⁷⁸. Approaches to metamaterials have taken the form of anisotropic property values for the material density ρ and bulk modulus κ as in Cummer et al^{19,37} as well as scalar properties with negative values^{79,80,81,82,83} such as investigations in simultaneously negative bulk modulus and density and negative modulus for sound attenuation. With the control of the acoustic waves residing the fluid domain, practically any propagation pattern is achievable through the control of these two parameters. Attaining these values are based on the sub-wavelength structure of the metamaterials, orientation, and the periodicity of the material layout. These collectively are the basis of phononic crystals as studied by numerous authors^{84,85,86,87,88,89}. Numerous modeling techniques have been utilized with a variety of approaches to attempt to predict effective material properties^{84,87,90,91,92,93,94}. In several cases, approaches were taken into the physical realm

in experimental setups for the acoustic metamaterials. Such demonstrations show off effective material densities ρ and the bulk moduli κ that are not solely a product of the material properties within the metamaterial^{88,89,95,96,97,98}. Furthermore, the approach of influencing the frequency response with addition of a mass or Helmholtz resonator has been utilized in for narrow bands^{79,99,100,101,102,103,104}. Characterization of acoustic metamaterials have also been carried out for several membrane based metamaterials^{105,106}. Similar characterizations will be utilized for the analysis of this prototype.

The prototype presented here by Akl and Baz is composed of a 1 dimensional cylindrical acrylic cavity with an encapsulated a water medium. The cylinder ends are enclosed with a PZT4 (Lead Zirconate Titanate) piezoelectric diaphragm bimorph with a brass constraining layer. The bimorph nature piezoelectric diaphragm allows the simplicity having one sensor and a separate actuator for this prototype.

Characterization of the cell is measure via impedance and transmission loss measurements using a standard impedance tube and based on the ISO 10534-2 and ASTM E1050 standards^{107,108}. A variety of feedback gains are applied to compare and characterize changes of the homogenized system. These in turn are compared against a finite element model of the physical setup.

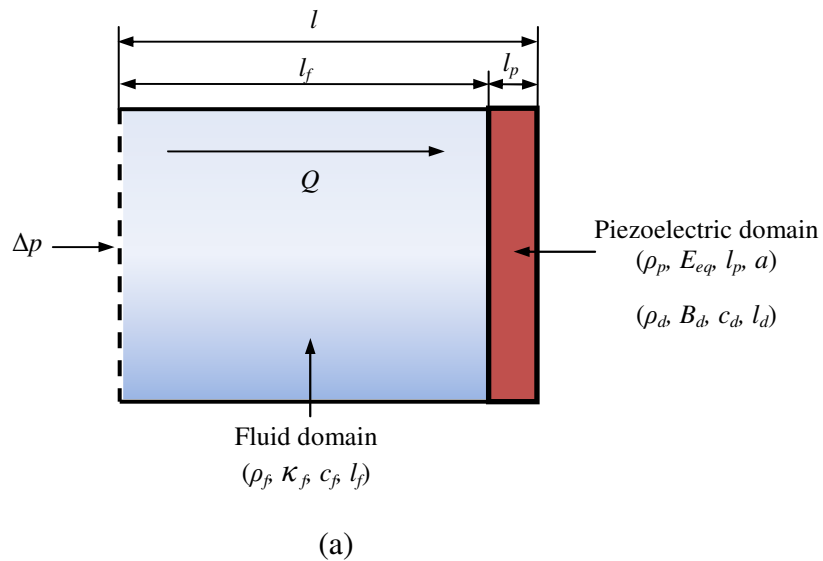
The presented work of Akl and Baz⁷⁸ will be extended in Chapter 6 to the independent control of both the density and bulk modulus of an active acoustic Metamaterial cell.

5.3: Analytical Model for the Developed Active Metamaterial Cell

The electro acoustic model on which the performance of the active acoustic metamaterial cell is based has been used in a number of previous studies such as Ding *et al.*⁸¹ and Blauert and Xiang¹⁰⁹.

The paper makes note that due to the dimensions of this prototype the primary movement for the piezoelectric diaphragm that will be considered for this model is bending as the compression mode will add little in comparison due to its small movement and high stiffness relative to that of the bending mode.

The authors begin by describing the model similar to that found in Figure 4.7 of the last chapter with its electro-acoustic equivalent circuit as shown in Figure 5.1.



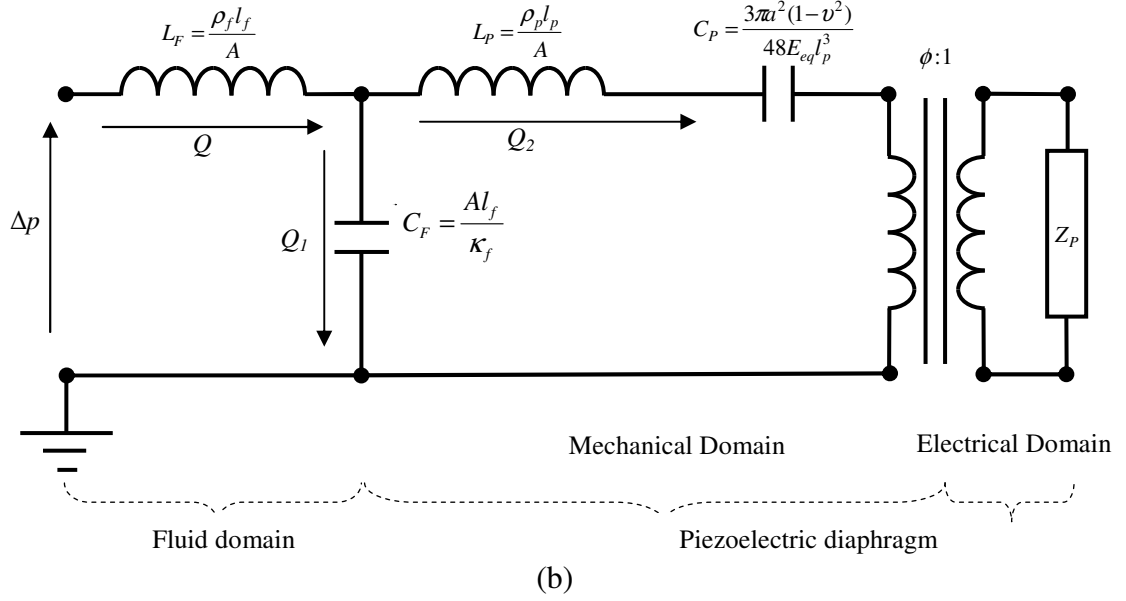


Figure 5.1: (a) Schematic of the metamaterial cell with property values. (b) electro-acoustic analogy circuit of the metamaterial cell (Akl and Baz⁷⁷)

The fluid components of density ρ_f and bulk modulus κ_f of those in Figure 5.1 are that of water, while ρ_p and E_{eq} represent the density and equivalent elasticity modulus of the piezoelectric domain. The piezoelectric electro-acoustic conversion factor ϕ is represented by the transformer in the schematic.

To determine the relation for the change in volume to that of the transverse pressure placed on the diaphragm, the authors begin with the linear plate bending theory with fixed edges following the method in the handbook by DiGiovanni¹¹⁰:

$$y = \frac{3(1-\nu^2)(a^2-r^2)^2}{16E_{eq}l_p^3} \Delta p \quad (5.1)$$

Equation (5.1) give the deflection of the plate y as a function of the radius r and the applied pressure Δp for a diaphragm with the components of radius, thickness, elastic modulus, and Poisson's ratio as a , l_p , E_{eq} , and ν respectively.

Integration of all the points of deflection on the bending plate gives the displaced volume of the diaphragm given by Eq. (5.1):

$$V = (1 - \nu^2) \frac{3\pi a^6}{48E_{eq}l_p^3} \Delta p \quad (5.2)$$

Using the adjusted constitutive equation (4.16) from the previous chapter, the acoustic impedance of the piezoelectric diaphragm can be described as:

$$Z_{CP} = \frac{1}{C_{pS}} = \frac{48E_{eq}l_p^3}{3\pi a^6(1 - \nu^2)s} \quad (5.3)$$

The authors use the electrical circuit reduction technique to get the overall acoustic impedance of the composite cell as shown in (5.4):

$$Z_t = \frac{\left(Z_p \phi^2 + \frac{1}{C_{pS}} + L_{pS} \right) \frac{1}{C_{fS}}}{Z_p \phi^2 + \frac{1}{C_{pS}} + L_{pS} + \frac{1}{C_{fS}}} + L_{fS} \quad (5.4)$$

The transfer function of the composite cell can then be given by:

$$\frac{\Delta p}{l} = -\frac{A}{ls} \left[\frac{\left(Z_p \phi^2 + \frac{1}{C_{pS}} + L_{pS} \right) \frac{1}{C_{fS}}}{Z_p \phi^2 + \frac{1}{C_{pS}} + L_{pS} + \frac{1}{C_{fS}}} + L_{fS} \right] su \quad (5.5)$$

The Euler form can then be converted into effective density as:

$$\rho_{eff} = \frac{A}{ls} \left[\frac{\left(Z_p \phi^2 + \frac{1}{C_{pS}} + L_{pS} \right) \frac{1}{C_{fS}}}{Z_p \phi^2 + \frac{1}{C_{pS}} + L_{pS} + \frac{1}{C_{fS}}} + L_{fS} \right] \quad (5.6)$$

It can be seen that controlling the compliance of the piezo diaphragm C_p controlled the overall homogenized density of the composite cell.

5.4: Calculation of the Acoustic Impedance using Two Microphone Measurements

The commercially manufactured impedance tube used includes two microphones spaced by 50.8 mm with the microphone at the end at a distance of 29.2 mm from the end of the impedance tube surface. The acoustic cell is mounted onto the end of the microphone as depicted in Figure 5.2. Measurements are made in compliance with ASTM E1050 and Iso 10534-2 standards

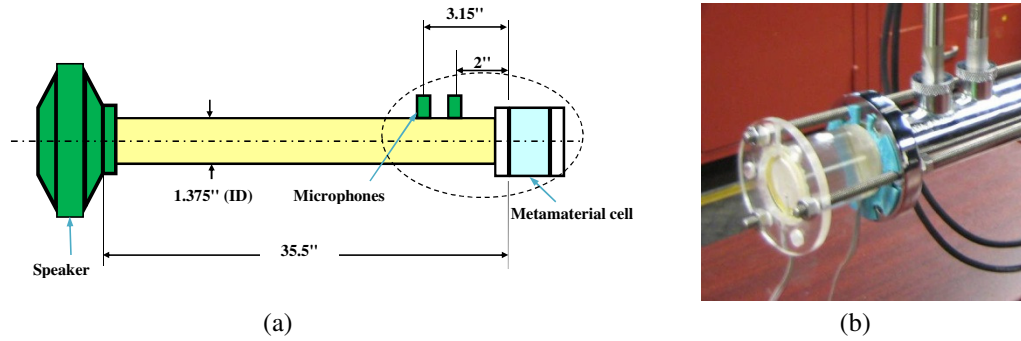


Figure 5.2: (a) Drawing of the impedance tube with metamaterial cell mounted (b) Actual mount of the metamaterial cell with holder (Akl and Baz⁷⁷)

To ensure proper measurement, the setup is calibrated for phase mismatch of the two microphones by placing each microphones in of the two slots and obtaining a transfer function between the two microphones then interchanging the microphone s and repeating the process¹⁰⁷. The microphones are then returned to their original location for measurements. Using the resulting transfer functions, a calibration transfer function

$(\bar{H}_c = |\bar{H}_c|e^{j\phi_c})$ is created and applied to subsequent measurements:

$$H = \bar{H} / \bar{H}_c = |H|e^{j\phi} = H_r + jH_i \quad (5.7)$$

where $(\bar{H} = |\bar{H}|e^{j\phi})$ denotes the transfer function of the subsequent measurements.

The coefficient R for the complex reflections can then be calculated with the corrected transfer function with equation (5.8):

$$R = |R|e^{j\phi_R} = R_r + jR_i = \frac{H - e^{-jks}}{e^{jks} - H} e^{2jk(l+s)} \quad (5.8)$$

The normal specific impedance can then be calculated as a function of the reflectance as follows:

$$\frac{z}{\rho c} = \frac{r}{\rho c} + j \frac{x}{\rho c} = \frac{1+R}{1-R} \quad (5.9)$$

5.5: Acoustic Metamaterial Cell Construction

The construction of the metamaterial cell begins with the sizing of the cylinder pipe and the addition of a 3mm hole at the middle of the cylinder. The hole is then refilled with silicon sealant to create a temporary self-sealing barrier for the introduction of water into the cavity with a syringe once the cavity is sealed. This is followed by the attachment leads of the PZT4 bimorph. Before the bimorph is mounted, a thin layer of non-conductive coating is applied to the bimorph. This prohibits interaction between the layers of the bimorph with the water in the cavity. The bimorph itself is 0.5mm thick with 0.135mm of that thickness coming from the brass constraining layer. The bimorph diameter is 0.045m, however, the inner radius of the cylindrical pipe is 0.035m. leaving the outer 0.005m of the bimorph available for mounting. Once the cavity is filled with the water and it must be inspected to ensure that no air bubbles are present. The cell can

then be permanently sealed with the addition of more sealant. The end result of the construction of the metamaterial cell can be seen in Figure 5.3a. The material properties of the piezoelectric bimorph components are listed in Table 5.1.

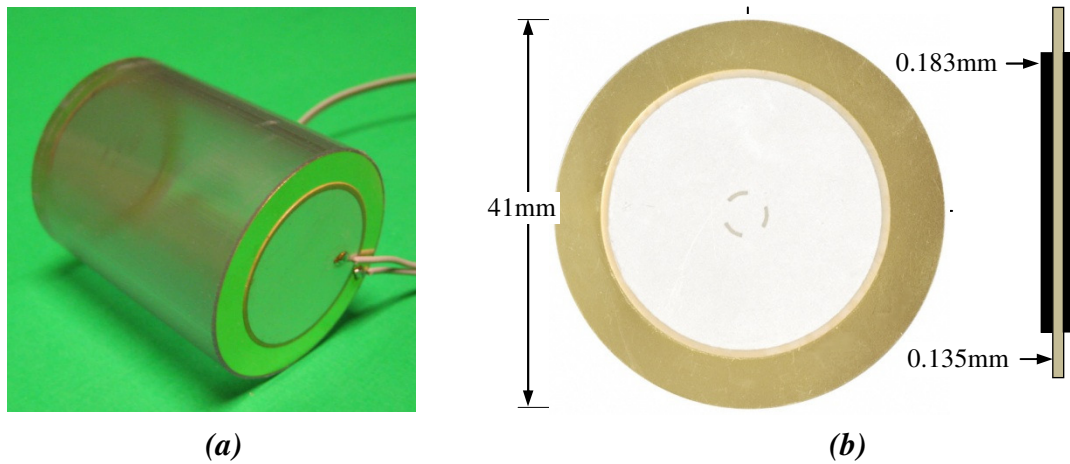


Figure 5.3: (a)End construction of metamaterial cell (b) Dimensional layout of the PZT4 bimorph (Akl and Baz⁷⁷)

Table 5.1: PZT4 material properties (adapted from Akl and Baz⁷⁷)

Material property	Value
Frequency	1.3 kHz
Capacitance @ frequency	150,000 pF @
Voltage Input (Maximum)	30V p-p
Impedance	200 Ohm

Figure 5.4 below depicts the basic interface of the metamaterial cell for control. The first piezoelectric diaphragm acts as a sensor which measures the acoustic pressure passing through the cell and feeds that signal through a power amplifier which energizes the actuator bimorph. This adjusts the stiffness of the second bimorph. Since the fluid is incompressible, the link to the second bimorph directly couples the system into a

homogeneous domain with a single degree for freedom. Therefore, the change of the stiffness of the piezo in turn changes the stiffness of the system as a whole and adjusts the dynamic density of the system. The authors reiterate, however, that it is vital that the system structure remain much shorter than the wavelength of excitation or the system will lose its homogeneity. This experiment conforms to the work with passive structures in fluid domains of Lee *et al.*¹³ where the effective dynamic density is a function of the frequency of excitation.

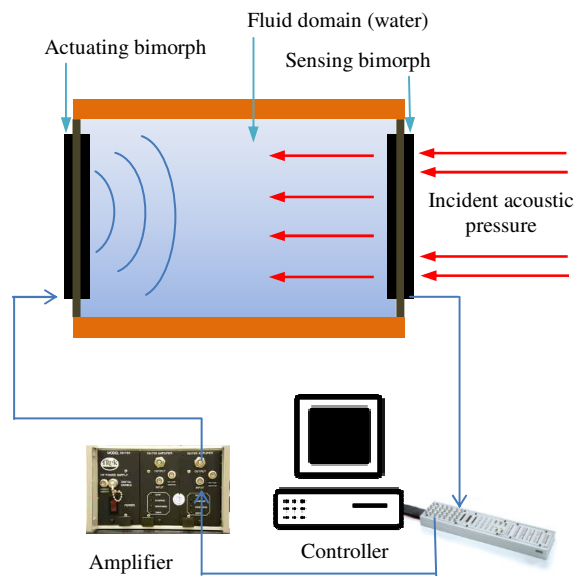


Figure 5.4: Schematic of the operation mechanism of the proposed cell (Akl and Baz⁷⁷)

5.6: Experimental Setup

In order to fully characterize the acoustic metamaterial cell, two sets of experiments were carried out by the authors. The first set focused on attaining the acoustic impedance of the metamaterial prototype. The impedance tube was set up and calibrated to ASTM and ISO specifications and modifications were added to hold the metamaterial sample as shown in Figure 5.2b. After the prototype was put in place, the

piezoelectric bimorph closest to the excitation speaker was fed to a proportional controller, through an amplifier, and back to the second actuator piezo. In the actual measurements of the metamaterial impedance, three cases were considered. The first of these was for the uncontrolled metamaterial. No feedback was sent to the second piezo rendering the cell passive. In the second and third cases, a negative and positive feedback was applied to the second piezoelectric diaphragm. These feedbacks increased and decreased the stiffness of the metamaterial cell as a whole respectively. For these measurements, the transfer function was run through a range frequencies from 200 Hz to 1 kHz.

The second set of experiments focused on the measurement of transmission loss through the prototype. For this setup the addition of the transmission loss attachment was added to allow for the placement of a secondary set of microphones on the far side of the prototype to measure the transmitted wave as shown in Figure 5.5.

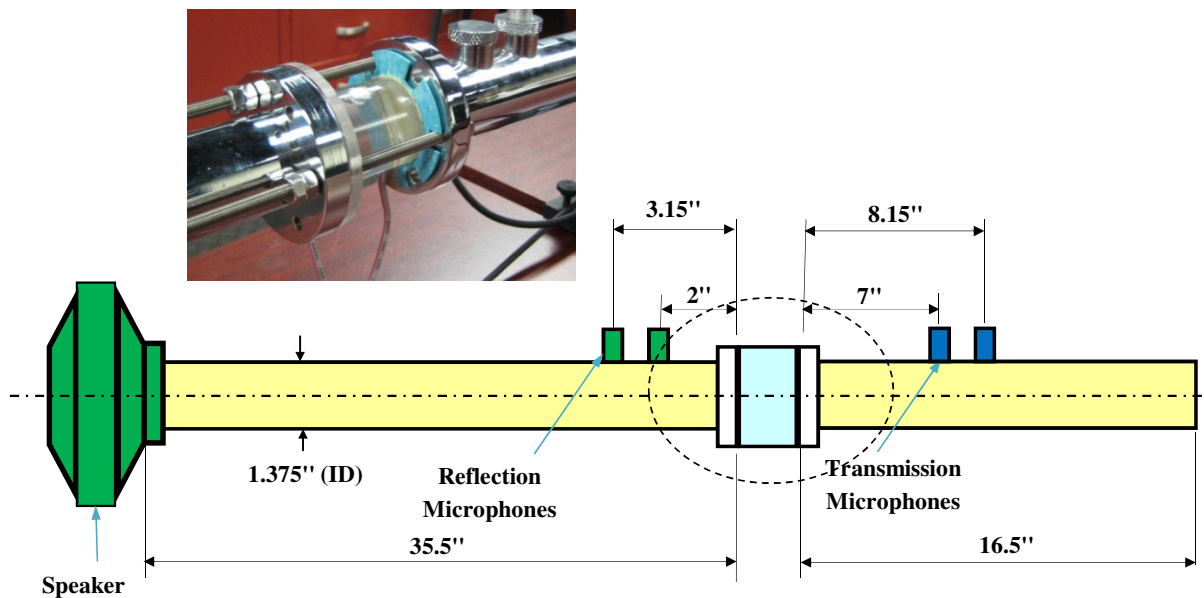


Figure 5.5: Schematic drawing and picture of the impedance tube with attached prototype and transmission loss attachment (Akl and Baz⁷⁷)

5.7: Finite Element Model

In the finite element section of the paper, the authors begin by describing the utilization of the ANSYS® 12.1 software package. The authors used axisymmetric elements of the type FLUID29 for the modeling of the air in the impedance tube as well as the water in the metamaterial cell. Furthermore PLANE223 and PLANE183 elements were used for the piezoelectric component and brass constraining layers respectively. An infinite boundary condition was then applied to eliminate boundary reflections.

The finite element model is then used to predict the pressure values at the locations of the microphones to calculate the acoustic impedance and transmission loss for the model. Figure 5.6 shows the mesh of the finite element cell alone while Figure 5.7 and Figure 5.8 depict the mesh for the entire setup used to attain the pressure values for the acoustic impedance modeling and the transmission loss modeling

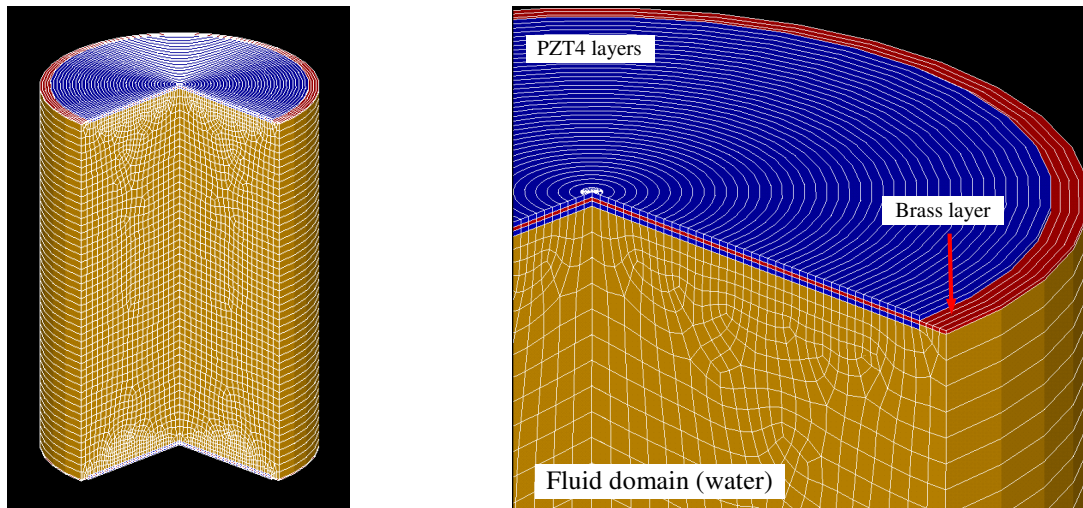


Figure 5.6: Finite element mesh of the engineered metamaterial cell (Akl and Baz⁷⁷)

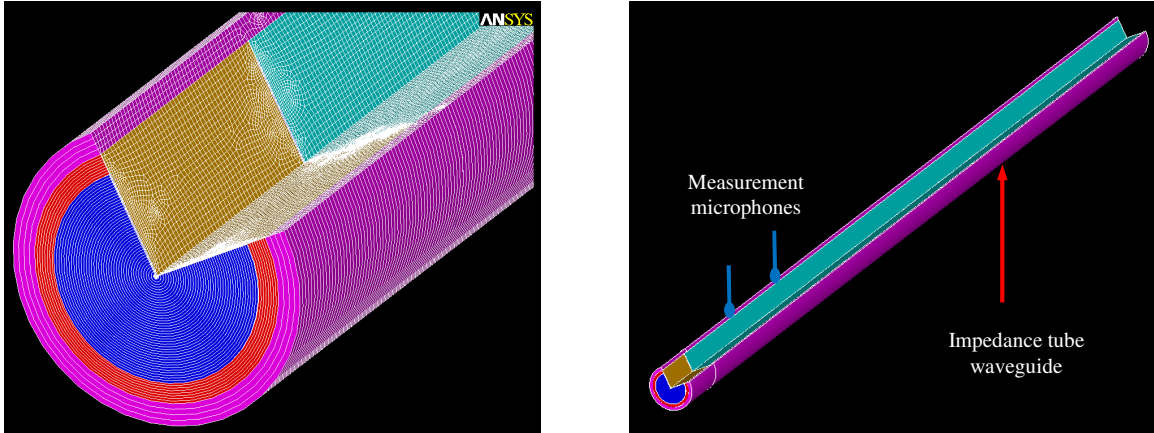


Figure 5.7: Finite element mesh of the engineered metamaterial cell coupled to the impedance tube and the finite element model of the impedance tube with microphone locations (Akl and Baz⁷⁷)

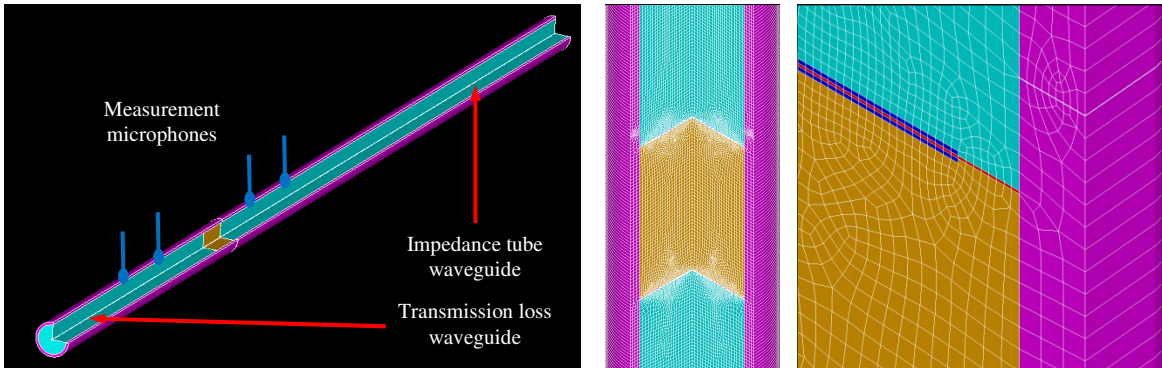


Figure 5.8: Finite element mesh of the engineered metamaterial cell coupled to the impedance tube with transmission loss attachment and the finite element model of the whole transmission loss measuring apparatus with microphone locations (Akl and Baz⁷⁷)

5.8: Results

The following figures depict the results of the modeling and experimental results for real and imaginary components of the acoustic impedance measurements and the transmission loss for the three cases of uncontrolled (Figure 5.9), positive feedback (Figure 5.10), and negative feedback (Figure 5.11) respectively.

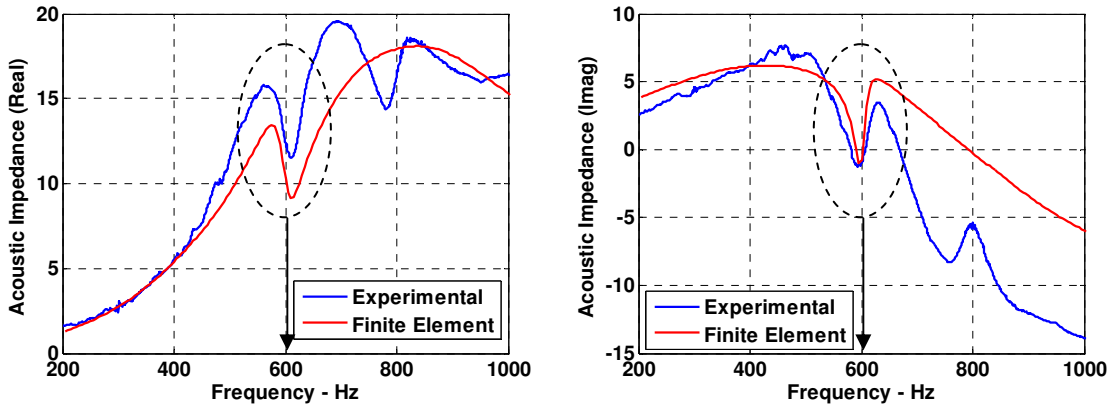


Figure 5.9: Real and imaginary components of the acoustic impedance in the uncontrolled case and comparison with the results obtained from the finite element model (Akl and Baz⁷⁷)

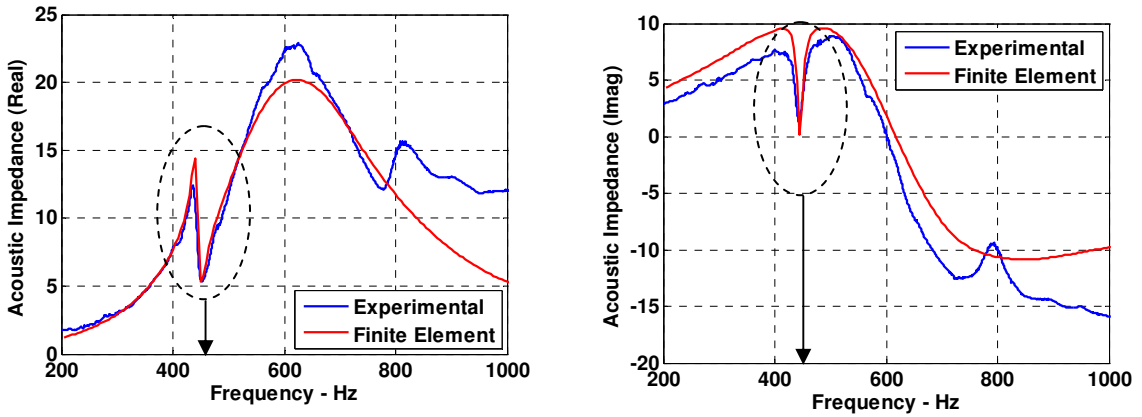


Figure 5.10: Real and imaginary components of the acoustic impedance in the positive feedback control case and comparison with the results obtained from the finite element model (Akl and Baz⁷⁷)

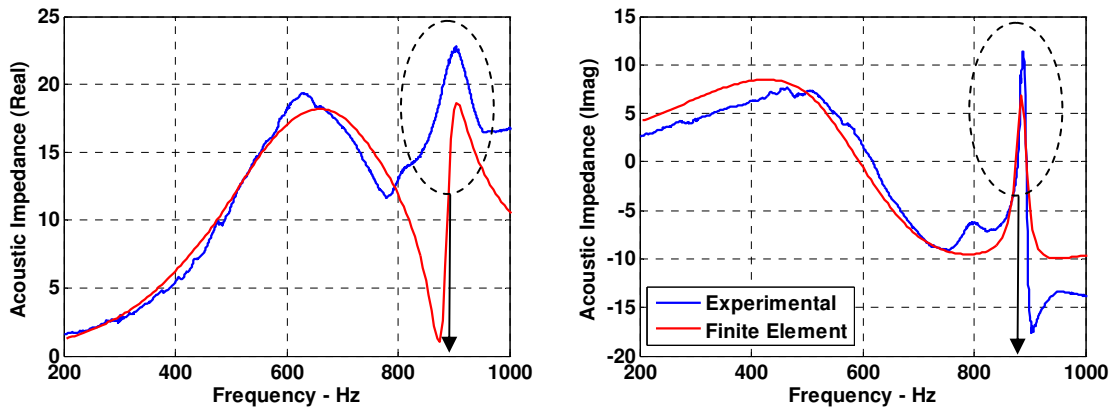


Figure 5.11: Real and imaginary components of the acoustic impedance in the negative feedback control case and comparison with the results obtained from the finite element model (Akl and Baz⁷⁷)

The authors note that there exists an additional node near 800Hz in the actual experiments which they attribute to a possible air bubble that may have leaked into the cavity cell. With the exception of the 800 Hz node, the experimental results match fairly close with those in the finite element model. The authors also note that this is particularly true when finding the locations of the shifting resonance peak. These peaks were shown to be moved from its uncontrolled 600Hz location to 450Hz and 900Hz for the positive and negative feedback gains respectively which corresponds to decreasing and increasing the overall stiffness of the cell as mention before.

The results of the authors' transmission loss measurements and calculations for the uncontrolled case, positive feedback case, and negative feedback case can be found in Figure 5.12, Figure 5.13, and Figure 5.14 respectively.

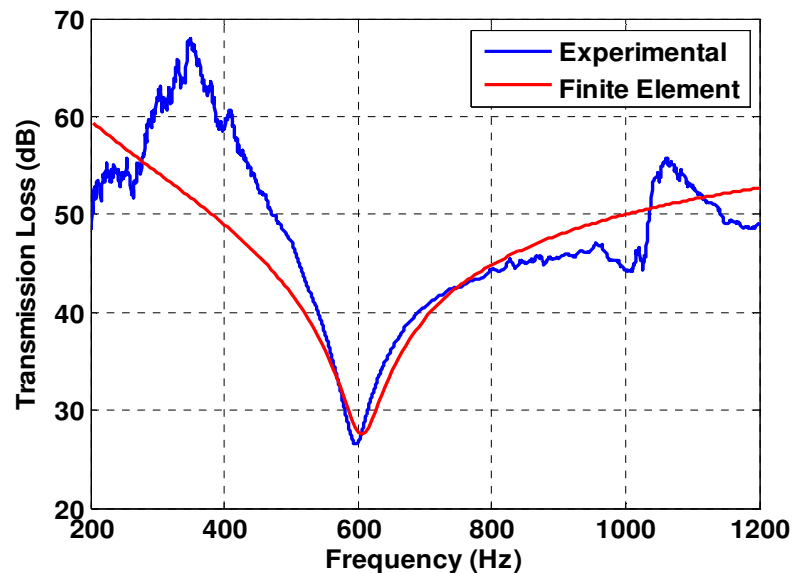


Figure 5.12: Transmission loss measurement of the developed cell and comparison with the results obtained from the finite element model for the uncontrolled case (Akl and Baz⁷⁷)

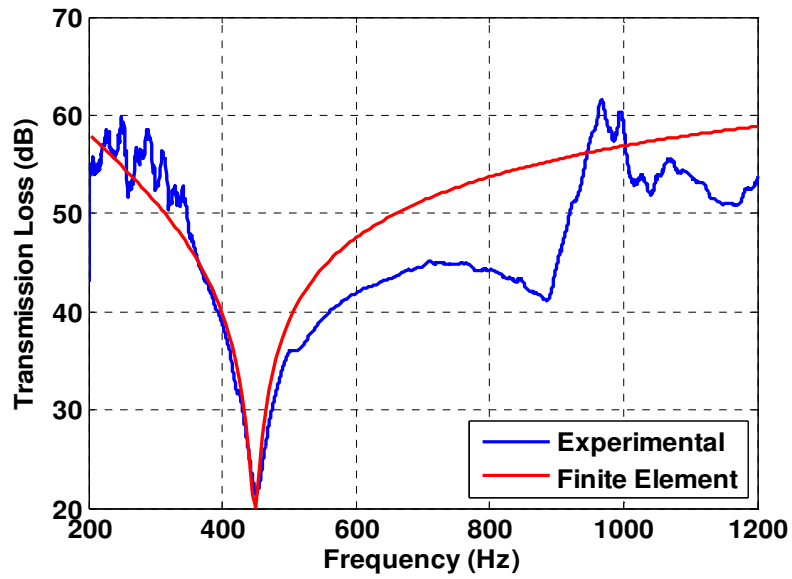


Figure 5.13: Transmission loss measurement of the developed cell and comparison with the results obtained from the finite element model for the positive feedback case (Akl and Baz⁷⁷)

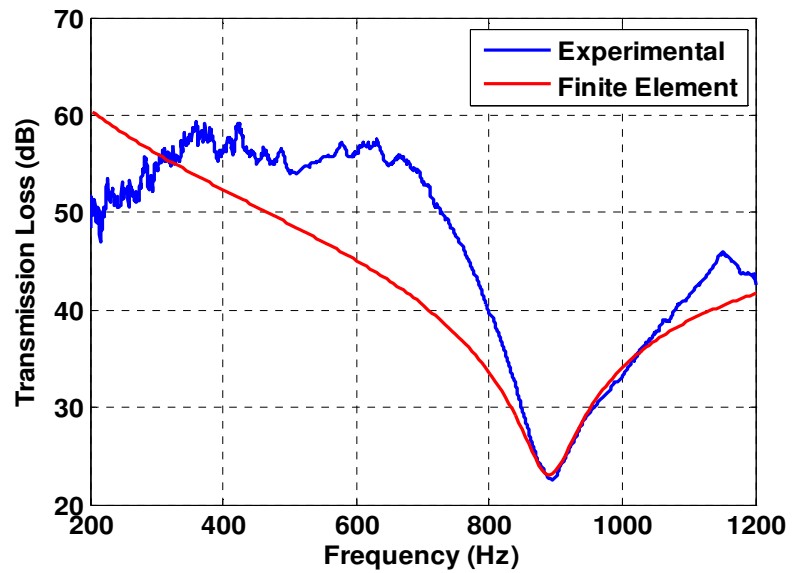


Figure 5.14: Transmission loss measurement of the developed cell and comparison with the results obtained from the finite element model for the negative feedback case (Akl and Baz⁷⁷)

Figures 5.12 through 5.14 illustrates the transmission loss results for the uncontrolled, positive feedback and negative feedback cases respectively. The authors note that a good agreement is found between the experimental results and the calculated values for the transmission loss near the peak values, but admits that larger deviations can be found outside this region. The author attributes these to the complex nature of the damping characteristics and losses in the prototype cell as compared to the simplified viscous damping in the finite element model.

The authors' final two graphs in Figure 5.15 depict the transfer function between the reference microphone and the first and second piezoelectric diaphragms respectively for the uncontrolled and positively controlled cases.

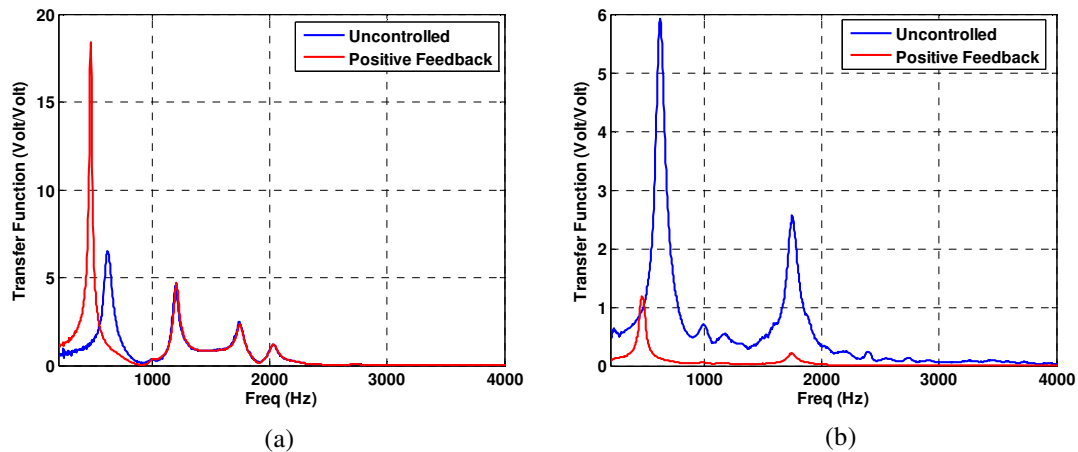


Figure 5.15: (a) Transfer function between the reference microphone and the adjacent piezoelectric diaphragm, (b) Transfer function between the reference microphone and the farther piezoelectric diaphragm (Akl and Baz⁷⁷)

The authors make the case that the only visible frequency shifts in both graphs occur over the targeted frequency range. In the positive feedback case the second piezo shows a reduction of magnitude over the entire spectrum, but the only shift occurs under the single peak in the target range leading to the single degree of freedom nature of the cell.

5.9: Summary

In summary, the authors have shown a characterization of a 1 dimensional metamaterial prototype with active control. The characterization was performed over a frequency range of 200 Hz to 1 kHz with measurements for acoustic impedance and transmission loss. Each of these measurements was taken for the uncontrolled case as well as the positive and negative feedback cases using the ASTM 1050-08 and ISO 10534-2 standards and were compared to values calculated using pressures found with and ANSYS[®] model.

The prototype cell was one based on the paper previously published by Baz⁶³ which is made up of cavity with piezo electric diaphragms for sensing and actuation. The active component of the metamaterial cell allows the prototype to increase as well as decrease stiffness as shown by the variation in peaks in the measurements of the acoustic impedance and transmission loss. The authors used the calculations from a finite element model to validate the experiments that were made. Moreover the transfer functions from the reference microphone the piezo diaphragms showed the one degree for freedom nature of the metamaterial cell for up to 4 kHz which was made apparent by the movement of a single peak with applied control. The author also notes that the strong coupling between the fluid and solid domains is important for the homogeneity of the system.

The authors finish with future work suggestion which involves the array of multiple cells. The author notes that such an arrangement can be thought of as a fluid domain equivalent to an array of spring-mass-damper system with controllable dynamic properties. Control of such dynamic properties with the active piezoelectric element would allow for controllable wave propagation properties.

The following chapter takes the fundamental aspects of the model design in chapter 4 and the experimental investigation described in this chapter to and extends it into the simultaneous control effective density and bulk modulus in a one dimensional metamaterial model.

Chapter 6 : Dually Tunable Effective Density and Bulk Modulus

Chapter 6 is drawn from an anticipated paper co-authored by Baz and Akl in conjunction with the author of this dissertation. The chapter draws from the designs both theoretical and physical to create a design that has simultaneous control of both density and bulk modulus.

6.1: Introduction

Over a decade now, many acoustics researchers have directed their attention towards the field of acoustic metamaterials, which prime objective is to engineer material structures in such a fashion to affect wave propagation pattern that cannot be realized using regular isotropic materials. This is expected and has been already implemented in various wave and noise control applications by Romero-García *et al.*⁸⁹ and Sánchez-Dehesa *et al.*¹¹¹, where in both cases, the authors have managed to create an acoustic stop band using periodic arrangements of cylinders that filtered out a noise bandwidth preventing it from propagating to the other side of the metamaterials domain. The concept behind acoustic metamaterials lies in designing the periodic structure to achieve certain values of the bulk modulus B and/or density ρ in the periodic cell (micro) scale to realize bulk modulus and/or density distributions in the structure (macro) scale that would yield pre-determined acoustic wave propagation patterns.

So far various attempts have been dedicated in changing the periodic cell bulk modulus OR the density separately. For the bulk modulus, two different approaches have been reported; the first approach focuses on combining two different isotropic materials

in a composite form to yield anisotropic properties that can influence the spatial wave propagation patterns^{80,83,112}. In the second approach, acoustic impedance mismatch is introduced along the path of wave propagation by integrating flexible sections into the rigid-walled ducts in order to vary the speed of sound and effective bulk modulus at these sections^{101,103}. Manipulation of the material density on the other hand has also been reported using two approaches; the first was by combining two different materials with different densities in a specific spatial arrangement that would yield homogenized value of the density all over the domain^{113,114,115} using phononic devices. In the second approach, the concept of dynamic density, which depends on the neighboring material stiffness, was implemented. This approach was manifested in the attempts of synthesizing prescribed dynamic acoustic densities in fluid domains by introducing lattice systems of mass-in-mass units^{71,116,117}. These attempts were merely focused on introducing negative effective density motivated by the mathematical analogy between acoustic and electromagnetic waves, where theoretical possibility of having negative electromagnetic permittivity and permeability was introduced by Pendry¹¹⁸.

In all the aforementioned attempts the focus was directed on either the bulk modulus or the dynamic density separately and passive metamaterials with fixed material properties were considered. The operating bandwidth limitation and the cross-influence of the density variation on the bulk modulus and vice versa have seriously limited the applicability of the proposed techniques. Initial attempts of introducing active piezoelectric elements in the periodic structure arrangement has been reported in the last few years^{92,93,119}, where the authors have introduced an electro-acoustic analogy model for periodic cell structure composed of fluid domain confined from both sides with

piezoelectric diaphragms to control the bulk modulus B or the density ρ . Doing so, the authors have managed to realize arbitrary effective bulk modulus OR density values above or below the nominal values of the fluid domain they are embedded in. The research has extended to physically realize the configuration for controlling the dynamic density. Controlling both the density and bulk modulus simultaneously has however not yet been introduced.

In the current paper, a cell forming the base of a periodic metamaterial structure has been developed using two piezoelectric diaphragms to control both the density and the bulk modulus simultaneously. In the proposed arrangement, the first piezoelectric diaphragm represents the flexible end of a Helmholtz resonator coupled to the fluid domain, while the second diaphragm is confining the fluid domain in the cell as presented in Figure 6.1. Controlling the first and second diaphragms separately affects the effective bulk modulus and density respectively. Electro-acoustic model as well as experimental verifications of the concept is introduced in the following sections.

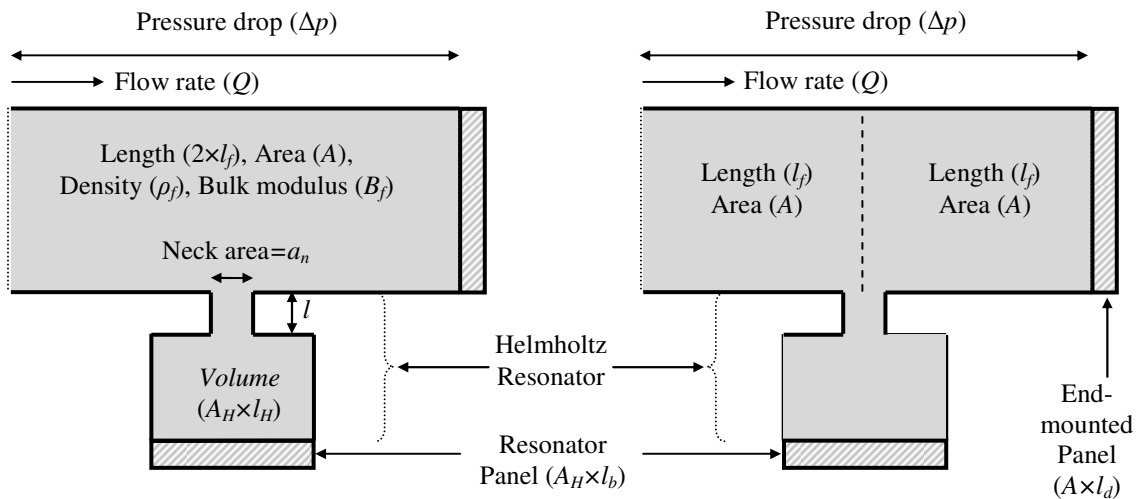


Figure 6.1: Schematic of the developed cell for density and bulk modulus control

6.2: Electro-Acoustic Analogy

A one dimensional acoustic cavity with uniform cross-sectional area A and length $2l_f$, subject to acoustic pressure drop Δp resulting in volumetric flow rate Q , is considered. The fluid inside the cavity is characterized with static fluid density ρ_f and bulk modulus B_f . The value of Q depends on three major forces; inertia forces due to the mass of the fluid inside the cavity, elastic forces due to the “stiffness” of the entrapped fluid volume and finally friction and damping forces, which are ignored in the current analysis.

6.2.1: Inertial Forces

Newton’s second law necessitates that the net force due to the pressure difference Δp equals the rate of change of fluid momentum as given by Eq. (1)

$$A\Delta p = \rho_f l_f A \frac{dv}{dt} \quad (6.1)$$

where v is the particle velocity.

For a uniform velocity along the cavity length, $\frac{dQ}{dt} = A \frac{dv}{dt}$. Rewriting (1) yields:

$$A\Delta P(s) = \rho_f l_f s Q(s) \quad (6.2)$$

where s is the Laplace operator. Hence,

$$\frac{\Delta P(s)}{Q(s)} = \frac{\rho_f l_f}{A} s = L_F s = Z_{LF}(s) \quad (6.3)$$

$Z_{LF}(s)$ denotes the inertial impedance of the cavity and is equal to the amount of pressure difference needed in order to drive a unit volume flow rate of the fluid inside the

cavity, which is proportional to the density of the fluid and the length of the cavity, while inversely proportional to its cross sectional area.

6.2.2: Elastic Forces

The second type of forces is due to the “stiffness” of the fluid inside. A pressure drop of Δp across the cavity will cause the fluid to be “strained” due to a change in its volume Vol by an amount of $d(Vol)$.

$$\varepsilon_v = -\frac{d(Vol)}{Vol} \quad (6.4)$$

and since the bulk modulus B_f is defined as the difference in pressure which yields a unit volume strain, Δp is defined as:

$$\Delta p = -B_f \frac{d(Vol)}{Vol} \quad (6.5)$$

The change in volume $d(Vol)$ along a period of time dt is defined as: $d(Vol) = -\int Q dt$. Hence applying Laplace transformation to Eq. (6.5) results in:

$$\Delta P(s) = \frac{Q}{s} \frac{B_f}{Al_f} \quad (6.6)$$

Consequently, the elastic impedance $Z_{CF}(s)$ equals:

$$Z_{CF}(s) = \frac{\Delta P(s)}{Q(s)} = \frac{1}{C_F s} = \frac{1}{s} \frac{B_f}{Al_f} \quad (6.7)$$

The total impedance of the straight cavity is therefore given as:

$$Z_t(s) = Z_{LF}(s) + Z_{CF}(s) = \frac{\rho_f l_f s}{A} + \frac{B_f}{Al_f s} \quad (6.8)$$

Utilizing the electro-acoustic analogy, the Helmholtz resonator is introduced adding to the total impedance of the proposed metamaterial cell. The mechanical stiffness and mass of the flexible panel coupled to the acoustic cavity are modeled using an ideal transformer, which in this case, couples the mechanical and the acoustical domains, where the transformation ratio is the surface area of the flexible panel. This is valid for the flexible panel mounted at the end of the fluid cell as well as that at the end of the Helmholtz resonator. The components in the mechanical side of the transformer are transferred to the acoustical side taking the transformation ratio into consideration. In the mechanical side the current would represent the mechanical velocity \dot{x} , the voltage drop would represent the mechanical force F and the system spring and mass would be represented by a capacitor $C_D = 1/K_D$ and inductor $L_D = M_D$ in the electrical circuit respectively. From equation (6.8), the acoustic mass and stiffness in each cavity section is represented by the inductor $L_F = \frac{\rho_f l_f}{A}$ and capacitor $C_F = \frac{A l_f}{B_f}$ respectively. The Helmholtz resonator is also represented as fluid inductance L_H , fluid capacitance C_H coupled with inductance L_B and capacitance C_B of the Helmholtz resonator flexible panel.

Putting all of the inductances and capacitances in one electrical circuit introduces the electrical analogous circuit shown in Figure 6.2, where Helmholtz resonator mass $M_H = \rho_f \times l \times a$, stiffness $K_H = B_f a^2 / (A_H \times l_H)$, a is the Helmholtz resonator's neck cross sectional area, l is its neck length, A_H and l_H are the resonator cavity's cross sectional area and length respectively.

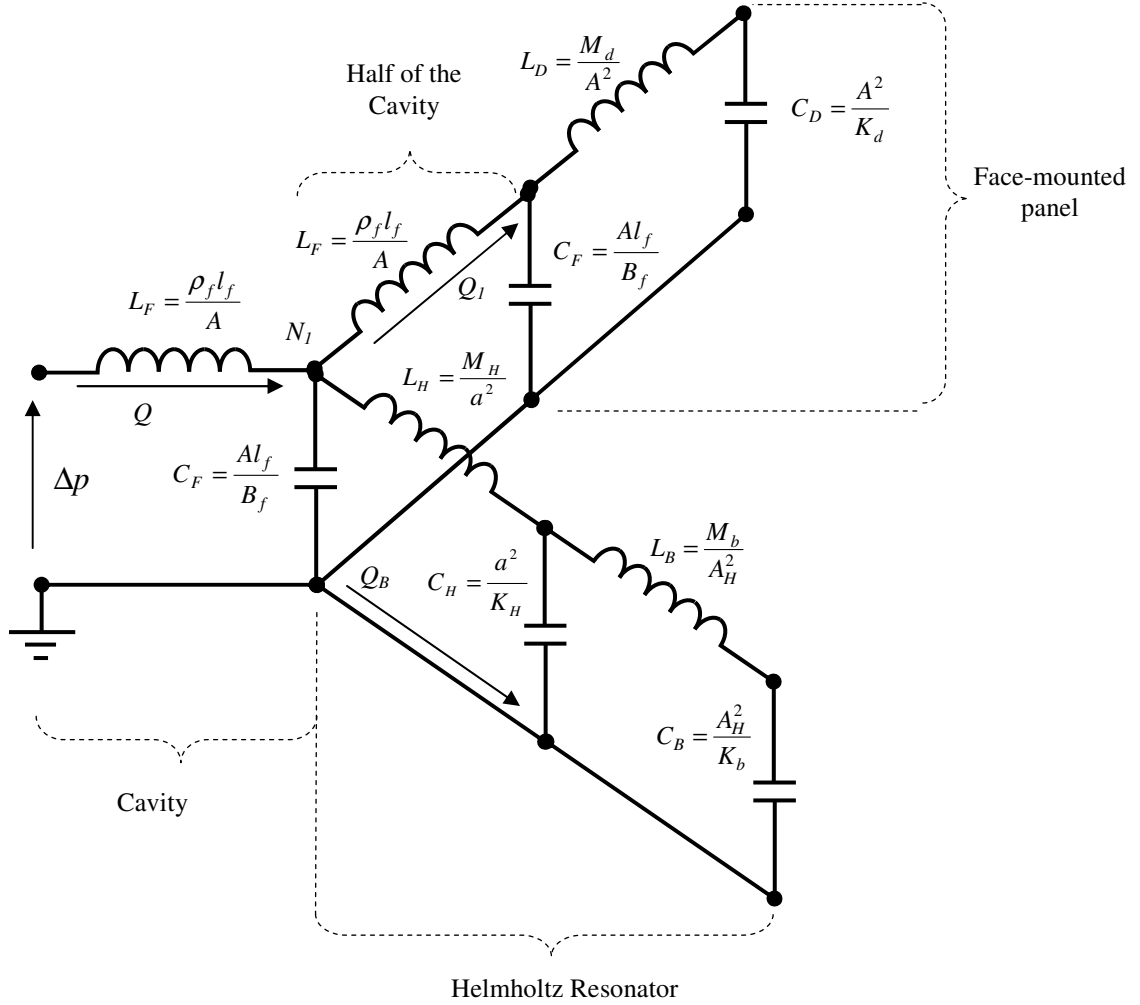


Figure 6.2: Electrical circuit analogous to the cavity with Helmholtz Resonator

From the circuit presented in Figure 6.2, the effective density and bulk modulus for the cavity can be calculated by considering volumetric rate of change of the acoustic cavity given as:

$$\dot{p} = -B_e \frac{Q - Q_H}{2Al_f} \quad (6.9)$$

$$\frac{\Delta p}{2l_f} = -\rho_e \frac{Q}{A_f} \quad (6.10)$$

where B_e , ρ_e is the effective bulk modulus and density respectively.

Equations (6.9) and (6.10) are two coupled equations, from which the effective bulk modulus B_e and density ρ_e can be calculated. However in the current scenario, the values of B_e and ρ_e are prescribed according to the wave propagation pattern dictated by the application of the metamaterial. Hence, the same equations can be used to calculate the stiffness of the two flexible diaphragms (K_b and K_d) that would yield the targeted values of B_e and ρ_e . Using electrical circuit reduction techniques the overall impedance Z_t can be calculated, which is a function of both K_b and K_d . Now let the junction of the two halves of the resonator and the cavity be node N_1 as in Figure 6.2. Using simple circuit analysis, one can find that the pressure at N_1 can be calculated as:

$$p_1 = p \left(1 - \frac{Z_{LF}}{Z_t} \right) \quad (6.11)$$

Recall that for the over all system

$$Q = p / Z_t. \quad (6.12)$$

In turn, the volume flow rate into the Helmholtz resonator is described by:

$$Q_H = \frac{p_1}{Z_H} \quad \text{or} \quad Q_H = \frac{p \left(1 - \frac{Z_{LF}}{Z_t} \right)}{Z_H}. \quad (6.13)$$

Equations (6.11) and (6.12) can then be used with (6.9) to calculate the effective bulk modulus B_e :

$$B_e = \frac{2Al_f s Z_B Z_t}{Z_t - Z_B - Z_{LF}} \quad (6.14)$$

And the density ρ_e is calculated as be as:

$$\rho_e = \frac{AZ_t}{2l_f} \quad (6.15)$$

where Z_B is the impedance of the Helmholtz resonator (cavity and piezoelectric panel) and Z_{LF} is the impedance of the fluid cavity of length l_f . Solving equations (6.14) and (6.15) simultaneously for any given B_e and ρ_e , results in the stiffness values (K_b and K_d) to achieve these effective cell properties.

For a cavity of 5cm length and $25 \times 10^{-4} \text{ m}^2$ cross sectional area, filled with water, the effective bulk modulus and effective density as a function of frequency are as shown in Figure 6.3. In Figure 6.3a, the bulk modulus starts with the static value of water ($2.25 \times 10^9 \text{ Pa}$) and drops as the excitation frequency increases. In Figure 6.3b, the linear and log scale frequency dependent dynamic density is presented, where it starts at high negative value at very low frequency and approaches the nominal value for water (1000 kg/m^3) as the excitation frequency increases. The shown peak occurs at the cavity resonance. Hence it is evident from these two plots that both the bulk modulus and the density are frequency dependent and vary dramatically with the excitation frequency. Hence in order to maintain a required wave propagation pattern over a wide frequency range within a domain, the density and bulk modulus of that domain have to maintain specific values over that frequency spectrum. This is why actively controlling the stiffness of both the face- and side-mounted panels is crucial in that sense.

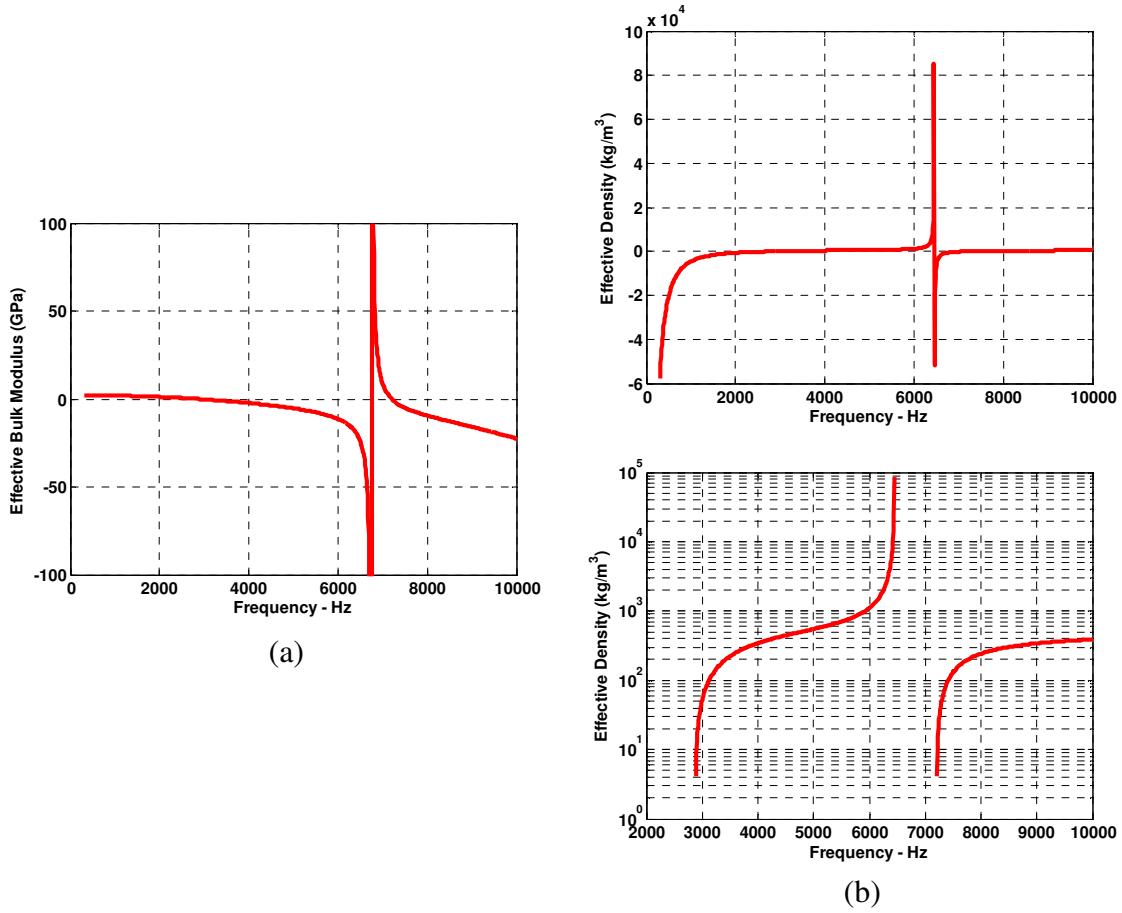


Figure 6.3: Uncontrolled homogenized bulk modulus and density for a cavity with Helmholtz resonator

Replacing the flexible panels with active piezoelectric elements upgrades the developed coupled acoustic cavity from passive to active nature, where the stiffness of both panels can be controlled using the piezoelectric electro-mechanical coupling factor.

The basic constitutive equation for a piezoelectric material is given by:

$$\begin{Bmatrix} S \\ D \end{Bmatrix} = \begin{bmatrix} s^E & d \\ d & \varepsilon \end{bmatrix} \begin{Bmatrix} T \\ E \end{Bmatrix} \quad (6.16)$$

where S = strain, D = electrical displacement, T = stress, E = electrical field, s^E =compliance, d = piezoelectric strain coefficient, and ε = permittivity. Equation (6.16) can be rewritten for active Helmholtz resonator and face-mounted piezoelectric panel as:

$$\begin{Bmatrix} \Delta Vol_b \\ q_b \end{Bmatrix} = \begin{bmatrix} C_B & d_{A_H b} \\ d_{A_H b} & 1/Z_{P_b S} \end{bmatrix} \begin{Bmatrix} \Delta p_b \\ V_b \end{Bmatrix}, \quad \begin{Bmatrix} \Delta Vol_d \\ q_d \end{Bmatrix} = \begin{bmatrix} C_D & d_{A_d} \\ d_{A_d} & 1/Z_{P_d S} \end{bmatrix} \begin{Bmatrix} \Delta p_d \\ V_d \end{Bmatrix} \quad (6.17)$$

where $q_{d,b}$, $\Delta Vol_{d,b}$ = electrical charge and change in face- and Helmholtz resonator mounted panels volume respectively. $\Delta p_{d,b}$ and $V_{d,b}$ = pressure and voltage applied to both panels. $C_{D,B} = 1 / K_{D,B}$ is panels compliance and Z_{P_d}, Z_{P_b} are the electrical impedances for the face and Helmholtz resonator panels respectively. Using the piezo-diaphragm as a self-sensing actuator, then the second row of equation (6.17) gives, for a short-circuit piezo-sensor, the following expressions:

$$q_b = d_{A_H b} \Delta p_b, \quad q_d = d_{A_d} \Delta p_d \quad (6.18)$$

Then, the voltage $V_{d,b}$ applied to both face- and side mounted panels can be generated by a direct feedback of the charge $q_{d,b}$ such that:

$$V_d = -G_d d_{A_d} \Delta p_d, \quad V_b = -G_b d_{A_H b} \Delta p_b \quad (6.19)$$

Then, the first row of equation (39) yields:

$$\Delta Vol_d = (C_D - d_{A_d}^2 G_d) \Delta p_d = C_{DC} \Delta p_d, \quad \Delta Vol_b = (C_B - d_{A_H b}^2 G_b) \Delta p_b = C_{BC} \Delta p_b \quad (6.20)$$

where C_{DC} and C_{BC} = Closed-Loop Compliance of piezoelectric face-mounted and Helmholtz panels respectively. The equivalent electric circuit for the composite cavity with active Helmholtz resonator and face-mounted panel is shown in Figure 6.4.

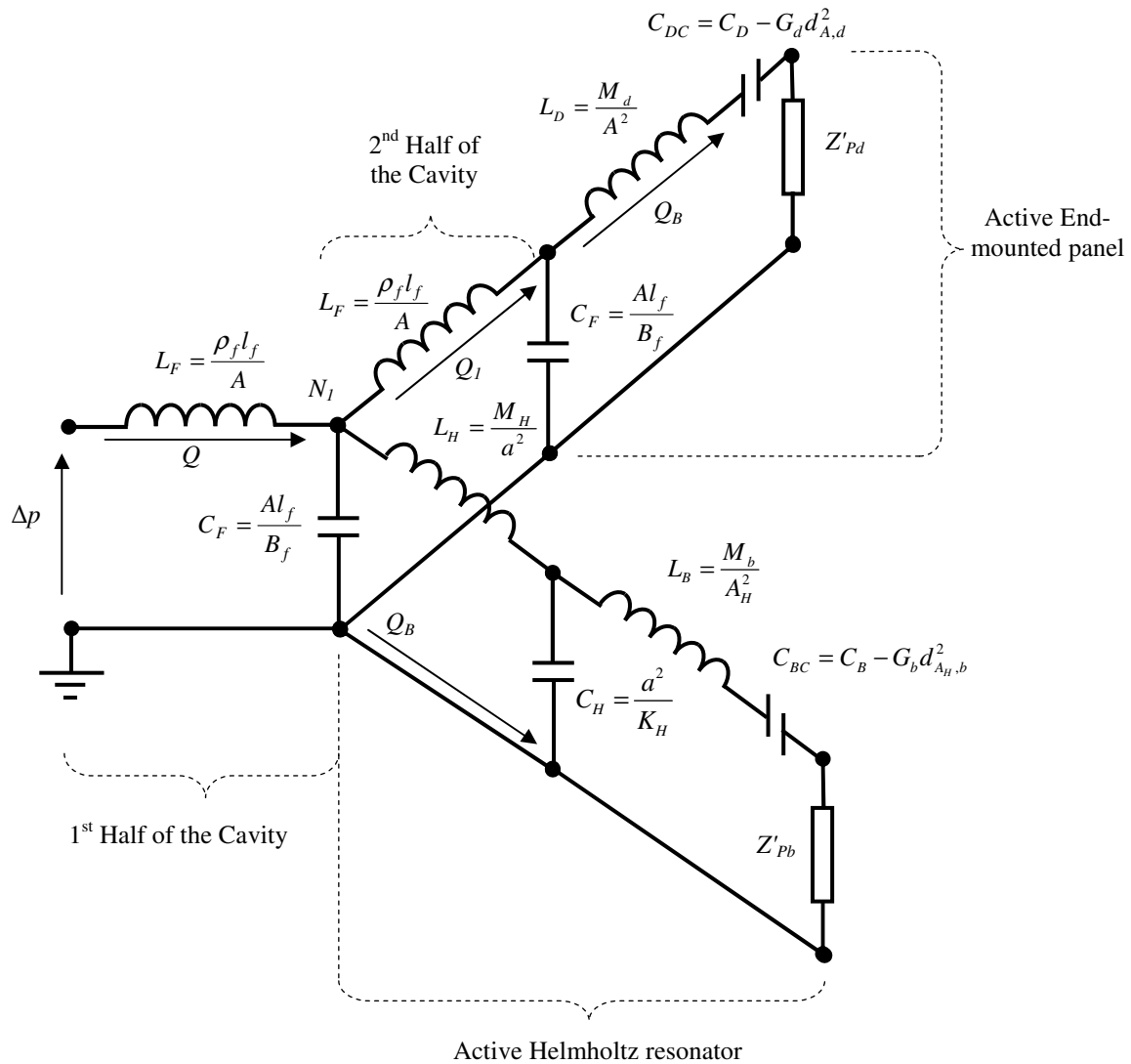


Figure 6.4: Electrical circuit analogous to the cavity with active Helmholtz resonator

A feedback control system has been applied to a cavity with the same parameters whose acoustic properties are plotted in Figure 6.3. The objective of the feedback algorithm was to control the stiffness of both the face-mounted and Helmholtz resonator piezoelectric panels to realize a composite cell filled with water that has an overall homogenized bulk modulus and density which are both 20 times that of water in one case (as shown in Figure 6.5) and 0.05 times in another case (as shown in Figure 6.6).

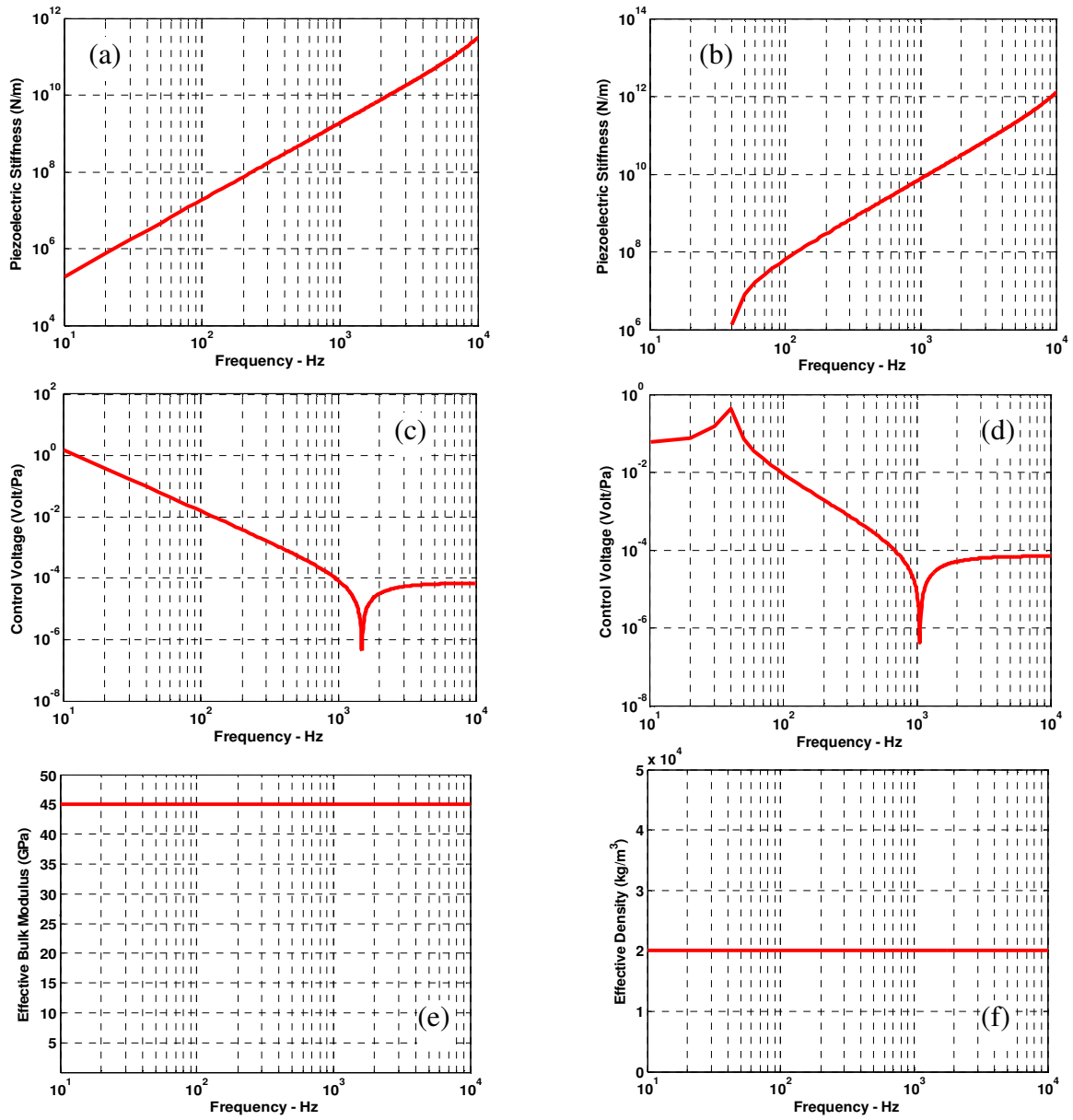


Figure 6.5: (a,c) Stiffness and control voltage for Helmholtz resonator (b,d) Stiffness and control voltage for end-mounted panels. (e,f) resultant homogenized bulk modulus and density (for 20 times that of water)

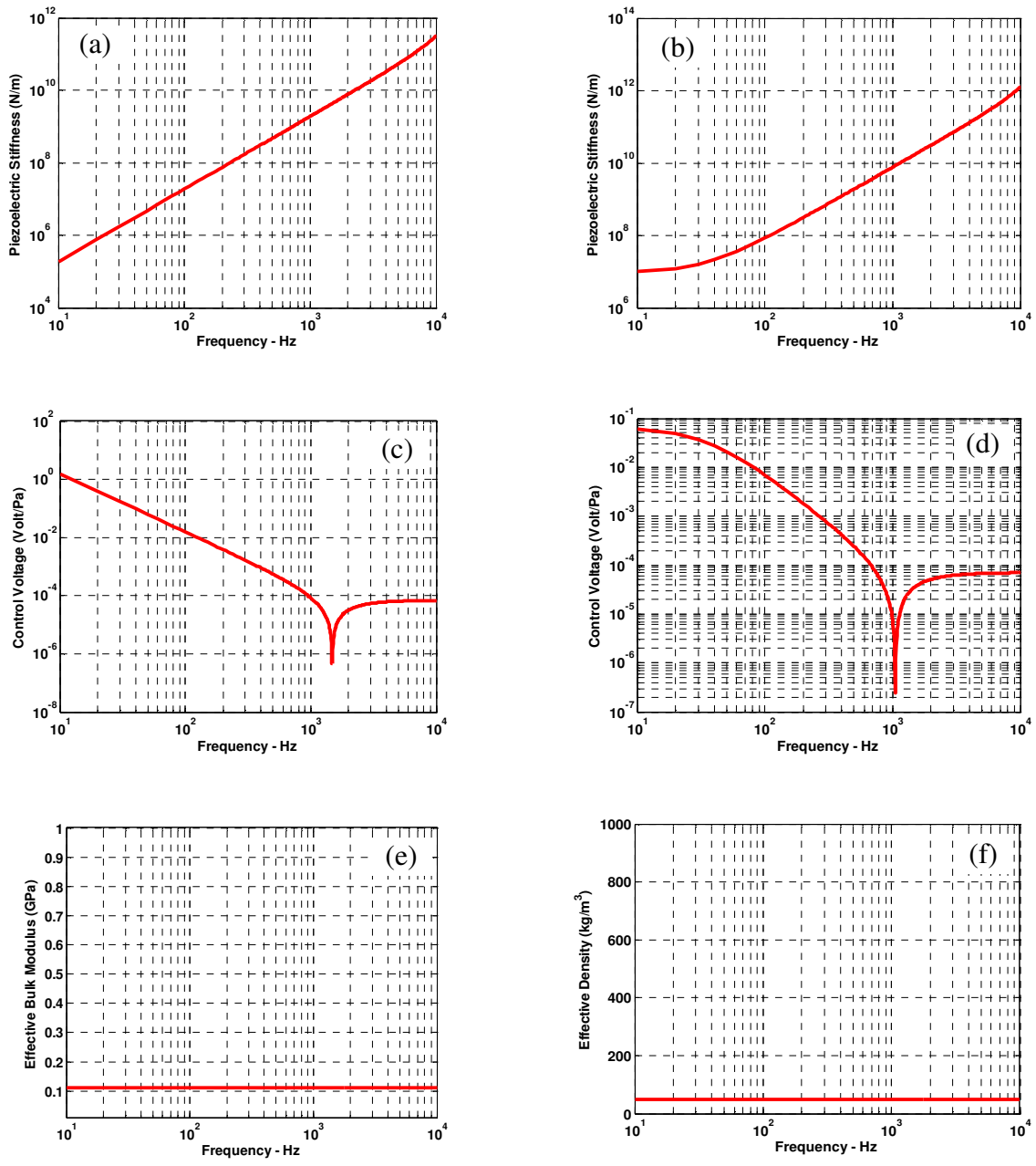


Figure 6.6: (a,c) Stiffness and control voltage for Helmholtz resonator (b,d) Stiffness and control voltage for end-mounted panels. (e,f) resultant homogenized bulk modulus and density (for 0.05 times that of water)

6.3: Experimental Realization of the Active Metamaterial Cell

The proposed active acoustic metamaterial cell investigated in this work is composed of three different materials as shown in Figure 6.7. Water, in a cylindrical pipe, is confined from both ends with two PZT4 piezoelectric bimorphs. In the middle of the acoustic cavity a Helmholtz resonator cavity has been attached, in which the rigid cap is replaced with the same PZT4 bimorph as in the main cavity. The bimorph itself is composed of intermediate Brass disk with PZT4 layers deposited on both surfaces. The internal cell diameter is 0.035m, its overall length is 0.045m and the overall diaphragm thickness is 0.5mm of which 0.135mm Brass intermediate disk thickness. The material properties of the piezoelectric bimorph components are listed in Table 6.1.

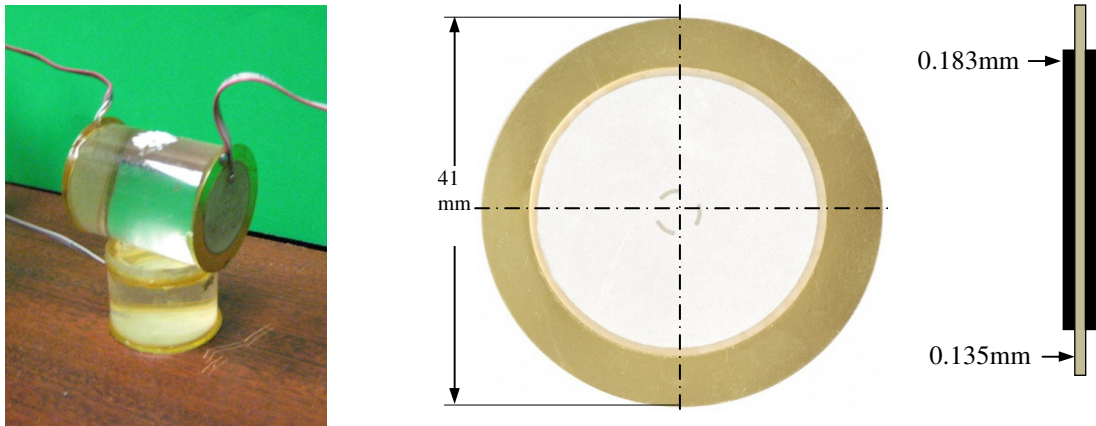


Figure 6.7: Construction and dimensions of the proposed active acoustic metamaterial cell

Table 6.1: Material Properties

MATERIAL PROPERTY	VALUE
Frequency	1.3 kHz
Capacitance @ frequency	150,000 pF @ 1kHz
Voltage Input (Maximum)	30V p-p
Impedance	200 Ohm

The cell is built by cutting the confinement Acrylic cylinder to the required length (for both the main fluid cavity and the Helmholtz resonator) and drilling a 3mm hole in the middle of its surface. The piezoelectric bimorph diaphragms are wired, then coated with electrical insulating coating and then glued to the annular faces of the cylinder confining a fixed volume. Water is then injected through the 3mm circumferential hole until it fills the entire cylindrical volume leaving no air bubbles inside the cell. The hole is then sealed, leaving a composite water-PZT metamaterial cell for testing and evaluation. The main cavity length ($2 \times l_f$) = 44.5mm, diameter = 32.6mm, Helmholtz resonator cavity length (l_H)=22.25mm, diameter = 32.6mm, Helmholtz resonator neck length (l) = 3mm and diameter = 3mm.

The basic concept of the AAMM lies (as illustrated in Figure 6.8) in that the (sensing bimorph) measures the acoustic pressure passing throughout the cell and submits the measured signal to a feedback control circuit to generate a consequent control signal to the actuating bimorphs via a power amplifier to change their stiffness. Due to the incompressible nature of the confined fluid, direct coupling to the actuating bimorphs is established forming a homogeneous fluid-solid domain that acts as a single degree of freedom (DOF) system, provided the excitation wavelength is much larger than the dimension of the entire composite cell. Hence, changing the stiffness of one of the actuating piezoelectric bimorphs affects directly the stiffness of the second one, resulting in a controllable dynamic density (resulting from the effect of the face-mounted bimorph) and the bulk modulus (resulting from the effect of the Helmholtz mounted bimorph) of the entire single DOF fluid domain as demonstrated in the electrical-acoustic circuit presented in Figure 6.4.

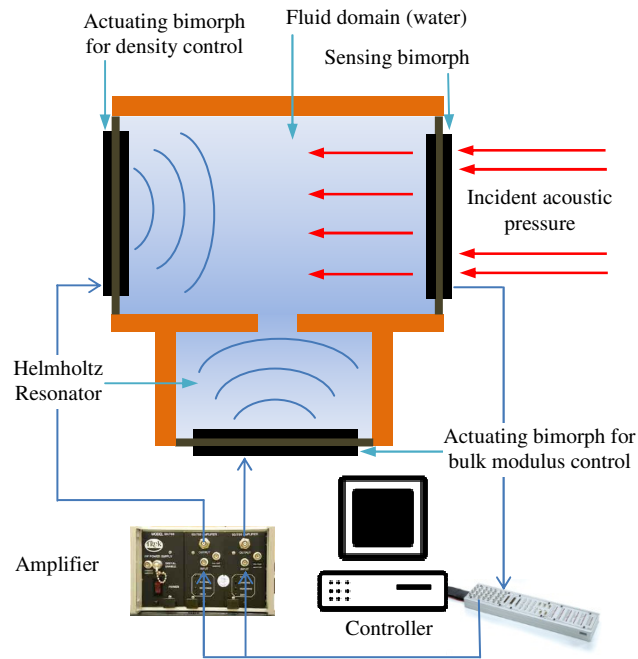


Figure 6.8: Schematic of the operation mechanism of the proposed cell

6.4: Experimental Verification

The verification process is carried out on two steps. In the first step, the face-mounted piezoelectric diaphragm (responsible for density control) is controlled, while the Helmholtz resonator mounted piezoelectric diaphragm (responsible for bulk modulus control) is maintained uncontrolled. In the second step, the opposite is carried out.

6.4.1: Density Control (First Step)

Figure 6.9 illustrates the frequency response of the face-mounted diaphragm in the uncontrolled, positive and negative feedback control gains. Figure 6.10 on the other hand is the frequency response of the Helmholtz resonator mounted piezoelectric

diaphragm as a result of the control of the face mounted one. In order to verify the change of dynamic density in the cell cavity, the pressure gradient inside the cavity is measured using the face-mounted piezoelectric diaphragm and a third diaphragm mounted on the opposite end of the fluid cavity. The response of each of these sensors represents the pressure inside the cavity measured at the cavity ends. Figure 6.11 illustrates the relative pressure gradient change as a result of both positive and negative feedback gains.

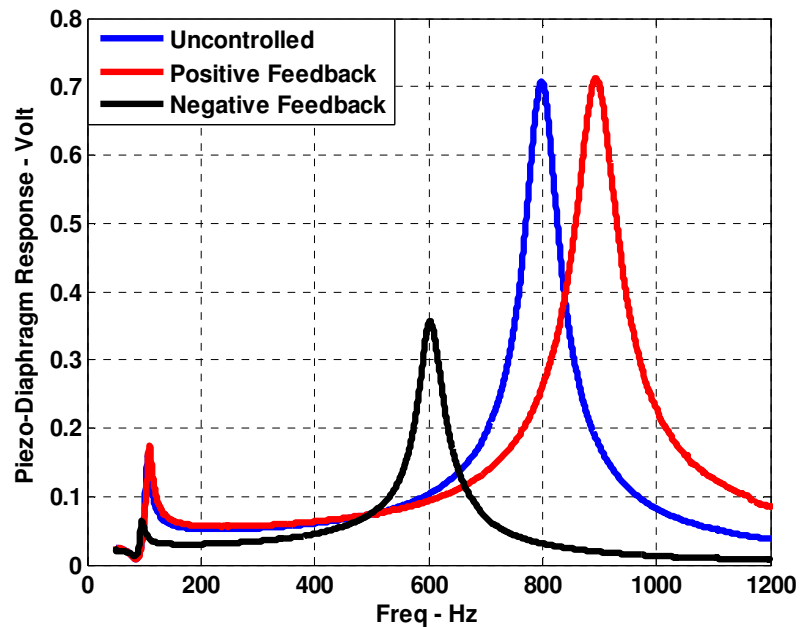


Figure 6.9: Frequency response of face-mounted piezoelectric diaphragm

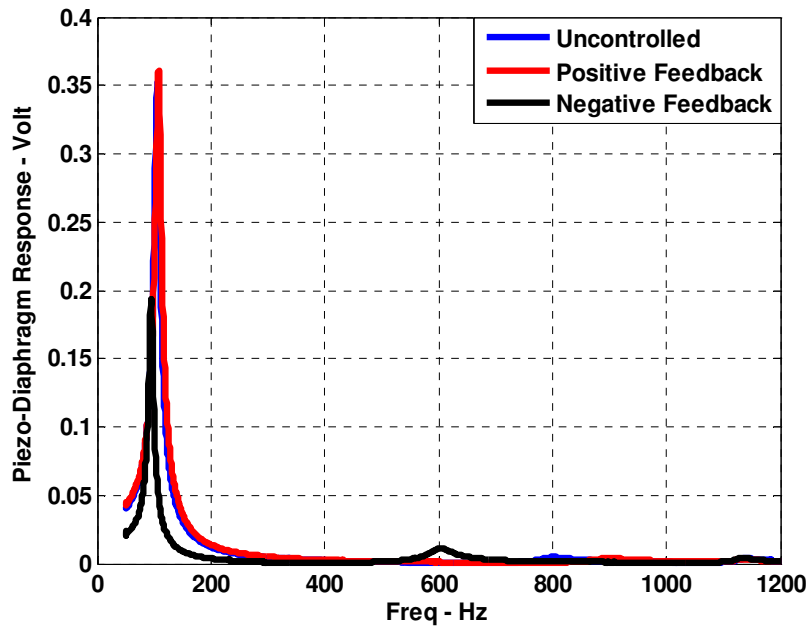


Figure 6.10: Frequency response of Helmholtz resonator mounted piezoelectric diaphragm

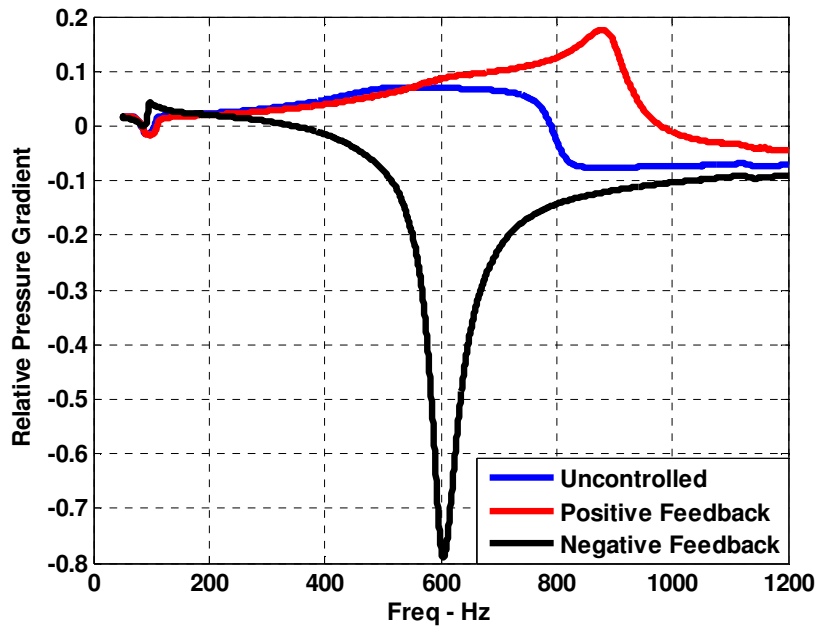


Figure 6.11: Frequency response of the pressure gradient in the uncontrolled and controlled cases

6.4.2: Bulk Modulus Control (Second Step)

Figure 6.12-14 illustrate the same spectra for the case of uncontrolled, positive and negative feedback control gains applied to the Helmholtz resonator mounted piezoelectric diaphragm.

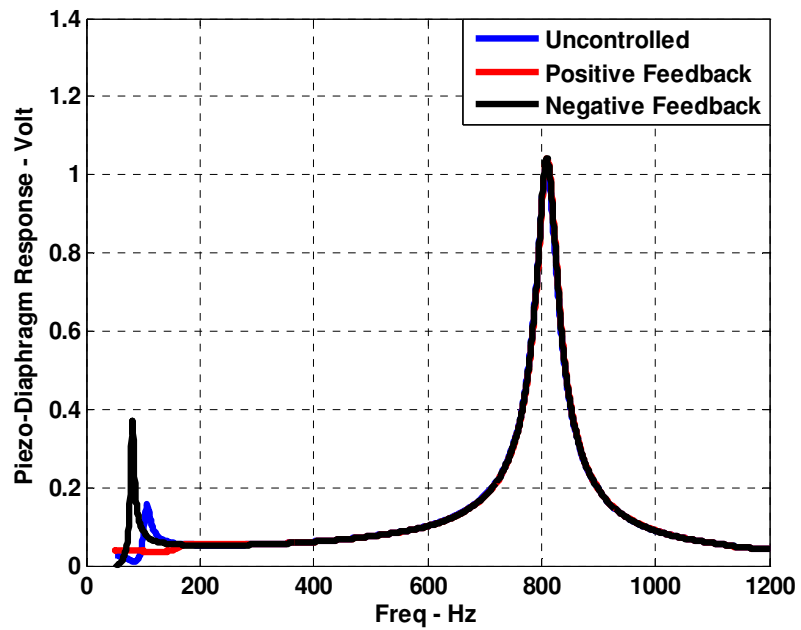


Figure 6.12: Frequency response of face-mounted piezoelectric diaphragm

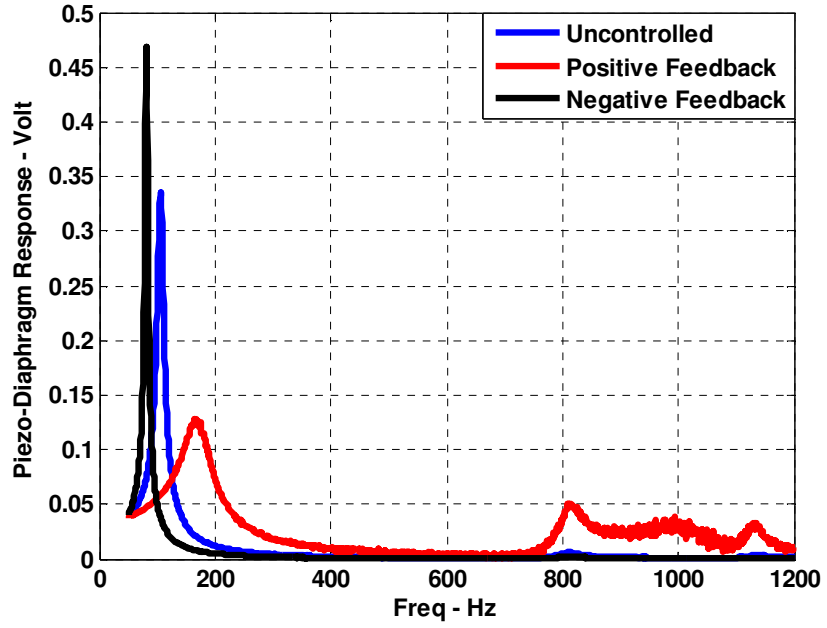


Figure 6.13: Frequency response of Helmholtz resonator mounted piezoelectric diaphragm

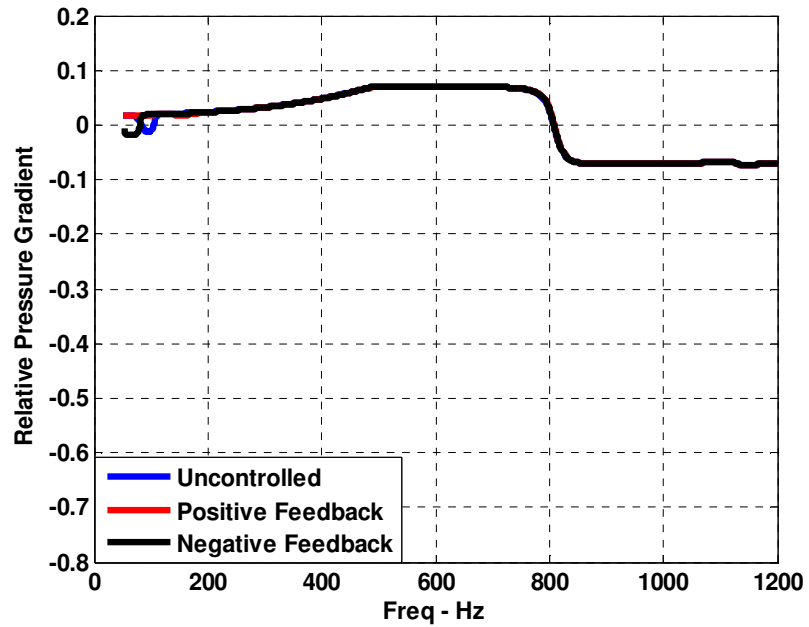


Figure 6.14: Frequency response of the pressure gradient in the uncontrolled and controlled cases

6.5: Summary and Conclusions

Based on the results obtained from the experimental measurements, it is evident that the composite acoustic metamaterial cell is acting as a single DOF system, whose natural frequency for the uncontrolled cases is 800 Hz. The Helmholtz resonator resonance frequency was measured to be 105 Hz. Applying positive/negative feedback control on the face mounted piezoelectric diaphragm has affected the main cavity natural frequency without significant effect on the Helmholtz resonator cavity as illustrated in Figure 6.10. Since the pressure gradient is a direct measure of the density in acoustic cavities, the gradient was measured using the two end-mounted piezoelectric diaphragms, which (as illustrated in Figure 6.11) reveals significant increase/decrease in the density of the fluid cavity, which eliminates the possibility that the resonance change in the uncontrolled, positive and negative feedback cases might be due to bulk modulus changes. Applying the same feedback control actions to the Helmholtz resonator mounted piezoelectric diaphragm didn't affect the resonance frequency of the main cavity, nor did it affect the pressure gradient as compared to the first case. However, significant effect on the Helmholtz resonator resonance frequency was measured. The Helmholtz resonance has ranged from 81 to 168Hz due to the negative and positive feedback control respectively. Projection of the Helmholtz resonator effect on the main cavity frequency response without significant change of the pressure gradient in that frequency band is an evident of the change of the main acoustic cavity's bulk modulus.

Hence an active acoustic metamaterial with programmable density and bulk modulus has been developed. Analytical analysis using electro-acoustic analogy has been developed. An active composite cell coupled with active Helmholtz Resonator was

manufactured and control actions were applied to both piezoelectric elements in the main cavity and in the Helmholtz resonator to change the density and the bulk modulus of the main cavity. The frequency band in which the density has been significantly controlled was 600-900Hz, while that in which the bulk modulus has been significantly controlled was 81-168Hz. Cross-effect of the two active elements is negligible, emphasizing the capability of the developed active acoustic metamaterial cell in simultaneous independent control of both the density and bulk modulus of the cell.

Chapter 7 : Loss Analysis

Thus far, the model of the system found through the electric analog method has been restricted to lossless components. This section looks at the effects of adding those losses back into the system. Use of resistive elements in a lumped element models has been used in many papers such as Liu *et al.*^{120, 121}, Prasad *et al.*¹²², and Gallas¹²³ when assessing lumped models of resonators and cavities with piezoelectric diaphragms.

7.1: Addition of Resistances to Model

For this model, these losses primarily will be assumed to come in two forms, the first of which is viscous losses in the different sections of the cavities. This can be described in its simplified form¹²³:

$$R_v = \frac{8\mu L}{\pi r^4} \quad (7.1)$$

where μ is the viscosity of fluid, l is the length of the cavity, and r is the radius of the cavity. The second form is the mechanical loss in the bending diaphragms. Using the method applied by Liu *et al.*¹²¹, the resistance can be described by:

$$R_d = 2\zeta \sqrt{\frac{M_d}{C_d}} \quad (7.2)$$

where M_d is the equivalent kinetic mass of the diaphragm, C_d is the short circuit acoustic compliance relating the acoustic pressure to displacement of the diaphragm, and ζ a damping coefficient that can be found experimentally. These resistance values can be inserted into the circuit portrayed in Figure 6.4 to result in Figure 7.1: Electric analog of the dually tunable system with added loss components shown below.

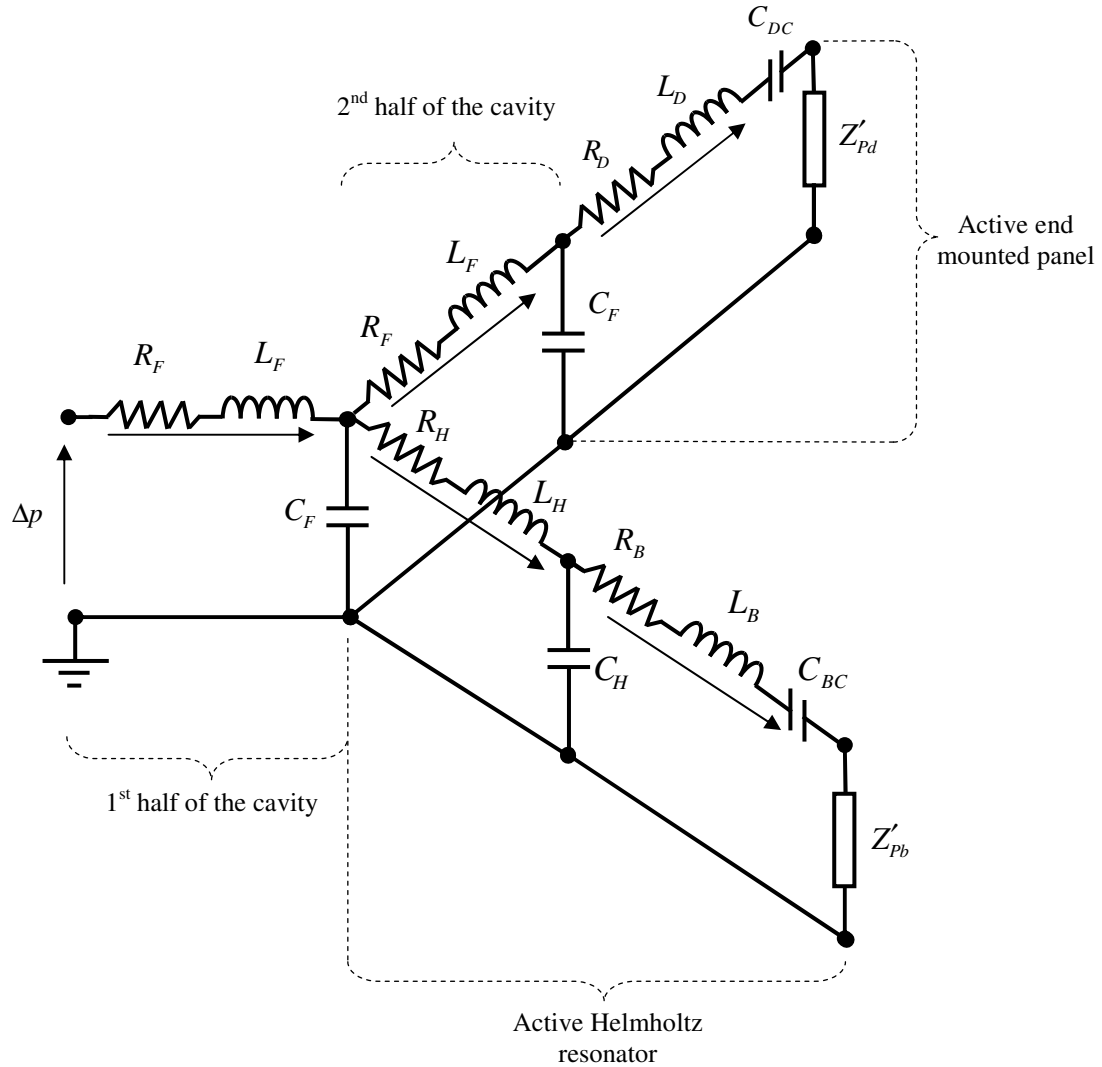


Figure 7.1: Electric analog of the dually tunable system with added loss components

As before, the total impedance Z_t of the above circuit can be broken down into Z_{1H} , Z_{2H} , Z_{HR} and Z_{CF} for the resistance and inductance of the first half of the cavity, the entire second half of the cavity, the Helmholtz resonator section, and the compliance of the first half of the cavity. These individually can be written as:

$$Z_{1H} = R_F + L_F s = R_F + \frac{\rho_f L s}{A} \quad (7.3)$$

$$Z_{2H} = \left(\frac{\rho_f L s}{A} + R_F + \frac{\frac{1}{C_F s} \left(Z_{pd} \phi^2 s + L_D s^2 + R_D s + \frac{1}{C_{DC}} \right)}{Z_{pd} \phi^2 s + L_D s^2 + R_D s + \frac{1}{C_{DC} s} + \frac{1}{C_F s}} \right) \quad (7.4)$$

$$Z_{HR} = \left(\frac{M_H s}{a^2} + R_H + \frac{\frac{1}{C_H s} \left(Z_{pb} \phi^2 s + L_B s^2 + R_B s + \frac{1}{C_{BC}} \right)}{Z_{pb} \phi^2 s + L_B s^2 + R_B s + \frac{1}{C_{BC} s} + \frac{1}{C_H s}} \right) \quad (7.5)$$

$$Z_{CF} = \frac{1}{C_F s} = \frac{B_f}{A L s} \quad (7.6)$$

And the total impedance Z_t is described as:

$$Z_t = Z_{1H} + \frac{Z_{CF} Z_{HH} Z_{2H}}{Z_{CF} Z_{HH} + Z_{CF} Z_{HH} Z_{2H} + Z_{HH} Z_{2H}} \quad (7.7)$$

which can be simplified a bit for the purpose of solving for the gain using Matlab by eliminating internal fractions:

$$\begin{aligned} Z_t &= Z_{1H} + \frac{\frac{n_{CF} n_{HH} n_{2H}}{d_{CF} d_{HH} d_{2H}}}{\frac{n_{CF} n_{HH}}{d_{CF} d_{HH}} + \frac{n_{1H} n_{2H}}{d_{1H} d_{2H}} + \frac{n_{HH} n_{2H}}{d_{HH} d_{2H}}} \\ &= Z_{1H} + \frac{n_{CF} n_{HH} n_{2H}}{d_{2H} n_{CF} n_{HH} + d_{HH} n_{CF} n_{2H} + d_{CF} n_{HH} n_{2H}} \end{aligned} \quad (7.8)$$

The equations for the density and bulk modulus are then solved as with equations (6.9)-(6.15).

7.2: Results

Modeling was done for an effective relative density of 1 and bulk modulus of 20 times that of the ambient medium which in this case was water. Parameters used in the model can be found in Table 7.1 below.

Table 7.1: Parameters of the model with resistance

PARAMETER	VALUE
A	$25 \times 10^{-4} \text{ m}^2$
a	$7.06 \times 10^{-6} \text{ m}^2$
ρ_f	1000 kg m^{-3}
β_f	$2.25 \times 10^9 \text{ Pa}$
l	.0225 m
l_H	.003 m
μ	$8.94 \times 10^{-4} \text{ Pa s}$
r	0.0163 m
r_H	0.0015 m
ϕ	138.3 PaV^{-1}
d_A	$-2.108 \times 10^{-11} \text{ m}^3 \text{V}^{-1}$
L_P	50 H
C_S	$0.2 \times 10^{-12} \text{ F}$
C_P	$18.239 \times 10^{-9} \text{ F}$
ζ	0.028

Five cases were modeled separating the various sources of resistance. The first results for the control voltage and closed loop compliance below serves as the baseline where all resistances are set to zero. The following two separately include the viscous effects in the cavity and in the neck of the Helmholtz resonator. The fourth case applies only the acoustic resistance of the diaphragm. The final case combined all the resistances.

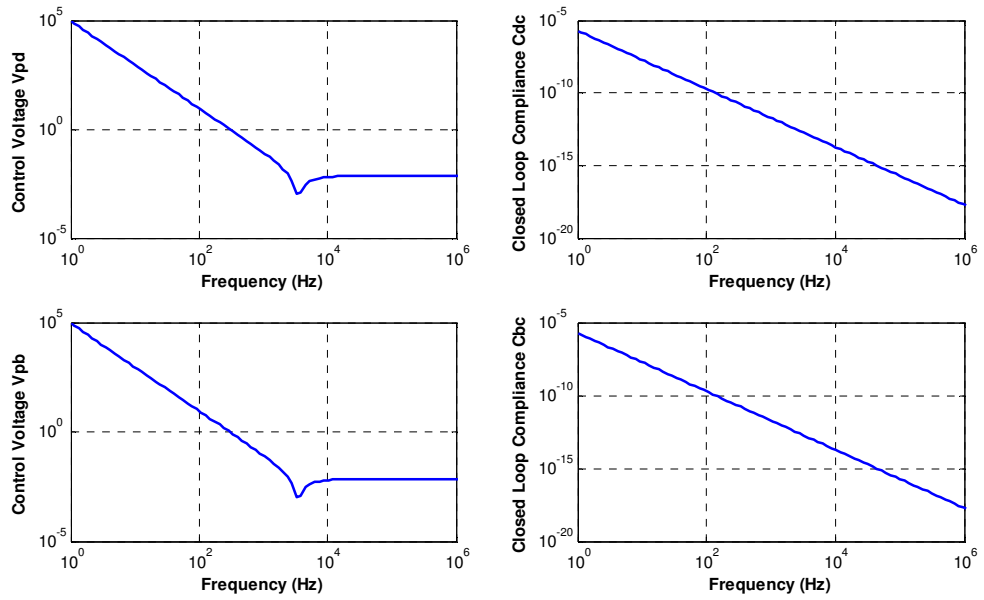


Figure 7.2: Resistances set to zero

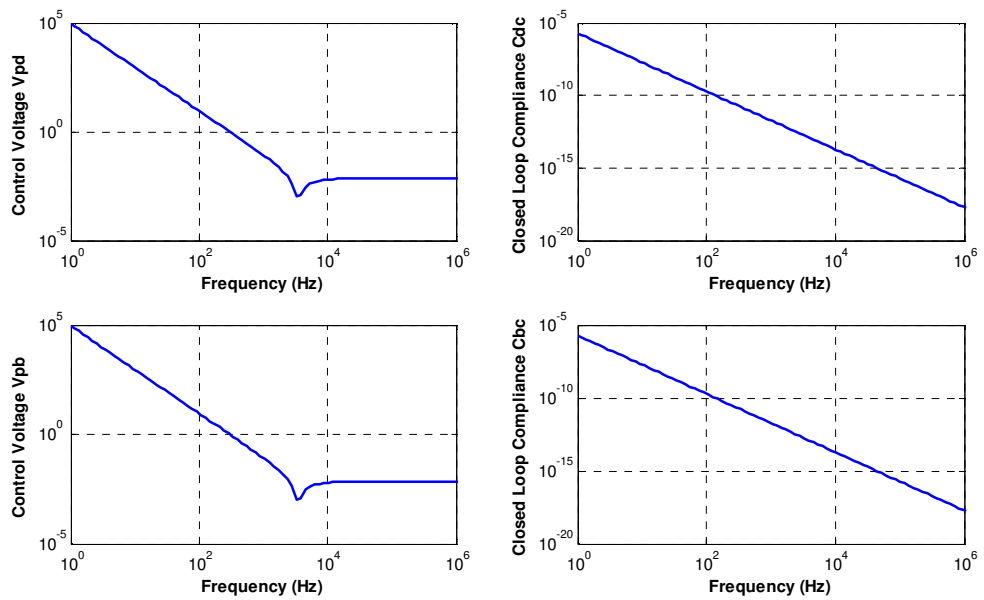


Figure 7.3: Only viscous resistance in cavities

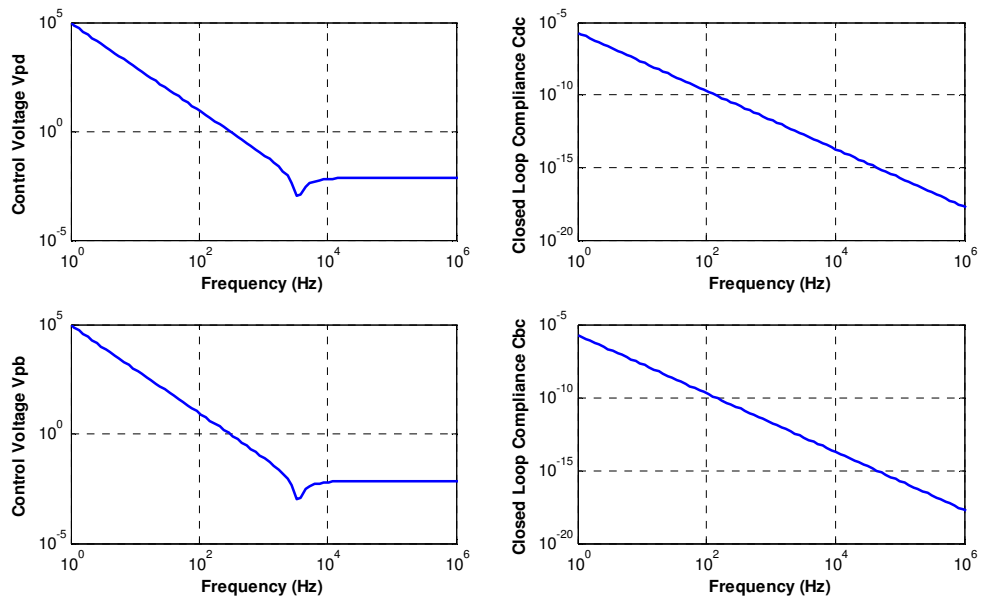


Figure 7.4: Only viscous resistance in Helmholtz neck

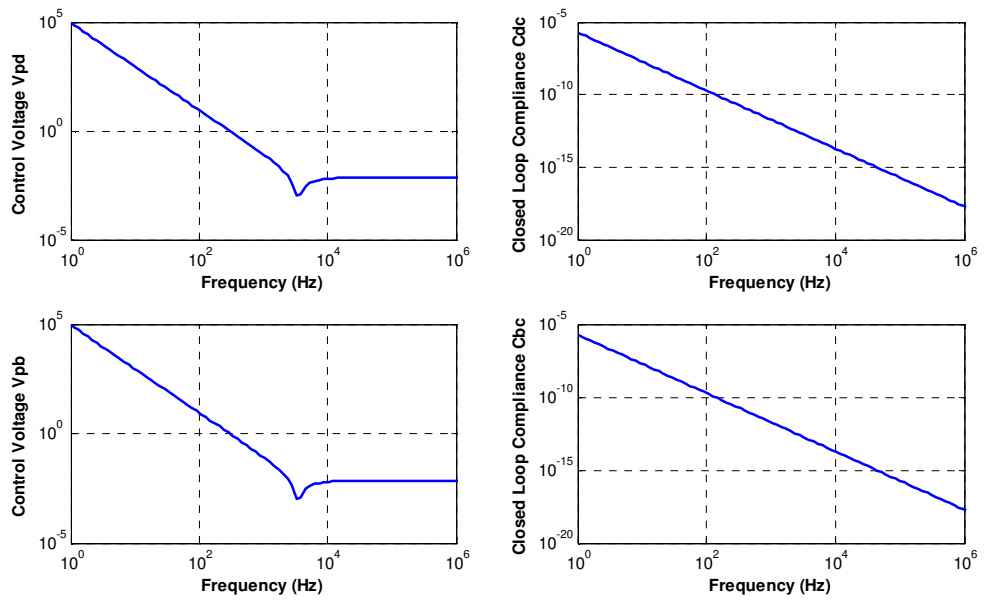


Figure 7.5: Only acoustic resistance from diaphragms

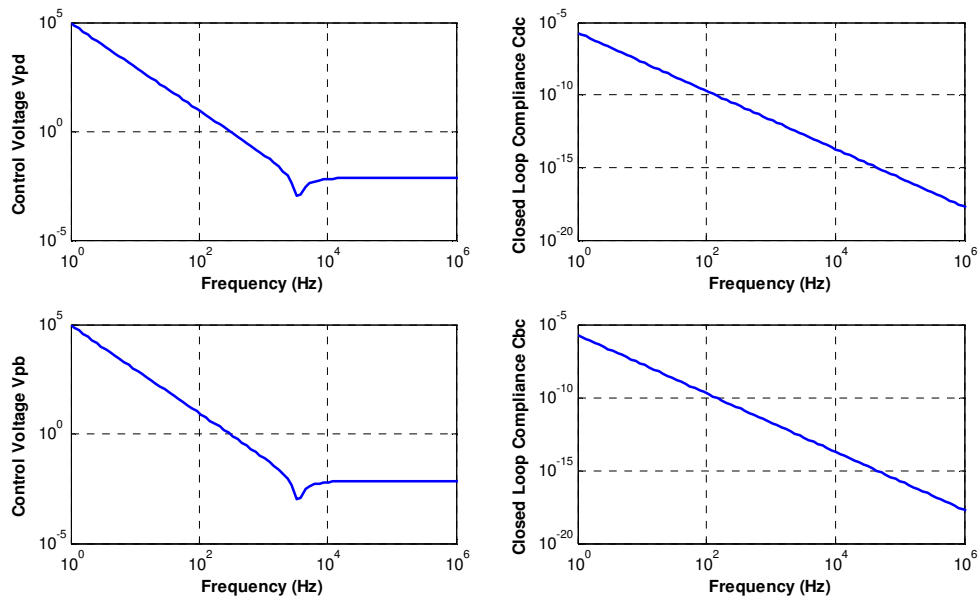


Figure 7.6: All inclusive resistances

Figure 7.7 subtracts the baseline case from the subsequent cases to solely look at the change in the control voltage caused by the addition of the resistances.

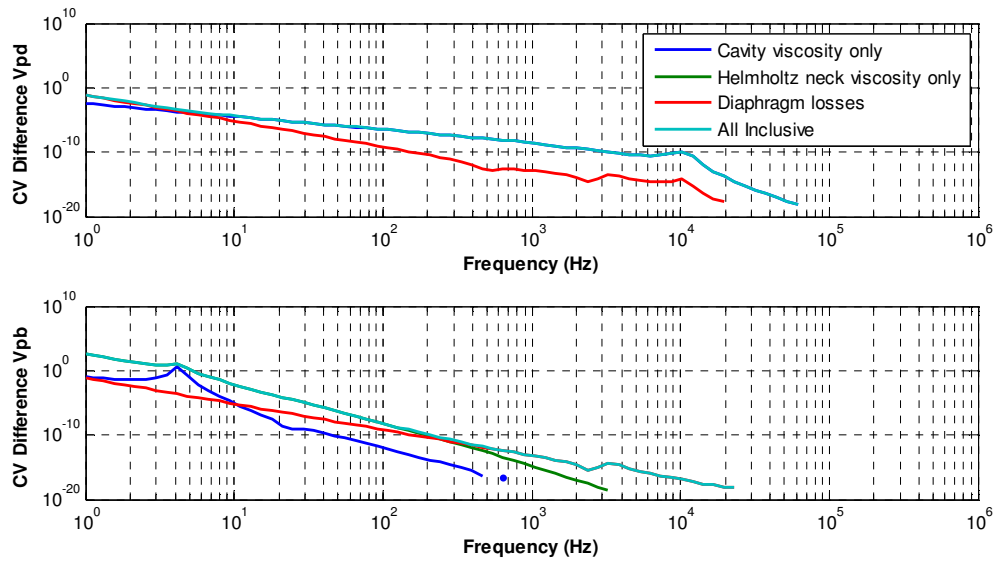


Figure 7.7: Subtracted from baseline

7.3: Summary and Conclusions

Figures 7.2 through 7.7 show that the addition of viscous resistance elements and elements for acoustic resistance of the diaphragm have very little effect. The maximum effect from these resistances occur at low frequencies but even at those low frequencies, the values for the control voltage are around five orders of magnitude greater than the differences caused by the resistances.

Chapter 8 : Conclusion

8.1: Summary

This dissertation presents the theory, modeling, manufacturing and experimental results of an Active Acoustic Metamaterial (AAMM). A thorough investigation of past developments has been made in both general metamaterials as well as metamaterial design based on coordinate changes such as those necessary to attain the parameters for an acoustic cloak. Furthermore, a generalized coordinate change formula has been presented for determining material parameters for desired directivity and dispersion control.

Custom Finite Difference Time Domain (FDTD) models have also been created through MATLAB scripts that match previous work and have shown agreement commercial software for both the material parameters of the cloak coordinate change as well as the directivity and dispersion coordinate change. The intuitive nature of the FDTD over the FEM allows for quick adaptation for other metamaterial projects. Only the knowledge of the material's geometry and property values of bulk modulus and density are necessary to input into the model. The limitation however, is that the FDTD model resides over a set grid domain and can not be readily refined for important locations in the metamaterials geometry. This may lead to some problems such as mismatched impedances at boundaries. For fine meshes, the FDTD can also be memory and time expensive.

With the necessary material parameters having been found, an approach was presented to achieve such material parameters in such a way that avoids the infinite mass

problem described by Norris²⁴. In addition, the approach allows for the metamaterial to be physically identical passive “off” form, but can be tuned to desired properties when becoming active. The first model for this approach was a single cavity with a self sensing piezoelectric diaphragm back as presented by Baz⁶³. This model allowed for tuning of the effective density of the metamaterial and was presented as a lumped element model taking advantage of the long wavelength assumption i.e. that the cavity itself would be smaller than the wavelength of the incoming wave. Parametric analysis of the design showed the flexibility of the design as well as tradeoffs between parameters such as bandwidth and control voltage. Single cavity metamaterial cells were then fabricated to test the theory of the density control model. The metamaterial cell was characterized by Baz and Akl⁷⁷ by measuring the acoustic impedance and transmission loss in the 200Hz to 1kHz range and the results were compared to a finite element model created to match the physical dimension of the acoustic cavity cell and were found to be a close agreement. Additionally, dynamic properties of the cell showed homogeneity up to 4kHz. This demonstration however, is only limited to the control of the effective density and lacks an investigation into viscous losses in the cavity and losses in the diaphragm.

The single cavity model was then taking a step further with the addition of an active Helmholtz resonator. This model allowed the simultaneous yet independent control of both the effective bulk modulus and the effective density of the metamaterial. This model was physically manufactured as well and was shown to behave as a single degree of freedom system. The effective density for the system was significantly controlled in the 600-900Hz range, while that in which the bulk modulus has been

significantly controlled was 81-168Hz. Additionally, it was shown that the cross-effect of the two active piezoelectric diaphragms was negligible demonstrating the effective independent control of the density and bulk modulus.

Finally the model with the Helmholtz resonator was re-evaluated using resistance elements to determine the impact of such element on the control voltage. Viscous damping elements from the fluid as well as elements of acoustic resistance from the diaphragm were added to the circuit analogy and the gain for the control voltage was reevaluated. The results of the resistive elements on the control voltage gain were found to have negligible effects, especially at higher frequencies.

8.2: Original Contributions

Research into the field of acoustic metamaterials is still in its infancy and still has a lot to offer in terms of research paths and approaches. This author has created a finite difference time domain package for use with metamaterials which allows for matrix form densities. This package has been compared with a commercial finite element package to reproduce results from past research as well as having been used for new research as well such as the presented contribution of a directivity and dispersion control. This control is based on the solution to a density matrix and bulk modulus scalar based on desired material property values. Such programmability can have numerous applications such as wave redirection and metamaterial lenses.

Also, the work of Baz and Akl has been extended to include both density and bulk modulus control which can be done independently of each other. This was also shown to have a single degree of freedom characteristic and the cross-effect was shown to be

negligible. All of the pre-described electro-acoustic circuit analogy models, however, lacked dissipative components. Chapter 7 contributes both viscous and mechanical losses to the model and finds for current models, these resistive elements change the control voltage and stiffness an insignificant amounts.

8.2: Future Work

Possible extensions come in several different forms. Fabrication of multi-cell arrays in a cascading arrangement could be carried out to demonstrate a controllable wave propagation pattern in a fluid domain.

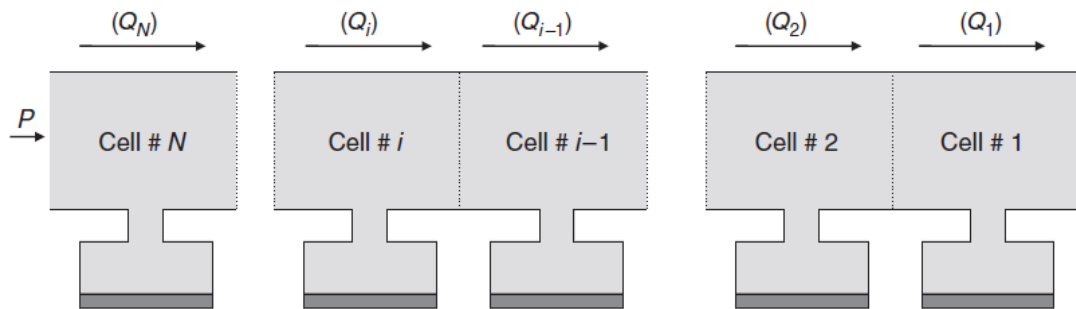


Figure 8.1: Schematic for cascading cells (Akl and Baz⁹²)

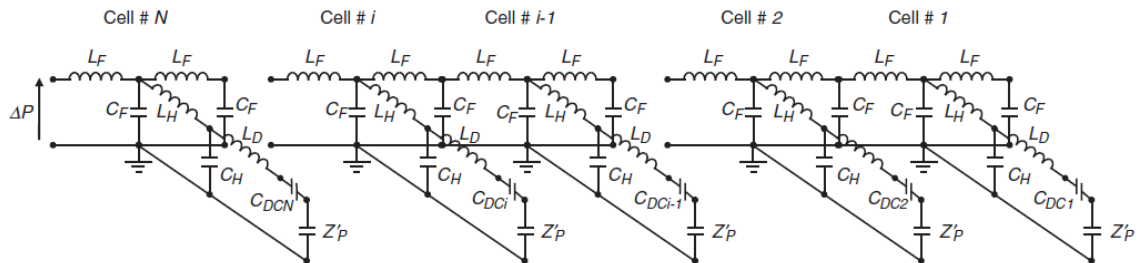
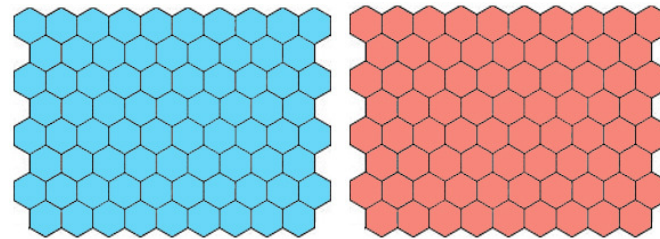
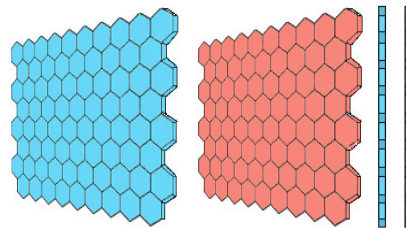


Figure 8.2: Electric Analog for cascading cells (Akl and Baz⁹²)

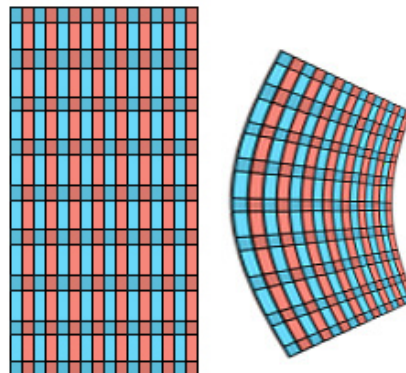
Furthermore, the model and array could be expanded into second and third dimensions to satisfy cloaking shells for cylindrical or spherical coordinate systems. Simplification or approximations of the electro-mechanical analog may be necessary as the solution for the control gain for the current model is very complex as is.



a)



b)



c)

Figure 8.3: Extension of metamaterial for cylindrical coordinates (a) Honeycomb layout for metamaterial A and B layers (b) Turning of the layers on side (c) Representation of layers for curved surface

Additionally, an investigation can be made on the effect of the thickness of the layers of materials A and B as compared to the thickness of the metamaterial structures as demonstrated in Figure 8.4.

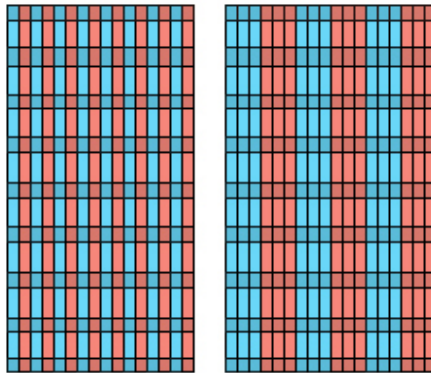


Figure 8.4: Different configurations of A and B metamaterial layers relative to the thickness of the structure.

Miniaturization is another path that may be taken for this metamaterial. In addition to the overt advantage of the reduction in bulk size, miniaturization would increase the bandwidth for which the necessary condition for the long wavelength assumption to hold. This could possibly be extended to micro-electromechanical systems (MEMS) level structures, though a more thorough investigation into viscous and damping effects would be necessary such miniaturizations.

Furthermore, a study of effect of S-Waves through the metamaterial cell could be performed for this structure. Though some theoretical research on the subject has been made such as Tang *et al.*¹²⁴ and Smith and Verrier¹²⁵, a practical experiment for acoustic cloaks or even any acoustic metamaterial has not yet been made. Resulting acoustic noise may become an issue or may be negligible compared to the pressure component.

Appendix I: Descritization into Finite Difference

Second order derivative conversions of pressure in time and space are:

$$\frac{\partial^2 P}{\partial t^2} \approx \frac{P(x, y, t+1) - 2P(x, y, t) + P(x, y, t-1)}{\Delta t^2}$$

$$\frac{\partial^2 P}{\partial x^2} \approx \frac{P(x+1, y, t) - 2P(x, y, t) + P(x-1, y, t)}{\Delta x^2}$$

$$\frac{\partial^2 P}{\partial x \partial y} \approx \frac{P(x+1, y+1, t) - P(x+1, y-1, t) - P(x-1, y+1, t) + P(x-1, y-1, t)}{4\Delta x \Delta y}$$

$$\frac{\partial P}{\partial y^2} \approx \frac{P(x, y+1, t) - 2P(x, y, t) + P(x, y-1, t)}{\Delta y^2}$$

First order derivative conversions of pressure in and space are:

$$\frac{\partial P}{\partial x} \approx \frac{P(x+1, y, t) - P(x-1, y, t)}{2\Delta x}$$

$$\frac{\partial P}{\partial y} \approx \frac{P(x, y+1, t) - P(x, y-1, t)}{2\Delta y}$$

First order time invariant derivative conversions of density in space are:

$$\frac{\partial \rho_{xx}^{-1}}{\partial x} \approx \frac{\rho_{xx}^{-1}(x+1, y) - \rho_{xx}^{-1}(x-1, y)}{2\Delta x}$$

$$\frac{\partial \rho_{yx}^{-1}}{\partial y} \approx \frac{\rho_{yx}^{-1}(x, y+1) - \rho_{yx}^{-1}(x, y-1)}{2\Delta y}$$

$$\frac{\partial \rho_{xy}^{-1}}{\partial x} \approx \frac{\rho_{xy}^{-1}(x+1, y) - \rho_{xy}^{-1}(x-1, y)}{2\Delta x}$$

$$\frac{\partial \rho_{yy}^{-1}}{\partial y} \approx \frac{\rho_{yy}^{-1}(x, y+1) - \rho_{yy}^{-1}(x, y-1)}{2\Delta y}$$

Using these conversions, we substitute back into the wave equation:

$$\frac{\partial^2 P}{\partial t^2} = \kappa \left[\rho_{xx}^{-1} \frac{\partial^2 P}{\partial x^2} + 2\rho_{xy}^{-1} \frac{\partial^2 P}{\partial x \partial y} + \rho_{yy}^{-1} \frac{\partial^2 P}{\partial y^2} + \left(\frac{\partial \rho_{xx}^{-1}}{\partial x} + \frac{\partial \rho_{yx}^{-1}}{\partial y} \right) \frac{\partial P}{\partial x} + \left(\frac{\partial \rho_{xy}^{-1}}{\partial x} + \frac{\partial \rho_{yy}^{-1}}{\partial y} \right) \frac{\partial P}{\partial y} \right]$$

to result in the following:

$$\left[\begin{array}{c} P(x, y, t+1) \\ -2P(x, y, t) \\ +P(x, y, t-1) \end{array} \right] \frac{1}{\Delta t^2} = \kappa \left\{ \begin{array}{l} \rho_{xx}^{-1} \frac{P(x+1, y, t) - 2P(x, y, t) + P(x-1, y, t)}{\Delta x^2} \\ + 2\rho_{xy}^{-1} \frac{P(x+1, y+1, t) - P(x+1, y-1, t) - P(x-1, y+1, t) + P(x-1, y-1, t)}{4\Delta x\Delta y} \\ + \rho_{yy}^{-1} \frac{P(x, y+1, t) - 2P(x, y, t) + P(x, y-1, t)}{\Delta y^2} \\ + \left(\frac{\rho_{xx}^{-1}(x+1, y, t) - \rho_{xx}^{-1}(x-1, y, t)}{2\Delta x} + \frac{\rho_{yx}^{-1}(x, y+1, t) - \rho_{yx}^{-1}(x, y-1, t)}{2\Delta y} \right) \\ \times \frac{P(x+1, y, t) - P(x-1, y, t)}{2\Delta x} \\ + \left(\frac{\rho_{xy}^{-1}(x+1, y, t) - \rho_{xy}^{-1}(x-1, y, t)}{2\Delta x} + \frac{\rho_{yy}^{-1}(x, y+1, t) - \rho_{yy}^{-1}(x, y-1, t)}{2\Delta y} \right) \\ \times \frac{P(x, y+1, t) - P(x, y-1, t)}{2\Delta y} \end{array} \right\}$$

Isolating the pressure for the future step we get:

$$P(x, y, t+1) = \kappa \Delta t^2 \left\{ \begin{array}{l} \rho_{xx}^{-1} \frac{P(x+1, y, t) - 2P(x, y, t) + P(x-1, y, t)}{\Delta x^2} \\ + 2\rho_{xy}^{-1} \frac{P(x+1, y+1, t) - P(x+1, y-1, t) - P(x-1, y+1, t) + P(x-1, y-1, t)}{4\Delta x\Delta y} \\ + \rho_{yy}^{-1} \frac{P(x, y+1, t) - 2P(x, y, t) + P(x, y-1, t)}{\Delta y^2} \\ + \left(\frac{\rho_{xx}^{-1}(x+1, y) - \rho_{xx}^{-1}(x-1, y)}{2\Delta x} + \frac{\rho_{yx}^{-1}(x, y+1) - \rho_{yx}^{-1}(x, y-1)}{2\Delta y} \right) \\ \times \frac{P(x+1, y, t) - P(x-1, y, t)}{2\Delta x} \\ + \left(\frac{\rho_{xy}^{-1}(x+1, y) - \rho_{xy}^{-1}(x-1, y)}{2\Delta x} + \frac{\rho_{yy}^{-1}(x, y+1, t) - \rho_{yy}^{-1}(x, y-1, t)}{2\Delta y} \right) \\ \times \frac{P(x, y+1, t) - P(x, y-1, t)}{2\Delta y} \\ + 2P(x, y, t) - P(x, y, t-1) \end{array} \right\}$$

Appendix II: Stability Analysis

Von Neumann:

Begin with the finite difference wave equation for time dependent variables

$$P(x, y, t+1) = \kappa \Delta t^2 \left\{ \begin{aligned} & \rho_{xx}^{-1} \frac{P(x+1, y, t) - 2P(x, y, t) + P(x-1, y, t)}{\Delta x^2} \\ & + 2\rho_{xy}^{-1} \frac{P(x+1, y+1, t) - P(x+1, y-1, t) - P(x-1, y+1, t) + P(x-1, y-1, t)}{4\Delta x \Delta y} \\ & + \rho_{yy}^{-1} \frac{P(x, y+1, t) - 2P(x, y, t) + P(x, y-1, t)}{\Delta y^2} \\ & + \left(\frac{\partial \rho_{xx}^{-1}}{\partial x} + \frac{\partial \rho_{yx}^{-1}}{\partial y} \right) \frac{P(x+1, y, t) - P(x-1, y, t)}{2\Delta x} \\ & + \left(\frac{\partial \rho_{xy}^{-1}}{\partial x} + \frac{\partial \rho_{yy}^{-1}}{\partial y} \right) \frac{P(x, y+1, t) - P(x, y-1, t)}{2\Delta y} \\ & + 2P(x, y, t) - P(x, y, t-1) \end{aligned} \right\}$$

The difference between the numerical solution and the true solution for the wave equation will be some round off error. Let round off error be defined as $\mathcal{E}_{i,j}^n = e^{at} e^{i(kx+ly)}$ and let the finite difference derivatives in time and space be as follows.

$$\begin{aligned} \mathcal{E}_{i,j}^{n+1} &= e^{a(t+\Delta t)} e^{i(kx+ly)} & \mathcal{E}_{i+1,j}^n &= e^{at} e^{i(k(x+\Delta x)+ly)} & \mathcal{E}_{i,j+1}^n &= e^{at} e^{i(kx+l(y+\Delta y))} \\ \mathcal{E}_{i,j}^{n-1} &= e^{a(t-\Delta t)} e^{i(kx+ly)} & \mathcal{E}_{i-1,j}^n &= e^{at} e^{i(k(x-\Delta x)+ly)} & \mathcal{E}_{i,j-1}^n &= e^{at} e^{i(kx+l(y-\Delta y))} \end{aligned}$$

With each iteration, the round off error may compound, so let us define some amplification factor as a fraction of the future time error over the current time

error $G = \frac{\mathcal{E}_{i,j}^{n+1}}{\mathcal{E}_{i,j}^n}$ which will acknowledge any growth in the error in each time period. For

the finite difference equation to stay stable over time, the absolute value of the amplification factor must remain below one.

$$|G| \leq 1$$

To begin the analysis of the equation, the Fourier transform of the second order wave equation using the aforementioned round off error and its derivatives in time and space. Note that the terms for the spatial derivative in density are untouched since they time invariant and will only act as coefficients for the growth factor.

$$\frac{\begin{bmatrix} e^{a(t+\Delta t)} e^{i(kx+ly)} \\ -2e^{at} e^{i(kx+ly)} \\ +e^{a(t-\Delta t)} e^{i(kx+ly)} \end{bmatrix}}{\Delta t^2} = \kappa \left\{ \begin{aligned} & \rho_{xx}^{-1} \frac{e^{at} e^{i(k(x+\Delta x)+ly)} - 2e^{at} e^{i(kx+ly)} + e^{at} e^{i(k(x-\Delta x)+ly)}}{\Delta x^2} \\ & + 2\rho_{xy}^{-1} \frac{e^{at} e^{i(k(x+\Delta x)+l(y+\Delta y))} - e^{at} e^{i(k(x+\Delta x)+l(y-\Delta y))} - e^{at} e^{i(k(x-\Delta x)+l(y+\Delta y))} + e^{at} e^{i(k(x-\Delta x)+l(y-\Delta y))}}{4\Delta x\Delta y} \\ & + \rho_{yy}^{-1} \frac{e^{at} e^{i(kx+l(y+\Delta y))} - 2e^{at} e^{i(kx+ly)} + e^{at} e^{i(kx+l(y-\Delta y))}}{\Delta y^2} \\ & + \left(\frac{\partial \rho_{xx}^{-1}}{\partial x} + \frac{\partial \rho_{yx}^{-1}}{\partial y} \right) \frac{e^{at} e^{i(k(x+0.5\Delta x)+ly)} - e^{at} e^{i(k(x-0.5\Delta x)+ly)}}{\Delta x} \\ & + \left(\frac{\partial \rho_{xy}^{-1}}{\partial x} + \frac{\partial \rho_{yy}^{-1}}{\partial y} \right) \frac{e^{at} e^{i(kx+l(y+0.5\Delta y))} - e^{at} e^{i(kx+l(y-0.5\Delta y))}}{\Delta y} \end{aligned} \right\}$$

Divide through by $\frac{e^{a(t-\Delta t)} e^{i(kx+ly)}}{\Delta t^2}$ and reorganize the exponents on the second line

$$\left(e^{i(k\Delta x + l\Delta y)} - e^{i(k\Delta x - l\Delta y)} - e^{-i(k\Delta x - l\Delta y)} + e^{-i(k\Delta x + l\Delta y)} \right)$$

into $\left(e^{ik\Delta x} e^{il\Delta y} - e^{ik\Delta x} e^{-il\Delta y} - e^{-ik\Delta x} e^{il\Delta y} + e^{-ik\Delta x} e^{-il\Delta y} \right)$

then factor into $(e^{ik\Delta x} - e^{-ik\Delta x})(e^{il\Delta y} - e^{-il\Delta y})$

and finally factor out $e^{a\Delta t}$

$$e^{2a\Delta t} - 2e^{a\Delta t} + 1 = \kappa\Delta t^2 \left\{ \begin{aligned} & \rho_{xx}^{-1} \frac{e^{ik\Delta x} - 2 + e^{-i\Delta x}}{\Delta x^2} + \rho_{yy}^{-1} \frac{e^{il\Delta y} - 2 + e^{-i\Delta y}}{\Delta y^2} \\ & + 2\rho_{xy}^{-1} \frac{(e^{ik\Delta x} - e^{-ik\Delta x})(e^{il\Delta y} - e^{-il\Delta y})}{4\Delta x\Delta y} \\ & + \left(\frac{\partial\rho_{xx}^{-1}}{\partial x} + \frac{\partial\rho_{yx}^{-1}}{\partial y} \right) \frac{e^{ik\Delta x} - e^{-i\Delta x}}{2\Delta x} \\ & + \left(\frac{\partial\rho_{xy}^{-1}}{\partial x} + \frac{\partial\rho_{yy}^{-1}}{\partial y} \right) \frac{e^{il\Delta y} - e^{-i\Delta y}}{2\Delta y} \end{aligned} \right\} e^{a\Delta t}$$

Now recall that $\frac{e^{i\alpha} + e^{-i\alpha}}{2} = \cos(\alpha)$ and $\frac{e^{i\alpha} - e^{-i\alpha}}{2i} = \sin(\alpha)$

$$e^{2a\Delta t} - 2e^{a\Delta t} + 1 = \kappa\Delta t^2 \left\{ \begin{aligned} & \rho_{xx}^{-1} \frac{2 \cos(k\Delta x) - 2}{\Delta x^2} + \rho_{yy}^{-1} \frac{2 \cos(l\Delta y) - 2}{\Delta y^2} \\ & + 2\rho_{xy}^{-1} \frac{2i \sin(k\Delta x) 2i \sin(l\Delta y)}{4\Delta x \Delta y} \\ & + \left(\frac{\partial \rho_{xx}^{-1}}{\partial x} + \frac{\partial \rho_{yx}^{-1}}{\partial y} \right) \frac{2i \sin(k\Delta x)}{2\Delta x} \\ & + \left(\frac{\partial \rho_{xy}^{-1}}{\partial x} + \frac{\partial \rho_{yy}^{-1}}{\partial y} \right) \frac{2i \sin(l\Delta y)}{2\Delta y} \end{aligned} \right\} e^{a\Delta t}$$

Using the half-angle formula and simplifying, we get:

$$e^{2a\Delta t} - 2e^{a\Delta t} + 1 = \kappa\Delta t^2 \left\{ \begin{aligned} & -\frac{4\rho_{xx}^{-1}}{\Delta x^2} \sin^2\left(\frac{k\Delta x}{2}\right) - \frac{4\rho_{yy}^{-1}}{\Delta y^2} \sin^2\left(\frac{l\Delta y}{2}\right) \\ & - \frac{2\rho_{xy}^{-1}}{\Delta x \Delta y} \sin(k\Delta x) \sin(l\Delta y) \\ & + \left(\frac{\partial \rho_{xx}^{-1}}{\partial x} + \frac{\partial \rho_{yx}^{-1}}{\partial y} \right) \frac{i \sin(k\Delta x)}{\Delta x} \\ & + \left(\frac{\partial \rho_{xy}^{-1}}{\partial x} + \frac{\partial \rho_{yy}^{-1}}{\partial y} \right) \frac{i \sin(l\Delta y)}{\Delta y} \end{aligned} \right\} e^{a\Delta t}$$

Recalling the definition of the amplification factor we can simplify it to:

$$G = \frac{\mathcal{E}_{i,j}^{n+1}}{\mathcal{E}_{i,j}^n} = \frac{e^{a(t+\Delta t)} e^{i(kx+ly)}}{e^{at} e^{i(kx+ly)}} = e^{a\Delta t}$$

Rewriting the above wave equation with the amplification factor substitution:

$$G^2 - 2G + 1 = \kappa \Delta t^2 \left\{ \begin{array}{l} -\frac{4\rho_{xx}^{-1}}{\Delta x^2} \sin^2\left(\frac{k\Delta x}{2}\right) - \frac{4\rho_{yy}^{-1}}{\Delta y^2} \sin^2\left(\frac{l\Delta y}{2}\right) \\ -\frac{2\rho_{xy}^{-1}}{\Delta x \Delta y} \sin(k\Delta x) \sin(l\Delta y) \\ + \left(\frac{\partial \rho_{xx}^{-1}}{\partial x} + \frac{\partial \rho_{yx}^{-1}}{\partial y} \right) \frac{i \sin(k\Delta x)}{\Delta x} \\ + \left(\frac{\partial \rho_{xy}^{-1}}{\partial x} + \frac{\partial \rho_{yy}^{-1}}{\partial y} \right) \frac{i \sin(l\Delta y)}{\Delta y} \end{array} \right\} G$$

At this point, one can clearly see that solving for the amplification factor is just a matter of solving the quadratic equation.

Bringing the right side of the equation to the left we get.

$$G^2 + \left\{ -2 + \kappa \Delta t^2 \left(\begin{array}{l} -\frac{4\rho_{xx}^{-1}}{\Delta x^2} \sin^2\left(\frac{k\Delta x}{2}\right) - \frac{4\rho_{yy}^{-1}}{\Delta y^2} \sin^2\left(\frac{l\Delta y}{2}\right) \\ -\frac{2\rho_{xy}^{-1}}{\Delta x \Delta y} \sin(k\Delta x) \sin(l\Delta y) \\ + \left(\frac{\partial \rho_{xx}^{-1}}{\partial x} + \frac{\partial \rho_{yx}^{-1}}{\partial y} \right) \frac{i \sin(k\Delta x)}{\Delta x} \\ + \left(\frac{\partial \rho_{xy}^{-1}}{\partial x} + \frac{\partial \rho_{yy}^{-1}}{\partial y} \right) \frac{i \sin(l\Delta y)}{\Delta y} \end{array} \right) \right\} G + 1 = 0$$

$$\text{So the solution becomes } G = \frac{b \pm \sqrt{b^2 - 4ac}}{2a} \text{ for } aG^2 + bG + c = 0$$

where $a = c = 1$ and

$$b = -2 + \kappa \Delta t^2 \left(\begin{array}{l} \frac{4\rho_{xx}^{-1}}{\Delta x^2} \sin^2\left(\frac{k\Delta x}{2}\right) + \frac{4\rho_{yy}^{-1}}{\Delta y^2} \sin^2\left(\frac{l\Delta y}{2}\right) + \frac{2\rho_{xy}^{-1}}{\Delta x \Delta y} \sin(k\Delta x) \sin(l\Delta y) \\ - \left(\frac{\partial \rho_{xx}^{-1}}{\partial x} + \frac{\partial \rho_{yx}^{-1}}{\partial y} \right) \frac{i \sin(k\Delta x)}{\Delta x} - \left(\frac{\partial \rho_{xy}^{-1}}{\partial x} + \frac{\partial \rho_{yy}^{-1}}{\partial y} \right) \frac{i \sin(l\Delta y)}{\Delta y} \end{array} \right)$$

Since only the minimum and maximum are important here, the frequencies determined by l and k not important. Looking only at the ranges we get:

$$b = -2 + \kappa\Delta t^2 \left(\begin{array}{l} \frac{4\rho_{xx}^{-1}}{\Delta x^2}(0 \rightarrow 1) + \frac{4\rho_{yy}^{-1}}{\Delta y^2}(0 \rightarrow 1) + \frac{2\rho_{xy}^{-1}}{\Delta x\Delta y}(-1 \rightarrow 1)(-1 \rightarrow 1) \\ -\left(\frac{\partial\rho_{xx}^{-1}}{\partial x} + \frac{\partial\rho_{yx}^{-1}}{\partial y}\right)(-1i \rightarrow 1i) - \left(\frac{\partial\rho_{xy}^{-1}}{\partial x} + \frac{\partial\rho_{yy}^{-1}}{\partial y}\right)(-1i \rightarrow 1i) \end{array} \right)$$

The knowing that the coefficients are all positive, the maximum possible is:

$$b = -2 + \kappa\Delta t^2 \left(\begin{array}{l} \frac{4\rho_{xx}^{-1}}{\Delta x^2} + \frac{4\rho_{yy}^{-1}}{\Delta y^2} + \frac{2\rho_{xy}^{-1}}{\Delta x\Delta y} \\ +\left(\frac{\partial\rho_{xx}^{-1}}{\partial x} + \frac{\partial\rho_{yx}^{-1}}{\partial y}\right)i + \left(\frac{\partial\rho_{xy}^{-1}}{\partial x} + \frac{\partial\rho_{yy}^{-1}}{\partial y}\right)i \end{array} \right)$$

and minimum is

$$b = -2 + \kappa\Delta t^2 \left(-\frac{2\rho_{xy}^{-1}}{\Delta x\Delta y} - \left(\frac{\partial\rho_{xx}^{-1}}{\partial x} + \frac{\partial\rho_{yx}^{-1}}{\partial y}\right)i - \left(\frac{\partial\rho_{xy}^{-1}}{\partial x} + \frac{\partial\rho_{yy}^{-1}}{\partial y}\right)i \right)$$

which is dependent on the values of the coefficients and must abide by $0 \leq |b| \leq 2$ for the

absolute value of $G = \frac{b \pm \sqrt{b^2 - 4ac}}{2a}$ to be less than 1.

Appendix III: Discretization of the Perfectly Matched Layer equations

The three equations needed for the x direction are:

$$\left(\frac{\partial}{\partial t} + \sigma(x)\right)^2 P_1 = \kappa \rho_{xx}^{-1} \frac{\partial P}{\partial x^2}$$

$$\left(\frac{\partial}{\partial t} + \sigma(x)\right)^2 \zeta_1 = -\kappa \rho_{xx}^{-1} \sigma'(x) \frac{\partial P}{\partial x}$$

and the intermediate variable $\zeta_1 = \left(\frac{\partial}{\partial t} + \sigma(x)\right) P_2$

Multiplying out the left side of the first two equations, we get:

$$\frac{\partial}{\partial t^2} P_1 + \frac{\partial}{\partial t} \sigma(x) P_1 + \sigma(x)^2 P_1 = \kappa \rho_{xx}^{-1} \frac{\partial P}{\partial x^2}$$

$$\frac{\partial}{\partial t^2} \zeta_1 + \frac{\partial}{\partial t} \sigma(x) \zeta_1 + \sigma(x)^2 \zeta_1 = -\kappa \rho_{xx}^{-1} \sigma'(x) \frac{\partial P}{\partial x}$$

Using the same discretization transformations as in Appendix I on the P_1 equation we get:

$$\begin{aligned} & \frac{P_1(x, y, t+1) - 2P_1(x, y, t) + P_1(x, y, t-1)}{\Delta t^2} + \sigma(x) \frac{P_1(x, y, t+1) - P_1(x, y, t-1)}{2\Delta t} \\ & + \sigma(x)^2 P_1(x, y, t) = \kappa \rho_{xx}^{-1} \frac{P(x+1, y, t) - 2P(x, y, t) + P(x-1, y, t)}{\Delta x^2} \end{aligned}$$

Then isolating the $P_1(x, y, t+1)$ terms results in

$$\begin{aligned} & \frac{P_1(x, y, t+1)}{\Delta t^2} + \sigma(x) \frac{P_1(x, y, t+1)}{2\Delta t} = \frac{2P_1(x, y, t) - P_1(x, y, t-1)}{\Delta t^2} + \sigma(x) \frac{P_1(x, y, t-1)}{2\Delta t} \\ & - \sigma(x)^2 P_1(x, y, t) + \kappa \rho_{xx}^{-1} \frac{P(x+1, y, t) - 2P(x, y, t) + P(x-1, y, t)}{\Delta x^2} \end{aligned}$$

This can then be simplified to:

$$P_1(x, y, t+1) = \frac{\Delta t^2}{1 + \Delta t \sigma(x)} \left(\frac{2P_1(x, y, t) - P_1(x, y, t-1)}{\Delta t^2} + 2\sigma(x) \frac{P_1(x, y, t-1)}{2\Delta t} \right. \\ \left. - \sigma(x)^2 P_1(x, y, t) + \kappa \rho_{xx}^{-1} \frac{P(x+1, y, t) - 2P(x, y, t) + P(x-1, y, t)}{\Delta x^2} \right)$$

The same can be done to the similar ζ_1 equation to result in the following.

$$\zeta_1(x, y, t+1) = \frac{\Delta t^2}{1 + \Delta t \sigma(x)} \left(\frac{2\zeta_1(x, y, t) - \zeta_1(x, y, t-1)}{\Delta t^2} + 2\sigma(x) \frac{\zeta_1(x, y, t-1)}{2\Delta t} \right. \\ \left. - \sigma(x)^2 \zeta_1(x, y, t) - \kappa \rho_{xx}^{-1} \sigma'(x) \frac{P(x+1, y, t) - P(x-1, y, t)}{2\Delta x} \right)$$

Finally, for the x direction, the intermediate variable can be rearranged and discretized to result in the following.

$$P_2(x, y, t+1) = 2\Delta t (\zeta_1 - \sigma(x) P_2(x, y, t)) + P_2(x, y, t-1)$$

The same can be done in the y direction to result in the following three equations.

$$P_3(x, y, t+1) = \frac{\Delta t^2}{1 + \Delta t \sigma(y)} \left(\frac{2P_3(x, y, t) - P_3(x, y, t-1)}{\Delta t^2} + \sigma(y) \frac{P_3(x, y, t-1)}{2\Delta t} \right. \\ \left. - \sigma(y)^2 P_3(x, y, t) + \kappa \rho_{xx}^{-1} \frac{P(x, y+1, t) - 2P(x, y, t) + P(x, y-1, t)}{\Delta y^2} \right)$$

$$\zeta_2(x, y, t+1) = \frac{\Delta t^2}{1 + \Delta t \sigma(y)} \left(\frac{2\zeta_2(x, y, t) - \zeta_2(x, y, t-1)}{\Delta t^2} + \frac{\zeta_2(x, y, t-1)}{2\Delta t} \right. \\ \left. - \sigma(y)^2 \zeta_2(x, y, t) - \kappa \rho_{xx}^{-1} \sigma'(y) \frac{P(x, y+1, t) - P(x, y-1, t)}{2\Delta y} \right)$$

$$P_4(x, y, t+1) = 2\Delta t (\zeta_2 - \sigma(x) P_4(x, y, t)) + P_4(x, y, t-1)$$

Bibliography

- ¹ Walser, R.M. , “Electromagnetic metamaterials”, *Proceedings of SPIE*, 4467, 1, 2001
- ² Shamonina, E. and Solymar, L. , “ Metamaterials: How the subject started”, *Metamaterials*, vol.1, 1, 2007
- ³ Liu, H., Liu, Y. M., Li, T., Wang, S. M., Zhu, S. N., and Zhang, X., “Coupled magnetic plasmons in metamaterials”, *Physica Status Solidi B*, vol. 246, 7, 2009
- ⁴ Veselago, V. G., “The electrodynamics of substances with simultaneously negative values of ϵ and μ ”. *Soviet Physics Uspekhi*, vol. 10, 4, 1968 (Russian text 1967)
- ⁵ Pendry, J.B., Schurig, D., and Smith, D., "Controlling electromagnetic fields", *Science*, vol. 312, 1780, 2006
- ⁶ Milton, G.W., Briane, M., and Willis, J.R., “On cloaking for elasticity and physical equations with a transformation invariant form”, *New Journal of Physics*, vol. 8, 23, 2006
- ⁷ ShalaeV, V., “Optical negative-index metamaterials”, *Nature Photonics*, vol. 1, 1, 2007
- ⁸ Tretyakov, S.A., “Research on negative refraction and backward-wave media: a historical perspective”, *EPFL Latsis Symposium*, 2005
- ⁹ Pendry, J.B., Holden, A.J., Robbins, D.J., and Stewart, W.J., “Magnetism from conductors, and enhanced non-linear phenomena”, *IEEE Transactions Microwave Theory Tech* ,1999
- ¹⁰ Liu, Y., and Zhang, X., “Metamaterials: a new frontier of science and technology”, *Chemical Society Reviews*, vol. 40, 5, 2011
- ¹¹ Ung, B., “Metamaterials: a metareview”, http://www.polymtl.ca/phys/doc/art_2_2.pdf, last accessed August 2011
- ¹² Sheng, P., Mei, J., Liu, Z., and Wen, W., “Dynamic mass density and acoustic metamaterials”, *Physica B: Condensed Matter*, vol. 394, 2, 2007
- ¹³ Lee, S.H., Park, C.M., Seo, Y.M., Wang, Z.G., and Kim, C.K., “Acoustic metamaterial with negative density.” *Physics Letters A*, vol. 373 , 4465, 2009
- ¹⁴ Ambati, M., and Fang, N., and Sun, C., and Zhang, X., “Surface resonant states and superlensing in acoustic metamaterials”, *Physics Review Letters B*, vol. 75, 195447, 2007
- ¹⁵ Guenneau, S., Movchan, A., Pétursson, G., and Ramakrishna, S.A., “Acoustic metamaterials for sound focusing and confinement”, *New Journal of Physics*, vol. 9, 399,2007

-
- ¹⁶ Schurig, D., Pendry, J., and Smith, D., “Calculation of material properties and ray tracing in transformation media”, *Optics Express*, vol. 14, 21, 2006
- ¹⁷ Cummer, S.A., Popa, B-I, Schurig, D., and Smith, D.R., “Full-wave simulations of electromagnetic cloaking structures”, *Physics Review Letters E*, vol. 74, 3, 2006
- ¹⁸ Schurig, D., Mock, J., Justice, B., Cummer, S., Pendry, J., Starr, A., and Smith, D., “Metamaterial Electromagnetic Cloak at Microwave Frequencies”, *Science*, vol. 314, 5801, 2006
- ¹⁹ Cummer, S.A. and Schurig, D., "One path to acoustic cloaking", *New Journal of Physics*, vol. 9, 45, 2007
- ²⁰ Cai, L-W and Sánchez-Dehesa, J., "Analysis of Cummer-Schurig acoustic cloaking", *New Journal of Physics*, vol. 9, 450, 2007
- ²¹ Chen, H. and Chan, C.T., "Acoustic cloaking in three dimensions using acoustic metamaterials", *Applied Physics Letters*, vol. 91, 183518, 2007
- ²² Cummer, S.A., Popa, B-I, Schurig, D., Smith, D.R., Pendry, J., Rahm, M., and Starr, A., "Scattering derivation of a 3D acoustic cloaking shell", *Physical Review Letters*, vol. 100, 024301, 2008
- ²³ Norris, A., “Acoustic cloaking in 2D and 3D using finite mass”, <http://arxiv.org/abs/0802.0701v1>
- ²⁴ Norris, A., “Acoustic cloaking theory”, *Proceedings of the Royal Society A*, vol. 464, 2097, 2008
- ²⁵ Milton, G. W. and Cherkaev, A. V. “Which elasticity tensors are realizable?”, *Journal of Engineering. Material Technology*, vol.117, 4,1995
- ²⁶ Norris, A.,“Acoustic metafluids”, *Journal of the Acoustic Society of America*, vol. 125, 839, 2009
- ²⁷ Scandrett, C.L., Boisvert, J.E., and Howarth, T.R., “Acoustic cloaking using layered pentamode materials”, *Journal of the Acoustic Society of America*, vol.127, 2856, 2010
- ²⁸ Cheng, Y., Yang, F., Xu, J-Y., and Liu, X-J, “A multilayer structured acoustic cloak with homogeneous isotropic materials”, *Applied Physics Letters*, vol. 92, 151913, 2008
- ²⁹ Torrent, D. and Sánchez-Dehesa, J., “Anisotropic mass density by two-dimensional acoustic metamaterials”, *New Journal of Physics*, vol. 10, 023004, 2008
- ³⁰ Schoenberg, M., and Sen, P.N., “Properties of a periodically stratified acoustic half-space and its relation to a Biot fluid”, *Journal of the Acoustic Society of America*, vol.73, 10, 1983
- ³¹ Farhat, M., Enoch, S., Guenneau, S., and Movchan A.B., “Broadband Cylindrical Acoustic Cloak for Linear Surface Waves in a Fluid”, *Physical Review Letters*, vol. 101, 134501, 2008

-
- ³² Pendry, J.B., and Jensen, L., "An acoustic metafluid: realizing a broadband acoustic cloak", *New Journal of Physics*, vol. 10, 115032, 2008
- ³³ Hu, J., Zhou, X., and Hu, G., "A numerical method for designing acoustic cloak with arbitrary shapes", *Computational Materials Science*, vol. 46, 3, 2009
- ³⁴ Ren, C.Y., Xiang, Z.H., and Cen, Z.Z., "Layered and isotropic acoustic cloak design based on conformal transformation acoustics", *Science China*, vol. 54, 4, 2011
- ³⁵ García-Chocano, V. M., Sanchis, L., Díaz-Rubio, A., Martínez-Pastor, J., Cervera, F., Llopis-Pontiveros, R., and Sánchez-Dehesa J., "Acoustic cloak for airborne sound by inverse design", *Applied Physics Letters*, vo. 99, 074102, 2011
- ³⁶ Ward, A.J., and Pendry, J.B., "Refraction and geometry in Maxwell's equations", *Journal of Modern Optics*, vol. 43, 4, 1996
- ³⁷ Cummer, S.A., Rahm, M., and Schurig, D., "Material parameters and vector scaling in transformation acoustics", *New Journal of Physics*, vol. 10, 115025, 2008
- ³⁸ Auld, B.A., *Acoustic fields and waves in solids*, Krieger Pub Co, 1990
- ³⁹ Yee, K., "Numerical solution of initial boundary value problems involving Maxwell's equations in isotropic media", *IEEE Transactions on Antennas and Propagation*, vol. 14, 3, 1966
- ⁴⁰ Taflove, A.; and Brodwin, M.E.; , "Computation of the Electromagnetic Fields and Induced Temperatures Within a Model of the Microwave-Irradiated Human Eye," , *IEEE Transactions on Microwave Theory and Techniques*, vol. 23 , 11, Nov 1975
- ⁴¹ Taflove, A., "Application of the finite-difference time-domain method to sinusoidal steady state electromagnetic penetration problems" *IEEE Transactions on Electromagnetic Compatibility*, vol. 22, 3, 1980
- ⁴² Sullivan, D. *Electromagnetic Simulation using the FTFT Method* Piscataway, NJ: IEEE Press, 2000
- ⁴³ Courant, R., Friedrichs, K., and Lewy, H., "On the partial difference equations of mathematical physics", *IBM Journal*, 1967 (English translation of the 1928 German original)
- ⁴⁴ Smith, G. D. *Numerical Solution of Partial Differential Equations: Finite Difference Methods*, 3rd ed. 1985

-
- ⁴⁵ Engquist, B., and Majda, A., “Absorbing Boundary Conditions for the Numerical Simulation of Waves”, *Mathematics of Computation* , vol. 31, 139, 1977
- ⁴⁶ Clayton, R., and Engquist, B., “Absorbing boundary conditions for acoustic and elastic wave equations”, *Bulletin of the Siesmological Society of America*, vol.67, 5, 1977
- ⁴⁷ Clayton, R., and Engquist, B., “Absorbing boundary conditions for wave-equation migration”, *Geophysics*, vol. 45, 5, 1980
- ⁴⁸ Mur, G., “Absorbing Boundary Conditions for the Finite-Difference Approximation of the Time-Domain Electromagnetic-Field Equations”, *IEEE Transactions on Electromagnetic Compatibility*, vol. 23, 4,1981
- ⁴⁹ Berenger, J.P., “A perfectly matched layer for the absorption of electromagnetic waves”, *Journal of Computational Physics*, vol. 114, 2, 1994
- ⁵⁰ Berenger, J.P., “Three-dimensional perfectly matched layer for the absorption of electromagnetic waves”, *Journal of Computational Physics*, vol. 127, 0181, 1996
- ⁵¹ Chew, W.C., and Liu, Q.H., “Perfectly matched layers for elastodynamics: A new absorbing boundary condition”, *Journal Computational Acoustics*, vol. 4, no. 4, pp.341{259, 1996
- ⁵² Hu, F. “On absorbing boundary conditions for linearized Euler equations by a perfectly matched layer”, *Journal of Computational Physics*, vol.129, 0224, 1996
- ⁵³ Liu, Q.H., and Tao, J., “The perfectly matched layer (PML) for acoustic waves in absorptive media”, *Journal of the Acoustical Society of America*, vol. 102, 4, 1997
- ⁵⁴ Li, X., “PML Condition for the numerical simulation for acoustic wave”, *IEEE International Conference on Computing, Control, and Industrial Engineering*, 2010
- ⁵⁵ Zheng Y. and Huang X., “Anisotropic perfectly matched layers for elastic waves in Cartesian and curvilinear co-ordinates”, *Technical Report, MIT Earth Resources Laboratory*, 2002
- ⁵⁶ Komatitsch, D. and Tromp, J., “A perfectly matched layer absorbing boundary condition for the second – order seismic wave equation”, *Geophysical Journal International*, vol. 154, 2003
- ⁵⁷ Roden J.A. and Gedney, S.D., "A convolutional PML for the effective absorption of evanescent waves in arbitrary media," *IEEE Transactions on Antennas and Propagation*, 2000.

-
- ⁵⁸ Cummer, S.A., “A Simple, Nearly Perfectly Matched Layer for General Electromagnetic Media”, *IEEE Microwave and Wireless Components letters*, vol. 13, 3, 2003
- ⁵⁹ Berenger, J.P., “On reflection from Cummer’s nearly perfectly matched layer”, *IEEE Microwave and Wireless Components Letters*, vol. 14, 7, 2004
- ⁶⁰ Hu, W. and Cummer, S.A., “The nearly perfectly matched layer is a perfectly matched layer” *IEEE Antennas and Wireless Propagation Letters*, vol. 3, 2004
- ⁶¹ Chen, J. and Bording, R.P., “Application of the nearly perfectly matched layer to the propagation of low-frequency acoustic waves”, *Journal of Geophysical Engineering*, vol. 7, 2010
- ⁶² Chen, J., Zhang, C. and Bording, R.P., “Comparison between the nearly perfectly matched layer and unsplit convolutional perfectly matched layer methods using acoustic wave modeling”, *Journal of seismic exploration*, vol. 19, 2, 2010
- ⁶³ Baz, A., “An active acoustic metamaterial with tunable effective density”, *Journal of Vibration and Acoustics*, vol. 132, 017002, 2010
- ⁶⁴ Lapine, M., “The Age of Metamaterials”, *Metamaterials*, vol. 1, 2007
- ⁶⁵ Gil, M., Bonache, J., and Martín, F., “Metamaterial Filters: A review”, *Metamaterials*, vol. 2, 2008
- ⁶⁶ Popa, B. I. and Cummer, S., “Cloaking with Optimized Homogenous Anisotropic Layers”, *Physical Review A*, 79, 023806, 2009
- ⁶⁷ Cheng, Y. and Liu, X. J., “Three Dimensional Multilayered Acoustic Cloak with Homogeneous Isotropic Materials”, *Journal Applied Physics A: Materials Science & Processing*, vol. 94, 1, 2009
- ⁶⁸ Chen, H.-Y., Yang, T., Luo, X.-D. and Ma, H.-R., “Impedance-Matched Reduced Acoustic Cloaking with Realizable Mass and Its Layered Design”, *Chinese Physics Letters*, vol. 25, 10, 2008
- ⁶⁹ Norris, A.N., “Acoustic metafluids”, *Journal of the Acoustical Society of America*, vol. 125, 2, 2009
- ⁷⁰ Lee, S. H., Park, C. M., Seo, Y. M., Wang, Z. G., and Kim, C. K., “Reverse Doppler Effect of Sound”, <http://arxiv.org/abs/0901.2772v2>, 2009
- ⁷¹ Yao, S., Zhou, X. and Hu, G., “Experimental study on negative effective mass in a 1D mass–spring system”, *New Journal of Physics*, vol. 10, 043020, 2008
- ⁷² Bauer, B.B., “Equivalent circuit analysis of mechano-acoustic structures”, *Transactions of Institute of Radio Engineers*, vol. AU-2, 1954

-
- ⁷³ Firestone, F.A., “A new analogy between mechanical and electrical systems”, *Journal of the Acoustical Society of America*, vol. 4, 3, 1933
- ⁷⁴ Kinsler, L., Frey, A., Coppens, A., and Sanders, J., *Fundamentals of Acoustics*, 4th ed., J. Wiley & Sons, Inc., 2000
- ⁷⁵ ANSI/IEEE, 1987, American National Standards/Institute of Electrical and Electronics Engineers “Standard on Piezoelectricity”, ANSI/IEEE Std:176-1987, IEEE, New York.
- ⁷⁶ Prasad S., Gallas, Q., Horowitz, S., Homeijer, B., Sankar, B., Cattafesta, L., and Sheplak, M., “Analytical electroacoustic model of a piezoelectric composite circular plate”, *Journal of American Institute of Aeronautics and Astronautics*, vol. 44, 10, 2006
- ⁷⁷ Akl, W. and Baz, A., “Analysis and experimental demonstration of an active acoustic metamaterial cell”, *Journal of Applied Physics*, 044505, 2012
- ⁷⁸ Akl, W., Smoker, J., and Baz, A., “Acoustic metamaterial with controllable directivity and dispersion characteristics”, *Proceedings of the Smart Structures Conference*, 7977-49 2011
- ⁷⁹ Cheng, Y., Xu, J., and Liu, X.J., “One-dimensional structured ultrasonic metamaterials with simultaneously negative dynamic density and modulus”, *Physical Review B*, vol. 77, 4, 2008
- ⁸⁰ Ding, Y., Liu, Z., Qiu C., and Shi, J., “Metamaterial with simultaneously negative bulk modulus and mass density”, *Physical Review Letters*, vol. 99, 9, 2007
- ⁸¹ Fang, N., Xi, D., Xu, J., Ambati, M., Srituravanich, W., Sun, C., and Zhang, X., “Ultrasonic metamaterials with negative modulus”, *Nature Materials*, vol. 5, 452, 2006
- ⁸² Lee, S.H., Park, C.M., Seo, Y.M., Wang Z.G., and Kim, C.K., “Composite acoustic medium with simultaneously negative density and modulus”, *Physical Review Letters*, vol. 104, 5, 2010
- ⁸³ Li, J. and Chan, C., “Double-negative acoustic metamaterial ”, *Physical Review E*, vol. 70, 5, 2004
- ⁸⁴ Sánchez-Pérez J., Caballero, D., Martínez-Sala, R., Rubio, C., Sánchez-Dehesa, J., Meseguer, F., Llinares J., and Gálvez, F., “Sound attenuation by a two-dimensional array of rigid cylinders”, *Physical Review Letters*, vol. 80, 24, 1998
- ⁸⁵ Caballero, D., Sánchez-Dehesa, J., Rubio, C., Martínez-Sala, R., Sánchez -Pérez, J., Meseguer, F., and Llinares, J., “ Large two-dimensional sonic band gaps”, *Physical Review E*, vol. 60, 1999

-
- ⁸⁶ Chen, Y. and Ye, Z., “Acoustic attenuation by two-dimensional arrays of rigid cylinders”, *Physical Review Letters*, vol. 87, 184301, 2001
- ⁸⁷ Sanchis, L., Cervera, F., Sánchez-Dehesa, J., Sánchez-Perez, J., Rubio, C., and Martínez-Sala, R., “Reflectance properties of two-dimensional sonic band-gap crystals”, *Journal of the Acoustical Society of America*, vol. 109, 2001
- ⁸⁸ Climente, A., Torrent D., and Sánchez-Dehesa, J., “ Sound focusing by gradient index sonic lenses”, *Applied Physics Letters*, vol. 97, 104103, 2010
- ⁸⁹ Sánchez-Dehesa, J., Garcia-Chocano, V., Torrent, D., Cervera, F., Cabrera S., and Simon, S., “Noise control by sonic crystal barriers made of recycled materials”, *Journal of the Acoustical Society of America*, vol. 129, 3, 2011
- ⁹⁰ Kushwaha, M., “Stop-bands for periodic metallic rods: sculptures that can filter the noise”, *Applied Physics Letters*, vol. 70, 24, 1997
- ⁹¹ Sigalas, M., and Economou, E., “Attenuation of multiple-scattered sound” , *Europhysics Letters*, vol. 36, 4, 1996
- ⁹² Akl, W., and Baz, A., “Multi-cell active acoustic metamaterial with programmable bulk’s modulus”, *Journal of Intelligent Material Systems and Structures*, vol. 21, 5, 2010
- ⁹³ Baz, A., “The structure of an active acoustic metamaterial with tunable effective density”, *New Journal of Physics*, vol. 11, 1230102009, 2009
- ⁹⁴ Baz, A., “An active acoustic metamaterial with tunable effective density”, *ASME Journal of Vibration and Acoustics*, vol. 132, 4, 2010
- ⁹⁵ Martin, T., Nicholas, M., Orris, G., Cai, L., Torrent, D., and Sánchez-Dehesa, J., “Sonic gradient index lens for aqueous applications”, *Applied Physics Letters*, vol. 97, 113503, 2010
- ⁹⁶ Popa, B.I., Zigoneanu, L., and Cummer, S.A., “Experimental acoustic ground cloak in air”, *Physical Review Letters*, vol. 106, 253901, 2011
- ⁹⁷ Zigoneanu, L., Popa, B.I., Starr, A.F., and Cummer, S.A., “Design and measurements of a broadband two-dimensional acoustic metamaterial with anisotropic effective mass density”, *Journal of Applied Physics*, vol. 109, 054906, 2011

-
- ⁹⁸ Zhang, S., Yin, L., and Fang, N., “Focusing Ultrasound with an Acoustic Metamaterial Network”, *Physical Review Letters*, vol. 102, 194301, 2009
- ⁹⁹ Kostek, T.M. and Francheck, M.A., “Hybrid noise control in ducts”, *Journal of Sound and Vibration*, vol. 237, 1, 2000
- ¹⁰⁰ Nagaya, K., Hano Y., and Suda, A., “Silencer consisting of two-stage Helmholtz resonator with auto-tuning control”, *Journal of the Acoustical Society of America*, vol. 110, 1, 2001
- ¹⁰¹ Choi, S. and Kim, Y.H., “Sound-wave propagation in a membrane–duct (L)”, *Journal of the Acoustical Society of America*, vol. 112, 5, 2002
- ¹⁰² Esteve S.J. and Johnson, M.E., “Adaptive Helmholtz resonators and passive vibration absorbers for cylinder interior noise control”, *Journal of Sound and Vibration*, vol. 288, 4-5, 2005
- ¹⁰³ Chiu, Y., Cheng, L., and Huang, L., “Drum-like silencers using magnetic forces in a pressurized cavity”, *Journal of Sound and Vibration*, vol. 297, 3-5, 2006
- ¹⁰⁴ Fang, N., Xi, D., Xu, J., Ambati, M., Srituravanich, W., Sun C., and Zhang, X., “Ultrasonic metamaterials with negative modulus”, *Nature Materials*, vol. 5, 6, 2006
- ¹⁰⁵ Naify, C.J., Chang, C.M., McKnight G., and Nutt, S., “Transmission loss and dynamic response of membrane-type locally resonant acoustic metamaterials”, *Journal of Applied Physics*, vol. 108, 114905, 2010
- ¹⁰⁶ Naify, C.J., Chang, C.M., McKnight G., Scheulen F., and Nutt, S., “Membrane-type metamaterials: Transmission loss of multi-celled arrays”, *Journal of Applied Physics*, vol. 109, 104902, 2011
- ¹⁰⁷ ISO 10534-2, *Acoustics – Determination of sound absorption coefficient and impedance in impedance tubes – Part 2: Transfer-function method*, International Organization for Standardization, 1998
- ¹⁰⁸ ASTM E1050, in *Thermal Insulation; Building and Environmental Acoustics*, ASTM International, Pennsylvania, 2009
- ¹⁰⁹ Blauert, J. and Xiang, N., *Acoustics for Engineers: Troy Lectures*, Springer Verlag, 2009
- ¹¹⁰ DiGiovanni, M., *Flat and Corrugated Diaphragm Design Handbook*, CRC, 1982
- ¹¹¹ Romero-García, V., Fuster, E., García-Raffi, L., Sánchez-Pérez, E., Sopena, M., Llinares, J., and Sánchez-Pérez, J., “Band gap creation using quasicrystalline structures based on sonic crystals”, *Applied Physics Letters*, vol. 88, 174104, 2006

-
- ¹¹² Yang, Z., Mei, J., Yang, M., Chan, N., and Sheng, P., “Membrane-type acoustic metamaterial with negative dynamic mass”, *Physical Review Letters*, vol. 101, p. 204301, 2008.
- ¹¹³ Cervera, F., Sanchis, L., Sánchez-Perez, J., Martínez-Sala, R., Rubio, C., Meseguer, F., López, C., Caballero, D., and Sánchez-Dehesa, J., “Refractive acoustic devices for airborne sound”, *Physical Review Letters*, vol. 88, p. 023902, 2002
- ¹¹⁴ Krokhnin, A., Arriaga, J., and Gumen, L., “Speed of sound in periodic elastic composites”, *Physical Review Letters*, vol. 91, 264302, 2003
- ¹¹⁵ Torrent, D., and Sánchez-Dehesa, J., “Acoustic metamaterials for new two-dimensional sonic devices”, *New Journal of Physics*, vol. 9, 323, 2007
- ¹¹⁶ Milton, G.W., and Willis, J. R., “On modifications of Newton's second law and linear continuum elastodynamics”, *Proceedings of the Royal Society A: Mathematical, Physical and Engineering Science*, vol. 463, 855, 2007
- ¹¹⁷ Huang, H., Sun, C., and Huang, G., “On the negative effective mass density in acoustic metamaterials”, *International Journal of Engineering Science*, vol. 47, 2009
- ¹¹⁸ Pendry, J.B., “Negative refraction makes a perfect lens”, *Physical Review Letters*, vol. 85, 3966-3969, 2000
- ¹¹⁹ Akl, W. and Baz, A., “Stability analysis of active acoustic metamaterial with programmable bulk modulus”, *Smart Materials and Structures*, vol. 20, 125010, 2011
- ¹²⁰ Liu, F., Horowitz, S., Nishida, T., Cattafesta, L., and Sheplak, M., “A tunable electromechanical Helmholtz resonator”, *Proceedings of 9th AIAA/CEAS Aeroacoustic Conference*, 3145, 2003
- ¹²¹ Liu, F., Horowitz, S., Nishida, T., Cattafesta, L., and Sheplak, M., “A multiple degree of freedom electromechanical Helmholtz resonator”, *Journal of the Acoustical Society of America*, 112, 1, 2007
- ¹²² Prasad, S.A.N., Sankar, B.V., Cattafesta, L.N., Horowitz, S., Gallas, W., and Sheplak, M., “Two-port electroacoustic model of an axisymmetric piezoelectric composite plate”, *Proceedings of the 43rd AIAA/ASME/ASCE/AHS/ASC Structures, Structural Dynamics, and Materials Conference*, 1365, 2002
- ¹²³ Gallas, Q., *Lumped element modeling of piezoelectric-driven synthetic jet actuators for active flow control*, Master Thesis, University of Florida, 2002

¹²⁴ Tang, Y., Robinson, J., and Silcox, R., “Sound transmission through a cylindrical sandwich shell with honeycomb core”, *NASA Technical Report*, 1996

¹²⁵ Smith, J., and Verrier, P., “The effect of shear on acoustic cloaking”, *Proceedings of the Royal Society A*, vol. 467, 2132, 2011